TALLINNA TEHNIKAÜLIKOOL
TALLINN UNIVERSITY OF TECHNOLOGY

Department of Electrical Power Engineering and Mechatronics

CONCEPT STUDIES FOR A CUBESAT MISSION TO THE HIGHLY ELLIPTICAL ORBIT

KONSEPTSIOONID CUBESATI MISSIONIKS KÖRGELT ELLIPTILISELE ORBIIDILE

MASTER THESIS

Student: Nodirkhon Yusupov

Student code: 177253MAHM

Supervisor: Dr Mart Tamre, Professor

Tallinn, 2019

AUTHOR'S DECLARATION

Hereby I declare, that I have written this thesis independently.
No academic degree has been applied for based on this material. All works, major viewpoints and data of the other authors used in this thesis have been referenced.

"....." ..... 201…..

Author: .....
/signature /

Thesis is in accordance with terms and requirements

"....." ..... 201….

Supervisor: …….....
/signature/

Accepted for defence

"....."…….....201… .

Chairman of theses defence commission: .....
/name and signature/

Department of Electrical Power Engineering and Mechatronics

THESIS TASK

Student: Nodirkhon Yusupov, 177253MAHM (name, student code)

Study programme, MAHM02/13 - Mechatronics (code and title)

main speciality: Mechatronics

Supervisor(s): Professor, Mart Tamre, 5120982 (position, name, phone)

Consultants: Jaan Praks, Assistant Professor; Andris Slavinskis, Postdoctoral Researcher (name, position)

Aalto University, +358 50 420 5847, jaan.praks@aalto.fi (company, phone, e-mail)

Thesis topic:

(in English) *Concept studies for a CubeSat mission to the Highly Elliptical Orbit*

(in Estonian) *Konseptsioonid CubeSati missioniks Kõrgelt Elliptilisele Orbiidile*

Thesis main objectives:

1. Develop science goals and objectives into traceable requirements for satellite engineers.
2. Analyse the feasibility of the proposed concept.
3. Produce trade space studies and identify alternative options to the implementation of the concept.

Thesis tasks and time schedule:

No	Task description	Deadline
1.	CML 1: Science and Mission Traceability	27.02.19
2.	CML 2: Feasibility Analysis	21.03.19
3.	CML 3: Trade Space; CML 4: Point Design	25.04.19

Language: English **Deadline for submission of thesis:** "21." May 2019 a

Student: Nodirkhon Yusupov ..... "....." .....201....a
/signature/

Supervisor: Mart Tamre ..... "....." .....201....a
/signature/

Consultant: Andris Slavinskis ..... "....." .....201....a
/signature/

CONTENTS

PREFACE

The concept studies for a CubeSat mission to the Highly Elliptical Orbit (HEO) were made for the FORESAIL-2 nanosatellite project of the Finnish Centre of Excellence in Research of Sustainable Space funded by the Academy of Finland.

The research was done during the Erasmus+ exchange programme and had academic supervisors from two universities, Assistant Professor Jaan Praks of Aalto University and Professor Mart Tamre of Tallinn University of Technology. Meanwhile, Postdoctoral Researcher at Aalto University and Senior Researcher at Tartu Observatory of the University of Tartu, Andris Slavinskis, was an advisor of this research work.

The author expresses his gratitude to his parents, organizers of the exchange programme, supervisors and advisor for all kinds of support provided in the course of work over this research. Furthermore, the author would like to thank Professor Minna Palmroth, Associate Professor Emilia Kilpua and her team at the University of Helsinki, research manager Pekka Janhunen and his team at FMI, and Professor Rami Vainio and his team at the University of Turku. Finally, the author would like to thank his teammates from the laboratory of Space Technology at Aalto University.

The main goal of this research was to analyse the feasibility of the proposed concept of a CubeSat mission to the HEO and perform trade space studies to identify alternatives for concept implementation. The concept studies were done within a Concept Maturity Level (CML) framework developed by the Jet Propulsion Laboratory (JPL) at NASA. Science and mission requirements were developed at CML 1. The CML 2 produced studies on feasibility which concluded that a 3U CubeSat was feasible on condition that solar panels were deployed to provide enough power, and volume and mass reduced to fit within limits. The CML 3 provided trade space studies on the possible use of a 6U CubeSat at the HEO such as geostationary transfer orbit (GTO). A 3U CubeSat configuration was set as the baseline, while a 6U one was defined as the threshold. Finally, the CML 4 produced point designs for operating phases, spacecraft system design, and subsystem product tree. The research concluded that the proposed mission to the HEO was feasible if certain conditions were to be followed. A 3U and 6U CubeSats were proposed as mission baseline and threshold spacecraft configurations, respectively.

Keywords: FORESAIL-2, HEO, GTO, CubeSat, nanosatellite, CML, space technology, master thesis

List of abbreviations and symbols

ADCS	Attitude Determination and Control System
CML	Concept Maturity Level
COM	Communication
COTS	Commercial Off-The-Shelf
EMI	Electromagnetic Interference
GNSS	Global Navigation Satellite System
GTO	Geostationary Transfer Orbit
HEO	Highly Elliptical Orbit
IGRF	International Geomagnetic Reference Field
MEL	Master Equipment List
MLT	Magnetic Local Time
MPPT	Maximum Power Point Tracking
MTM	Mission Traceability Matrix
OBC	On-Board Computer
PEL	Power Equipment List
P-POD	Poly-Picosatellite Orbital Deployer
PROP	Propulsion
SEE	Single Event Effect
SEU	Single Event Upset
SRD	Science Return Diagram
STM	Science Traceability Matrix
STRUCT	Structure
TID	Total Ionizing Dose
UHF	Ultra High Frequency
ULF	Ultra Low Frequency
UTC	Coordinated Universal Time

1 INTRODUCTION

A concept of small satellites, such as CubeSat, has brought significant growth to Low Earth Orbit space missions with commercial and scientific goals [1]. The progress achieved in miniaturisation of space technology in the last decade allowed producing CubeSat missions for not only Low-Earth Orbit (LEO) trajectories but higher ones too [2].

The CubeSat mission under study aims to provide answers to the following science and technology related questions developed by members of the Finnish Centre of Excellence in Research of Sustainable Space (FORESAIL) [3]:

- What is the role of Ultra Low Frequency (ULF) waves in transporting and scattering of electrons in the Earth's radiation belts as a function of solar wind driving and magnetospheric activity?
- What are the novel radiation mitigation techniques?
- Is a CubeSat application technically feasible in challenging environments?

The desirable orbit parameters to achieve the aforesaid science goals are the orbit with low inclination from ecliptic plane, highly elliptical to access regions close to magnetopause, and with high radiation environment to perform radiation mitigation experiment [3]. The type of orbits that falls under these requirements is the Highly-Elliptical Orbit (HEO) [4]. Since piggyback launch for nanosatellite is more probable than a dedicated one, the most available type of HEO for launch is the Geostationary Transfer Orbit (GTO) [5].

A technology for CubeSat reached the new level when robotic deep space missions were demonstrated successfully by MarCO mission to Mars [6]. Despite that, HEO such as GTO, still has not been accessed with CubeSat technology. This orbit is frequently used to transfer telecommunication satellites to the Geostationary Orbit (GEO), and it is characterised by the presence of radiation belts populated by high-energy charged particles, resulting from dynamic radiation belts phenomena in Earth magnetosphere [7].

Furthermore, the radiation doses at the GTO are high and cause damages to onboard electronics of spacecraft, and possess health risks for astronauts working in the open space [7]. Therefore, it is vital to have direct sensing observations at the GTO to characterise the radiation environment and

develop technical solutions for radiation damage mitigation for small satellites. Currently, there are only three (3) science missions at the GTO producing direct sensing observations such as Van Allen Probes A and B (NASA) [8], and ARASE.ERG (JAXA) [9].

Therefore, an independent research is to be done to produce a systematic concept study of a CubeSat science mission to the Geostationary Transfer Orbit (GTO) for FORESAIL. The current space mission concept is to be developed to the stage where a baseline could be engineered, budgeted and benchmarked.

Furthermore, the current mission under study is to be built on the previous achievements of the FORESAIL consortium such as Aalto-1 [10], FORESAIL-1 [11], ESTCube-1 [12] and 2 [13], and Vlasiator [14]. The concept maturity of the space mission under study is at the stage where science and technology goals have been specified by the consortium [3], and mission requirements are available. Meanwhile, the hypothesis, that the CubeSat mission to the GTO fulfilling the given [3] science goals with the current technology is feasible will be tested in the course of this research.

The results of this research will be of interest to the academic and commercial institutions as scientific observation and technology demonstration at the GTO onboard of a CubeSat are yet to be validated for the first time. Furthermore, the Concept Maturity Level (CML) framework developed by the Jet Propulsion Laboratory of NASA [15] for space mission design will be applied for the first time to a non-NASA CubeSat mission to the GTO. Nevertheless, the scope of the framework mentioned above will be narrowed to several technical attributes to provide an engineering perspective rather than science and management ones. Since the specialisation in mechatronics requires the ability to integrate products of different engineering disciplines, different aspects of space mission concept development specified in a CML matrix [15] will be addressed in this research.

The first deliverable of this research will be a mission concept matured through CML framework to level 3 with Science traceability matrix, Feasibility assessment, and Trade Space analysis. Furthermore, solutions to mitigating different challenges associated with GTO environmental characteristics will be provided. Finally, this research will result at the end in a Master Equipment List (MEL) and system design of the CubeSat.

The structure is divided into five chapters where the chapter 2 will provide a literature review on current and future CubeSat missions to the GTO, characteristics of the GTO, available technology

for nanosatellites for use at the GTO, and available launch services. Meanwhile, chapter 3 will explain the problem this research is going to solve and the methodology of solving the problem above. Subsequently, chapter 4 will explain the maturing of the space mission concept via feasibility and trade space analysis, and conclusions on concept maturity developments for the next level will be provided.

The theoretical part is to be covered in chapter 2 and 3, while implementation part where work of author is showcased is to be presented in chapter 4. The author will provide numerical and analytical solutions illustrated with graphs and summarized with tables on such topics as orbital lifetime and evolution, total ionizing doses, geomagnetic field conjugation with spacecraft, electron and proton fluxes, telemetry and link budgets, power supply, thermal conditions, delta-v budget, spacecraft system design and technical risk assessment.

2 LITERATURE REVIEW

2.1 CubeSat missions to the GTO

No known nanosatellite missions are operating at the GTO at the moment [1]. Nevertheless, the nearest launch of a CubeSat (Orbital Factory II) to the GTO is planned to take place in December of 2019 [1]. Moreover, the mission of two (2) CubeSats (MarCO-A and MarCO-B) to the orbit of Mars has successfully commenced in May [16] and ended in November 2018 [2].

Table 2.1 A list of current and future CubeSat missions to the GTO and deep space.

#	CubeSat	Size	Thermal	Radiation	COM	ADCS	Launch date
GTO							
1	GTOSat [7] [17] [18] [19] [20] [7], [21]	6U	Thermal louvres (GSFC) UNDER DEVELOPMENT	Rad-tolerant parts Vault of shielding (7 mm) UNDER DEVELOPMENT	S-BAND	Reaction wheels with magnetorquers	DEC-20 or 2021
2	SpectroCube [22]	3U	N/A	N/A	N/A	N/A	DEC-20
3	Orbital Factory II [23]	1U	Chassis (AL6061)	Chassis (Vault) made of AL6061	UHF	NONE	DEC-19
4	LACCE [24] [25]	3U	N/A	N/A	N/A	N/A	Initially: DEC-18. Now: DELAY
5	ADE [26] [27]	1U	NONE	NONE	UHF(?)	NONE	DEC-19
6	M-BARC/ DSM-BRAC [28] [29] [30] [31] [32]	3U	N/A	Radiation shielding with 2 mm thick walls on all six sides	UHF	N/A RF Ion propulsion system	DEC-19
7	Shields-1 [33] [34] [35]	3U	Al/Tantalum Z-grade shielding vaults	Al/Tantalum Z-grade shielding vaults Electrostatic discharge solar panels Charge Dissipation Film	UHF	NONE	DEC-18 SSO/ Polar LEO

#	CubeSat	Size	Thermal	Radiation	COM	ADCS	Launch date
-	BIRDY-GTO [36]	3U	N/A	N/A	UHF INTERSAT GRND	Star tracker Object Tracker Liquid Pulsed Plasma Thruster	Cancelled
-	ALCEK [1]	6U	N/A	N/A	N/A	N/A	Cancelled
Initially GTO							
1	mDot [37] [38] [39]	6U	Insulation with low emissivity coating	No shielding Fault tolerant OBC Software watchdog	UHF	Reaction wheels Magnetorquer Sun sensor Star Tracker 3-axis gyroscope	DEC-20 SSO
Deep Space Mission to the Mars							
1	MarCO [40] [6] [16] [41]	6U	Thermal blanket; Radiator; Heater	Radiation tolerant components	UHF X-BAND	Two coarse sun sensors 1 star tracker Gyroscope 3 Reaction wheels Cold Gas Propulsion	MAY-18

There are eight (8) announced CubeSat missions to the GTO/HEO with launch dates spread from the December of 2018 to December of 2021 (Table 2.1). Another two (2) CubeSat missions were cancelled. While it is believed that not all of these missions are to be launched or successful once launched, it is worth reviewing their approaches to spacecraft design. These approaches are to be further studied to generate viable suggestions for the design of FORESAIL-2 CubeSat mission.

GTOSat project [7] is to host similar to FORESAIL-2 mission science instruments: (1) an energetic particle detector and (2) boom-mounted magnetometer [19]. Moreover, the primary investigator of the GTOSat project justified the use of 6U instead of 3U by the argument that this size is to provide more room for the science instruments [19].

The Dellingr mission uses no-boom magnetometer [20]. The use of magnetometer in close proximity to satellite subsystems was found to deteriorate its performance due to electromagnetic interference (EMI) caused by onboard electronics. Therefore, it was decided by NASA that

magnetometers would be placed outside of the CubeSat frame on a boom to avoid issues with the EMI in future nanosatellite missions [7], [21].

The radiation mitigation strategy of GTOSat includes usage of radiation tolerant components and 7 mm thickness of shielding to achieve targeted TID of less than 10 krad [18]. Meanwhile, the communication system is planned to be based on the S radio frequency band (S-band) [18]. Finally, the in-house developed Microsemi RTG4 FPGA is to be used for communication and data handling (C&DH) along with in-house developed electric power system (EPS) [18]. The GTOSat is to be based on an improved version of the Dellingr CubeSat platform [42], and thus, there might be similarities in the design of specific subsystems (Table 2.2).

Table 2.2 An overview of subsystems of interest onboard of the Dellingr CubeSat [43]

Size	Mission Status
6U	Operating; Experienced several hardware anomalies and failures; Now, commissioning one of its science payloads
Subsystem	**Description**
ADCS	Components: 3-axis reaction wheels, magnetometers, inertial rate sensors, magnetorquer, sun sensors Strategy: Sun-pointing.
Thermal control	Interior coating with low emissivity materials; Heat conduction from powered components to the aluminium baseplate radiating to space; Nadir side used as baseplate and radiator Metal behind solar cells was coated with high emissivity Teflon impregnated anodise The baseplate was made to be higher in mass to compensate for the transient temperature swing during the change to an eclipse phase Batteries use internal heaters and radiator. It was found that communication session produces a total of 10W of power dissipation. Radio was mounted on the housing with NuSil thermal interface material applied. The magnetometer was anodised for high emissivity. Finally, thermal louvre with bimetallic springs successfully passed the test of 12900 cycles at a range of 32 to 55 degree Celsius and eight thermal-vacuum tests at a range from -20 to 85 degree Celsius.
Communication	L3 Cadet-U: half-duplex UHF; downlink: 3 Mbit/s; High FIFO; Low FIFO
Payload	An advanced gated time-of-flight ion/neutral mass spectrometer (INMS), three fluxgate magnetometers (2 internal, 1 is on the end of a 52cm boom)

Dellingr CubeSat experienced severe anomalies once on the orbit, and in nearly two months after deployment, it failed to communicate with the ground stations [44][45]. Contact with the CubeSat was established only after 11 days since the loss of communication channel (Table 2.3).

Table 2.3 A list of anomalies and mitigation strategy associated with the Dellingr mission [45]

Date	Anomaly	Cause	Mitigation strategy
Unknown	The CubeSat turned on inside the deployer	The unexpected release of switch button due to friction and other mechanical impacts	This anomaly was tested, and the CubeSat was designed to continue operation in a normal mode
20-Nov-2017	Deployment from ISS	Not an anomaly. The reference date for the start of significant anomalies.	
30-Nov-2017	Anomalous gyro and sun pointing accuracy	Instability on the I^2C bus for IMU. Massive torques on wheels (rapid switches in directions). The noise made it impossible to use the Kalman filter to produce an accurate attitude.	Turning off IMU.
19-Dec-2017	GPS unresponsive	Lack of real-time ephemeris required for INMS science payload	No solution due to lack of onboard computer (OBC) processing power
21-Dec-2017	Unusually noisy fine sun sensor (FSS)	Faulty operation of the in-house fine sun sensor	Switching to the 2nd fine sun sensor of GomSpace. A software update was required to make sure that only one fine sensor is being used.
25-Jan-2018	Spacecraft data deleted - unknown cause	Lost around 650 000 packets of data. The CubeSat was near the South Atlantic Anomaly (SAA).	NONE. No exact cause has been established.
26-Jan - 6-Feb 2018	Loss of contact. Permanent reset state.	13000 resets every 63 seconds.	Jamming communication session with “RESET” requests from the ground station to force EPS watchdog to power cycle the CubeSat.
6-Feb-2018	Recovery	It was found that high traffic on the I^2C bus and the degradation of some components on the bus caused previous problems with resets. The source of high traffic was found to be generated from the reaction wheels.	The reaction wheels were disabled immediately after recovery. Each of three wheels communicated at 10 Hz frequency each. It was decided to turn on the wheels only a few times in a week to adjust sun-pointing attitude.
26-Mar-2018	Spacecraft data deleted - unknown cause	Around 700 000 packets lost.	

Date	Anomaly	Cause	Mitigation strategy
Mitigation of anomalies			
29-Mar - 15-May 2018	A series of B-dot (ADCS control algorithm) updates (V1 to V3)	The CubeSat was found to be spinning at 17.5 RPM. Reason: software implementation issue of a magnetic control during the eclipse.	The initial version B-dot algorithms did not work for such a high spin rate. Thus, patches for B-dot were uploaded to resolve the issue.

The Dellingr CubeSat crossed the region near to the South Atlantic Anomaly (SAA) during the first case of SEU with data deletion [45]. The SAA is an extension of the Van Allen radiation belts into the lower Earth orbits [46]. Since the FORESAIL-2 mission is aimed for the launch to the GTO where Van Allen radiation belts are present, the risk of SEU leading to the deletion of data on memory storage is high.

One of the mitigation strategies for the mentioned anomalies was the Failure Detection and Correction (FDC) scheme with a 25-hour reset for power cycling the CubeSat [45]. The FDC saved the CubeSat mission from several anomalies (Single event upsets (SEU)) but made troubleshooting and scheduling harder to perform.

The Dellingr team identified the primary sources of problems for failed ADCS and software implementation issues as the lack of extensive testing where a scenario with faulty GPS and IMU would have been simulated, limited human resources for thorough analysis and lack of sufficient documentation.

Key factors to increase odds of mission success as suggested by the Dellingr team [45] are as follows:

- Daily resets are useful for failure detection and correction.
- Capability to provide patches is vital.
- Size of uploads must be minimised.
- More telemetry, better for troubleshooting.
- Use redundant systems.
- The case with sun sensors where one failed, and another worked and thus, provided data for ADCS.
- Allocate more engineers for checkout and corrective actions on-orbit than a regular mission (not CubeSat).

- Allocate more time for data reduction, analysis and trending to detect hardware issues at early stages.
- FDC must be able to detect malfunctioning hardware rather than only failed components.
- Introduce hardware diagnostics to a software application.
- To isolate problems to a specific area.
- Capability to reconfigure between different ADCS control modes and science payload usages.
- To gain extra resilience for the mission.
- Good to have a full flatsat along with flight software testing with hardware in the loop and a physics simulator.
- Fewer devices share a communication bus the better.
- Sensor and actuator hardware must match the processing power of OBC.
- Low-level hardware (drivers) must be accessible with ground control software during the mission.
- Three systems cannot fail to keep the mission alive: Electric Power System (EPS), Communication (COM), and Communication and Data Handling (C&DH).

Dellingr X is the latest advancement in the development of Dellingr CubeSat platforms currently done by NASA Goddard Space Flight Centre (Table 2.5) [18]. The Dellingr X spacecraft bus aims to provide a robust and reliable platform able to operate at challenging and harsh space environments for the future NASA Class-D missions [18].

Table 2.5 List of targeted capabilities for each primary subsystem of a Dellingr X [18]

Subsystems	Targeted performance
Protection from radiation	SEE <37 MeV/cm^2 TID per component > 30 krad TID with part upgrades and shielding >100 krad
Communication	S-band SDR; IRIS compatible radio
Navigation	IRIS transponder or optical navigation
ADCS	Pointing determination: .005 deg (18 arcsec) (1 sigma) Quaternion at > 4 Hz Pointing accuracy - < 1 deg Autonomous protection of predefined exclusion zones
EPS	50 W-250 W at 1 AU Watchdogs, commandable reset
C&DH	Softcore LEON3 FT in an RTG4 FPGA

Subsystems	Targeted performance
	10 MB SRAM, 250 KB MRAM, 4 GB FLASH Digital, analogue, actuator, and telemetry interfaces
Mechanical structure and thermal control	Customised design for each mission

The radiation mitigation strategy of Orbital Factory II CubeSat mission does not consider using shielded components but focuses on putting all onboard electronics within a chassis [23]. The chassis is a hollow structure called vault and made of an Al6061 type of aluminium alloy. The Orbital Factory II team assumed that continuous chassis would minimise impact from ionising radiation. The justification for the said was that with continuous structure there would be a low number of ingress paths for particles to reach electronic components contained within the chassis [23]. Furthermore, the chassis was made to be electrically conductive with bonding terminations applied where applicable.

The radiation mitigation strategy of M-BARC mission is to use a shielding with 2 mm thick walls on all six sides of the CubeSat surface while keeping the total weight of the aluminium structure down to 2 kg [28]. It must be noted that this mission planned to stay at the GTO not more than two months prior to parking at the Medium Earth Orbit (MEO)

Meanwhile, the Shields-1 mission is made of several subsystems such as vault electronics (4-6 TRL) from MXL and AstroDev designed to fit the inner CubeSat vault form factor [35]. Furthermore, the OBC logs all data to a dual redundant, secure digital (SD) card systems as one of the single event effect (SEE) mitigation strategies. Additionally, electrostatic discharge cleaned CubeSat solar panels (4-8 TRL) were developed by Vanguard Space Technologies Inc. to provide solar power converter capable of operating in extreme radiation environments. Finally, the communication subsystem for the Shields-1 was realised with a Lithium-1 radio module by AstroDev for a half-duplex transmissions in the ultra-high frequency (UHF) band [35].

The structure of the mDOT A is to be made of aluminium and provided by Pumpkin Supernova or ISIS. The total mass of the structure is estimated to be not more than 12 kg [39]. Nevertheless, it was found that the science payload for this mission would require cooling to -40 and -100 °C, while transitions to eclipse would produce a sudden drop from -53°C to -113°C leading to the strain of 0.013% of an aluminium structure [37]. The mDOT mission team concluded that the thermal control could be realised with a set of measures such as insulation with a low emissivity coating to reduce

temperature swings and internal heating to reduce the risk of electronics and propellants to be frozen during the eclipse period.

Furthermore, the mDOT mission team concluded that the use of magnetorquers for attitude control at the GTO would be of small use as magnetic field was found to be too weak at the altitudes of this orbit due to the large distance from the Earth [47]. Therefore, a propulsion system was proposed for the mDOT A to control momentum caused by the reaction wheels and for alignment with mDOT B during the science phases of the mission. The VACCO MiPS CPOD propulsion with 2U storage tank was selected with the following properties:

- Power = 5 W
- Thrust = 25 mN
- *Isp* = 40 s; specific impulse
- Propellant = R134a cold gas
- Wet mass = 2,5 kg
- ΔV = 31 m/s; change in velocity
- No. of valves = 8

The mDOT mission team compared the mentioned above cold gas thruster from VACCO to an electrospray thruster from Busek and found out that while it had low thrust and high specific impulse, the translation in one axis was only possible with this thruster.

Finally, the last noteworthy point about this mission is the navigation (Table 2.6). The mDOT team found that Global Navigation Satellite System (GNSS) was based in the Medium Earth Orbit (MEO) transmitting signals to the Earth, and thus, it was not possible to directly use it for position knowledge determination in the GTO, GEO or HEO [37]. Nevertheless, it was found that the carrier-phase differential Global Positioning System (GPS) can be applied in the perigee region of the HEO or GTO which can be propagated to the apogee with the uncertainty range of 100 m. The said method was successfully tested on the PRISMA mission [37].

Table 2.6 A comparison of tracking methods applied for position determination in GTO and HEO

Method	Accuracy	Range/FOV	Uncertainty
GNSS	Coarse	Whole orbit	100 m
Star tracker and beacon	Medium	10° x 12°	50 m (36’’/2)
Telescope and beacon	Fine	400’’ x 400’’	0.1 m (0.2’’/2)
Wavefront sensing	Ultra-Fine	20 cm	1 cm

The attitude determination and control system (ADCS) of MarCO CubeSat is fused into an integrated platform made of a star tracker, gyro, coarse sun sensors, and 3-axis reaction wheels [40]. Furthermore, the propulsion system has been added to provide eight thrusters (4 for altitude control, 4 for trajectory correction manoeuvres) operating on R-236FA propellant (cold-gas used in fire extinguishers) adding 40 m/s of delta-V [6]. Noteworthy, thrusters are used not only for trajectory adjustments but to desaturate the reaction wheels also.

The thermal control subsystem on the MarCO CubeSats is made of two discrete radiators, thermal blanket, onboard heaters, and a large number of temperature sensors at different onboard locations [40]. Moreover, there is a dedicated radiator for batteries to protect them against large temperature swings.

While there were eight (8) CubeSat missions planned for launch to the GTO, during reviews done in this paper it was found that only five (5) of them had not changed their orbit and followed their initial plan. Another one was postponed until the further notice. The remaining two (2) missions corrected their plans to include the SSO as their injection orbit.

Some of the missions are not intended for an extended stay at the GTO such as ADE, Orbital Factory II and M-BARC. Some missions do not implement the Attitude Determination and Control System (ADCS) such as Shields-1, ADE and Orbital Factory II. The observed common diversion from the initial plans indicates high risks associated with the GTO environment and lack of environment tested technologies. Nevertheless, each of the reviewed missions has technical solutions that might be useful for the CubeSat mission at the GTO (Table 2.7).

Table 2.7 A list of reviewed missions with an indication of advanced technology solutions and critical lessons to take away

Mission	Advanced technologies	Key takeaways from the review
Dellingr	Thermal control system Deployment mechanism	Resilience is preferred over reliability
Orbital Factory	Radiation shielding chassis	AL6061 is suitable for shielding purposes
Shields-1	Radiation shielding vaults Electrostatic discharged solar panels	Atomic number Z-grade coating is the best for shielding of CubeSats

Mission	Advanced technologies	Key takeaways from the review
MarCO	Communication system Thermal control system ADCS Propulsion system	The CubeSat is capable of performing deep space missions and accommodate communication system capable of performing a DTE communication.
M-BARC	Electric propulsion system Satellite tracking	A CubeSat can change its orbit using the propulsion system with manoeuvres similar to that of larger satellites
mDOT	ADCS Propulsion system Satellite tracking	The CubeSat can be tracked at altitudes above the MEO given corrections to GPS are done at passes in the perigee region of the HEO/GTO.

2.2 Characteristics of the GTO

The geosynchronous transfer orbit (GTO) also known as geostationary transfer orbit is a highly elliptical orbit with its perigee intersecting with the LEO and apogee crossing to geosynchronous earth orbit (GEO) [48]. The properties of the GTO in terms of Keplerian elements are provided in Table 2.8. It must be noted, that parameters for the GTO depend on the launch site (e.g. inclination) and parameters attributed to the launch of the specific rocket [49].

Table 2.8 Properties of the GTO as Keplerian elements [50]

Property	Value
Eccentricity	$e \in [0, 0{,}9]$; Highly elliptical
Perigee (Periapsis)	$hp \in [0, 2000]$ (depends on injection orbit and orbit evolution)
Apogee (Apoapsis)	$ha \in [31570, 40002]$ (depends on injection orbit and orbit evolution)
Inclination	$i < 90°$ (depends on the launch site and injection orbit); most missions are in $i < 10°$ range.
Argument of perigee	180°
Period	≅ 1,.5 hrs

The GTO is characterised by a high level of eccentricity and low degree of inclination. The said characteristics indicate that the CubeSat will be subjected to wide temperature swings [37]. The primary sources of thermal radiation are the Earth and Sun loads (Table 2.9).

Table 2.9 A list of significant heat sources in the space [51]

Sources of heat in space	Power
Solar flux	1367 W/m^2; 1414 W/m^2 at the boreal winter; 1322 W/m^2 at the boreal summer
Earth albedo	~400 W/m^2 (at perigee); ~0 (at apogee)
Earth IR	~200 W/m^2 (at perigee); ~0 (at apogee)
Charged particle heating	n/a

The Earth loads such as infrared radiation and albedo will be useful only at the region near the perigee while Solar loads are the main source of thermal radiation at the apogee. The velocity of the CubeSat will increase at the perigee and decrease at the apogee causing the spacecraft to spend most of its orbital period exposed to the thermal radiation from the Sun [51].

Nevertheless, the period the CubeSat is in the eclipse region depends on the season and can vary from 0 to around 70 minutes. Since the degree of inclination is low for the GTO, the eclipse can occur around the vernal and autumnal equinox also, periods known as “eclipse seasons”. The vernal equinox takes place around the March and April, while the autumn equinox happens around September and October [51]. Another factor which might contribute to the increase in the period of the eclipse is the Moon; nevertheless, the probability of this happening is low.

2.2.1 The Van Allen radiation belts

The GTO is characterised by the presence of the radiation belts located in the inner region of the Earth’s magnetosphere and made of high-energy particles originating from solar wind and cosmic rays formed as a part of a universe space-weather system [52]. These radiation belts are known as Van Allen radiation belts in respect to its discoverer in 1958, James Van Allen [53].

The behaviour of particles in the radiation belts can be described as gyrating and bouncing [54]. These particles are trapped to two concentric rings in the magnetosphere of the Earth to prevent them from entering the atmosphere of the Earth. Nevertheless, these particles swell and shrink, and from time to time manage to enter the atmosphere [7].

The negative impact of the ionising radiation with the mentioned above particles is visible in the disruption of satellites and GPS communication and risks for health and safety of astronauts at the

LEO [55]. Therefore, further scientific research is required to be taken regarding the Van Allen radiation belts as this region of the Earth magnetosphere is not well studied [33].

2.2.2 Current application of GTO

The name of this orbit suggests that its primary application is to provide energy efficient transfer of spacecraft to the GEO [7]. Therefore, most of communication and broadcast satellites are sent to the GEO via the GTO. Even though it consumes less energy to transfer a spacecraft from the GTO to GEO than direct insertion into the desired orbit, it takes more time to accomplish the transfer [49]. The long exposure to radiation is required to be minimised as it reduces a lifetime of an onboard electronics of a spacecraft. The mentioned above challenges with radiation make this orbit unsuitable for long period missions. The shortened lifetime of the mission makes utilisation of this orbit non-feasible or too expensive for spacecraft more massive than the size of microsatellites [7].

2.3 Technology availability for GTO

Attitude Determination and Control System for FORESAIL-2 requires attitude knowledge of 0.6 degrees of phase angle at minimum for determination and spin stabilisation with either active or passive method [3]. The list in Table 2.10 shows the current state-of-the-art in ADCS technologies.

Table 2.10 A list of technologies for ADCS available for CubeSats [56], [57], [58]

Type	Highest TRL	Performance	COTS availability (# of models)	Highest radiation tolerance (krad)
Integrated Units	9	0.002° pointing capability	> 8	N/A
Attitude Control				
Reaction wheels	9	0.001 – 0.3 Nm peak torque, 0.015 – 8 Nms storage	> 10	N/A
Magnetorquers	9	0.1 Nm peak torque, 1.5 Nms storage	> 6	5
Thrusters	9	>1100 mN >3000 s	>20	N/A
Attitude Determination				
Star Trackers	9	25 arcsec pointing knowledge	> 5	75 (Other: 11)
Magnetometers	9	Resolution: 10 nT	> 5	10

Type	Highest TRL	Performance	COTS availability (# of models)	Highest radiation tolerance (krad)
		Orthogonality: < 1°		
Sun Sensors	9	0.1° accuracy	> 8	1100 (Other: 20, 10)
Earth Sensors	9	0.25° accuracy	> 2	n/a
Gyros	9	1° h-1 bias stability, 0.1° h-1/2 random walk	> 3	10 (5)
Navigation				
GPS	9	1.5 m accuracy	> 4	10
Deep Space Navigation	9	X, Ka, S, UHF	IRIS V2 (Only 1 model)	n/a

The magnetorquers are not enough to perform manoeuvres required by FORESAIL-2 in the GTO (Table 2.11) as the more substantial portion of the orbit lays in the regions where the magnetic field of the Earth is weak. Nevertheless, the portion of the orbit at the perigee and nearby it has a strong influence of the magnetic field and as such the use of magnetorquers would be possible in the areas close to the perigee.

Table 2.11 Applicability of ADCS components for GTO environment

Reaction wheels	Fully applicable	Unlike the similar systems at the LEO, needs a combination of a propulsion system with magnetorquers
Magnetorquers	Conditionally applicable	Only at the region near to the perigee
Thrusters	Fully applicable	Any thrusters can be used at the GTO
Star trackers	Conditionally applicable	There might be blackout periods. Furthermore, start trackers are susceptible to radiation from high energy protons.
Magnetometers (for attitude knowledge)	Conditionally applicable	Because the magnetic field of the Earth goes down with the cube of the distance, and thus for most of the orbit the field strength is weak. Besides, the magnetometer is highly sensitive to onboard generated noises.
Sun sensors	Fully applicable	Except for the eclipse region
Earth sensors	Conditionally applicable	Only at the perigee and the region within its proximity
Gyros	Fully applicable	Only attitude and spin rate determination

GPS	Conditionally applicable	Most of the orbit lay above the altitudes of the GPS satellites, and thus, no GPS signal would be available for most of the time for GNSS
Deep Space Navigation	Not applicable	The GTO is not considered to be deep space, and thus, no navigation of this kind is required for the mission to this orbit.

Meanwhile the use of thrusters for attitude control in the GTO is suitable and recommended. While a star tracker is an accurate tool for attitude determination, the presence of high energy protons in this environment may lead to the creation of false stars [57]. Moreover, the magnetic field was found by several researchers to be weak for most of the period of highly elliptical orbits making the use of magnetometers inefficient for attitude determination [37].

Currently, available sun sensors produce a full 2-axis estimate of Sun location [59] and are suitable for use in the GTO. Meanwhile, there are two types of gyros used in CubeSats, fibre optic gyros (FOG) and MEMS gyros. While the FOG offers better performance, it downgrades mass and cost factors [59]. The use of gyroscope is not only suitable for use at the GTO but essential to fulfilling science observation goals.

Thermal control system (TCS). The typical range of operating temperatures for the CubeSat onboard subsystems (Table 2.12) indicates the batteries to be the most sensitive in large temperature swings in the environment, and thus, might require a dedicated thermal control solution [6].

Table 2.12 A typical range of operating temperatures for different components onboard of a typical spacecraft [60]

Component	$T_{min, OP}$ / ℃	$T_{max, OP}$ / ℃	Survival range ℃
Batteries	0	15	-10 to 25
Reaction Wheels	-10	40	-20 to 50
Solar Panels	-150	110	-200 to 130
Gyros/IMUs	0	40	-10 to 50
Star Trackers	0	30	-10 to 40
Antennas	-100	100	-120 to 120
C&DH Box Baseplates	-20	60	-40 to 75
EPS Box Baseplates	-10	50	-20 to 60

On the other hand, while most of the thermal control technology achieved TRL of 9 or 8, the availability of these technologies is limited (Table 2.13). Furthermore, thermal control technology is being miniaturised for CubeSats and still require tests in the space environment. The latest tests in the space environment for thermal control systems were conducted for storage units and thermal louvres [61].

Table 2.13 A list of technology solutions applied for the thermal protection of a CubeSat [57][57], [62][61]

Technology	TRL	Availability
Passive Systems		
MLI Blanket	9	MODERATE (>5)
Thermal coating and tapes	9	MODERATE (>4)
Sun Shields	7	LOW (1)
Metal Thermal Straps	9	MODERATE (>4)
Composite Thermal Straps	7	MODERATE (>4)
Passive Thermal Louvers	9	LOW (1)
Deployable Radiators	6	LOW (2)
Passive Heat Pipes	6	LOW (2)
Thin Plate Heat Switch	n/a	n/a
Storage Units	8	LOW (2)
Active Systems		
Flexible and Enhanced Active Thermal Straps (FEATS)	6	LOW (1)
Electrical Heaters	9	LOW (2)
Mini Cryocoolers	6	MODERATE (6)
Kapton heater	n/a	n/a
Emerging systems		
Fluid Loops	3	LOW
Deployable Passive Radiators	4/5	LOW

Thermal insulation and coating. The insulation limits heat transfer between the CubeSat and environment, and thus, protects from wide temperature swings. While the multilayer insulation blanket (MLI) is efficiently used on large spacecraft, there are several limitations when it is scaled to the standard size of the CubeSat such as [61]:

- drops efficiency if gets compressed;
- drops efficiency if its size been decreased.
- efficiency depends on the way it is attached to the body of the CubeSat.

Thus, MLI is not a preferred option for the CubeSat mission to the GTO. It was found that low emissivity coatings perform better for exterior and interior application on the surface of CubeSat than MLI [51][51], [63]. On the other hand, silvered tapes proved to be efficient and more reliable than paint for the thermal control but were found to not bond well with curved surfaces.

Another method for passive temperature control, matte paint, defines its optical characteristics according to chosen colours [51]. For instance, the black paint has high absorbance to emittance ratio while white colour produces different results. Since the CubeSat at the GTO is exposed to the solar radiation for most of its orbit period, the white paint would be preferred on the side pointed to the Sun, while black paint could be applied to the interior surface to maintain thermal balance within the CubeSat.

Nevertheless, the MLI blanket should not be dismissed as an option for thermal control as there are developments and tests done by several companies for CubeSats. For instance, Dunmore Aerospace Corporation produces four (4) models of MLI blankets for CubeSats with the TRL of 6, and MLI tapes for insulation of cables with the TRL of 7 [61].

Thermal louvres proved to be efficient onboard of the large spacecraft, but its implementation for CubeSats was found to be challenging to weight and power constraints. Nevertheless, the Goddard Space Flight Centre of NASA successfully demonstrated its technology onboard of Dellingr 6U CubeSat increasing its TRL to 9. The maximum power dissipation for CubeSat achieved with this technology was 14 W [64].

The electrical resistance heaters proved to efficient for maintaining temperature balance of batteries on CubeSats such as Compass-1, MASAT-1 and OUTFI-1 [61]. The heaters might be required for the CubeSat missions at the GTO since large temperature swings are expected during transitions to and from eclipse. Furthermore, NASA Ames used this type of heaters on a number of its nanosatellite missions to maintain temperature balance for biological payloads. The current TRL of this technology is 9, and its history of use in CubeSats makes it suitable for the CubeSat mission to the GTO [61].

Protection from ionizing radiation. The GTO is characterized by a high density of high energy charged particles of proton and electron in the Van Allen belts region. The radiation caused by particles hitting the electronics components and printed circuit boards (PCB) can lead to the damage of electronics, and thus, fail the mission or shorten its lifetime [46]. Other characteristics of radiation environment related to the operation of electronics are single event upset (SEU) [65] and single event latch-up (SEL) (Table 2.14).

Table 2.14 A list of causes and effects of the SEE on electronics [52]

Cause	Effect	Severity
Single event upsets (SEU)	Disturbance on the logic state of the memory	Non-destructive
Single event transients (SET)		
Multiple Bit Upsets (MBU)		
A single-event hard error (SHE)		
Single event latch-up (SEL)	Disturbance on the output transistors and on CMOS logic leading to the high-current state	Destructive
Single event gate rupture (SEGR)		
Single event burnout (SEB)		

Meanwhile, Table 2.15 shows high availability of different hardware and software technologies for protection from ionizing radiation.

Table 2.15 A list of technology solutions for radiation mitigation strategies [66], [67]

Technology	Radiation tolerance	Availability
Inherent Mass Shielding	Depends on shielding thickness and materials	HIGH
Ad Hoc Shielding	Depends on shielding thickness and materials	HIGH
Protection Circuits	n/a	HIGH
Memory Protection	n/a	HIGH
Communication Protection	n/a	HIGH
Parallel Processing and Voting	n/a	HIGH

Proton upset rate has a small dependence on shielding depth [52]. Thus, software algorithms and hardware circuits should be implemented in the CubeSat at the GTO to provide adequate protection from SEUs.

Communication system. The most common frequency band for CubeSats communication is the UHF as the process of acquiring the amateur licence is more comfortable, faster and cheaper than for other bands [68]. Thus, there is the most significant number of UHF transceivers and antennas with TRL of 9 available on the market for CubeSats (Table 2.16).

Table 2.16 A list of communication bands available for use on the CubeSat [69]

Technology	Bandwidth	EMI	Highest TRL	Availability (models)
VHF/ UHF	30-300 MHz 300 MHz - 3 GHz	HIGH	9	> 18
L-band	1-2 GHz	MODERATE	9	> 6
S-band	2-4 GHz	LOW	9	>16
X-band	8-12 GHz	LOW	9	>12
Lasercom	100-800 THz	LOW	6-7	<3

UHF is the most popular frequency band not only for communication but RFIDs and other ground-based devices, and thus, presents a high risk of electromagnetic interference for CubeSat communication [70].

The UHF band has the highest number of antennas and communication modules available as COTS components for the CubeSat. Furthermore, around 30% of available communication components operating in the UHF band and developed for the CubeSat have reached TRL of 9 [69]. Noteworthy, most of the UHF band antennas designed for CubeSats do not require pointing to the Earth and can be used in an omnidirectional mode. The highest nominal downlink rate for the UHF is 500 kbps for most of the CubeSats, while the real downlink rate can be as low as 8 kbps.

S-band is congested with space operations and research missions, military links, NASA communications for the ISS and Space Shuttle, and others [71]. There are more than 11 models of S-band communication modules with antennas available for CubeSats [69].

The advantage of using this band at the GTO is the availability of lightweight (80 or 20 gr for patch only) omnidirectional antennas and higher than UHF downlink rate such as around 1Gbps.

Therefore, the use of S-band will reduce risks of communication session and packet losses during the passes by the CubeSat.

X-band. The most famous one is IRIS V2 by the JPL that is currently used onboard of MarCO CubeSat mission to the Mars [41]. Meanwhile, Utah State University develops an X-band antenna integrated into solar panels that have the potential to reduce space consumption on the CubeSat. The main advantage of this band is the high symbol rate which is around 312,5 Msps and 8,3 Msps for different modulation modes [57].

Propulsion systems for satellites are considered to be mature technologies when micro and larger sizes are taken into account [72]. Nevertheless, the current trend is miniaturization of propulsion systems used in more massive than CubeSat size satellites and testing in the Space environment as a part of technology demonstration [73]–[77]. Thus, the TRLs for most of the propulsion systems available for the CubeSat is less than 8 (Table 2.17).

Table 2.17 A list of technology solutions for the propulsion system of the CubeSat [78]

Technology	Propellant	Specific Impulse (s)	Thrust (mN)	TRL
Cold and Warm Gas Propulsion (CGP) system	Liquid Butane SF6 Argon Methane R134A	43 <35 43 50-75 40	50 10-40 1 1 25	9 (Butane)
Liquid Propulsion (LP) system	AF-M315E Hydrazine ADN LMP-103S Liquid water	214-240 215 231-232 256	1,5 - 1100 260 1000 250-600	6
Solid Rocket Propulsion system (SRP)	Al and Ammonium perchlorate HIPEP-501A AP/HTPB	269,4 245-269 226	37 13 76	7
Resistojets	Xe SO_2 R134a, R236fa Water	48 @ 30 W 65 @ 15 W 82-150 @ 15-30 W 79,2	18 5,4 10 - 30 0,129	8 (Xenon)
Radio Frequency (RF) Ion Thruster (RIT)	Xe, Iodine Iodine	2150-3200@28 W 2500@75 W	0,1-0,18 1,15	8 (Xenon) 4 (Iodine)

Technology	Propellant	Specific Impulse (s)	Thrust (mN)	TRL
	Xe	300-3200@50-145 W	0,05-25	
Hall Effect Propulsion	Xe, I, Kr Xe, Kr Xe, Ar Xe	1390-1530@200-600 W 1100@100 W 1139@200 W 1750@100 W	12,8-39,1 10 1-10 50	8 (Xenon) 4 (Iodine)
Electrospray	Ionic liquid	800-1800@1,5-30W	0,005 – 1,5	6
Pulsed Plasma and Vacuum Arc Thruster	Teflon PTFE Nickel Aluminium Titanium, Tungsten	536-1150@7,5-12.5W 578-830@2-10 W 3000@10 W @4 W 900-1100 @0,5-2 W	0,14 0,144 0,001-0,02 0,054 0,002-0,01	8 (PTFE) 7 (Titanium only)

The lowest impulse is produced by Cold Gas propulsion systems and the largest one comes from Ion based electric propulsion systems [78]. Meanwhile, the highest thrust is generated by solid rockets. All the options below 10 mN of thrust and 300 s of specific impulse are suitable for the FORESAIL-2 mission to the GTO as based on estimations in following sections these values are the threshold ones. Thus, the most suitable types of propulsion systems are Cold Gas, Resistojets, and Liquid.

2.4 Launch services

The orbit parameters for simulations were defined concerning launching sites and rocket specifications. Furthermore, research on current science satellite missions to the GTO was done to define launch history and orbit corrections. Meanwhile, since there were no dedicated launchers for CubeSats to the GTO, the parameters for the projected orbit were taken from the existing launchers of microsatellites (Table 2.18).

Table 2.18 A list of launch sites and respective rockets with a track of launches and capabilities to reach the GTO

Launch site	Rocket (for GTO)	Country
Xichang Satellite Launch Centre[79]	Long March 3D	China

Launch site	Rocket (for GTO)	Country
Uchinoura Space Centre[80]	Epsilon	Japan
Florida Launch Site [81]	Falcon 9	USA
Cape Canaveral [81]	Atlas 5, Delta 2, Falcon 9 (SpaceX has an agreement with NASA), Electron (RocketLab has an agreement with NASA, but all of its future ride-share launches are planned for SSO up to 2024)	USA
Guiana Space Centre [82]	Ariane 5 ECA, Soyuz	France
Satish Dhawan Space Centre [5]	GSLV II	India

Furthermore, all satellites sent to the GTO corrected their orbit from the initial one to increase their perigee up to 600 km such as in the case of Van Allen Probes (Table 2.19).

Table 2.19 A list of current science missions to the GTO with respective orbit parameters

Current satellites at GTO	Date of Launch	Inclinations *i*°	Eccentricity	Perigee / km	Apogee / km	Period / hr	Launch site	Rocket
ARASE.ERG [9]	20.12.2016	31	0,706	460	33200	9.6	USC	Epsilon
SPIRALE-A [83]	11.2.2009	2	0,702	240	31342	9.1	GSC	Arian 5
Van Allen Probe A [84]	30.8.2012	10	0,683	591	30534	8.98	CC	Atlas 5
Van Allen Probe B [84]	30.8.2012	10	0,683	596	30657	9.02	CC	Atlas 5

There was found to be a high probability of the rocket for the FORESAIL-2 mission to be the Atlas V (Table 2.20) since future CubeSat launches to the GTO would be all using this rocket [85]. The launch site was expected to be the Cape Canaveral Air Force Base due to its close location (Latitude of 27 degrees North) to the equator line which made this site suitable for injections to low inclination orbits. Other options such as Epsilon and Arian 5 were not found to be used for the launches of CubeSats to the GTO [85].

Table 2.20 A list of rockets designed for launches to the GTO with parameters of orbit for the second stage

Rocket	Inclination / °	Perigee / km	Apogee / km	The argument of perigee / °
Atlas V [81]	27	185	35786	180
Falcon 9 [81]	27	185	35786	180
Ariane 5 [82]	6	250	35950	178
Soyuz [82]	6	250	35950	178
GSLV II [86]	20.61	170	35975	180

The first option selected for the feasibility analysis was the most probable candidate [85] for launching FORESAIL-2 to the GTO, Atlas V or Falcon 9 both launched from Cape Canaveral US Air Force Base (Table 2.21).

Table 2.21 A list of essential parameters for the simulated launch of the FORESAIL-2

Parameters	Value
Start date	01.12.2021
End date	01.12.2023
Launch site	Cape Canaveral US Air Force Base
Rocket	Atlas V/ Falcon 9
Launch provider	ULA

2.5 Summary

There have been no nanosatellite missions to the GTO, and only five (5) missions declared plans for future launches to this orbit. Furthermore, there are only two (2) future missions aiming to stay on orbit for an extended period and produce science measurements. Meanwhile, all other manifested missions are planned for a period not exceeding three (3) months and set as their primary purpose to do technology demonstration. Moreover, there are only four (4) satellites in total placed to the GTO orbit with only three (3) of them producing in-situ measurements in Van Allen belts.

The said above suggests that GTO remains mostly unexplored and requires a more significant number of in-situ science measurements. Furthermore, a low number of missions to the GTO and

absence of such among nanosatellites indicates that there are no tested in this environment space technology available for CubeSats.

The study of GTO characteristics indicates that this is a highly elliptical orbit with a high-radiation environment. The high-radiation environment is found to be formed by a large number of high-energy electrons and protons trapped in radiation belts known as Van Allen belts. This radiation environment was found to be a cause of fast degradation of electronics and malfunctioning of systems onboard of spacecraft, and negative impacts on the health of astronauts working at LEO.

Finally, the most probable launch site and rockets to the GTO were identified as Cape Canaveral US Air Force Base and Atlas V and Falcon 9, respectively.

3 RESEARCH OBJECTIVES AND METHODOLOGY

3.1 Problem statement

The literature review in the previous chapter highlighted the issue with a lack of missions to the GTO and, specifically, those producing in-situ measurements for science. Currently, there are only three (3) science missions at the GTO producing direct sensing observations such as Van Allen Probes A and B (NASA), and ARASE.ERG (JAXA). The mentioned satellites are more significant than those of nanosatellite class. The lack of these measurements produces an incomplete understanding of dynamic processes underlying the formation of radiation belts. It is vital to have direct sensing observations at the GTO to characterise the radiation environment and develop technical solutions to mitigate high radiation doses.

Furthermore, it was found that missions of minisatellite size and larger would have had higher risks at the GTO than nanosatellites. The reason for that was in a dramatically lower cost of production and launch for nanosatellites. Therefore, proving the feasibility of nanosatellite mission in harsh environment such as at the GTO is another motivation for this research.

The current research aims to verify that the proposed science and technology goals for FORESAIL-2 [3] are feasible to achieve in a CubeSat form factor of nanosatellite class of spacecraft. If the analysis shows that the mission is feasible, different engineering solutions will be compared in trade space analysis. The questions investigated within the scope of this research are summarised in Table 3.1.

Table 3.1 A list of leading questions to be answered in the course of this research

Category	Research questions
Mission development	What would be the orbital lifetime? Will a CubeSat maintain the orbit for the minimum of mission lifetime? Do orbital parameters change within the range sufficient to fulfil science and technology goals?
Radiation in space	What is the total ionising dose (TID) for the mission lifetime? Are there components able to tolerate the TID for the mission lifetime? Is an increase in the mass of CubeSat due to the required shielding thickness within an acceptable range?
Geomagnetic field conjugation with local field in spacecraft	Is magnetic intensity strong enough to make efficient use of magnetorquers for desaturation of reaction wheels and spinning spacecraft to release the tether?

Category	Research questions
Communication links	Is the duration of the line-of-sight between a CubeSat and ground control station (GCS) long enough to facilitate downlink of science and systems health data?
Power supply	Is eclipse period short enough to maintain a CubeSat operational with onboard batteries? Will the power generated for the basic CubeSat configuration be enough to maintain all subsystems functional?
Spacecraft System Design	What components can be selected preliminarily for each subsystem of a CubeSat? What is the minimum volume and mass to accommodate all payloads and subsystems?
Technical risk assessment	What are the risks? What are the areas of significant concern?
Technical margins	What are the high-risk areas that need significant margin?
CML3: Trade space analysis Launch services	What are the differences to mission goals if a CubeSat launched from other launch sites and rocket types? Different scenarios for orbital parameters.
CML3: Trade space analysis Science observation scenarios	How different orbital and design parameters will affect science observations?
CML3: Trade space analysis Spacecraft system design	Different payload and spacecraft configurations (e.g. 3U vs 6U). What are the strengths, weaknesses, opportunities, and risks?

3.2 Methodology

A design of mission to the GTO will produce a higher number of challenges than a mission to the LEO due to the presence of a harsher environment. Therefore, while nanosatellite mission to LEO could be built solely with a NewSpace approach similar to the agile software development, nanosatellite mission design for GTO would require a more rigorous approach similar to the one implemented at the space agencies such as NASA and ESA. This research will combine some elements of NewSpace approach with the framework developed by JPL of NASA known as Concept Maturity Levels (CML). This framework allows drawing a relationship between stages of concept development in Pre-phase A of mission development [15].

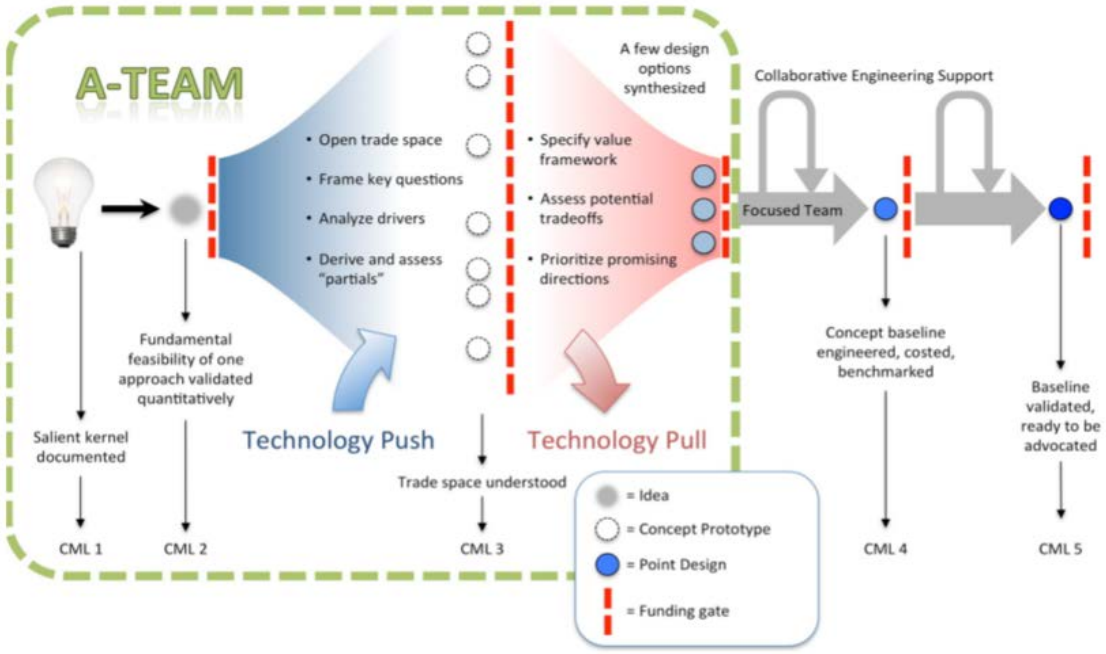

Figure 3.1 Concept Maturity Levels (CML) framework developed and applied at NASA. The illustration shows only the first five levels of the CML. [87]

The current research will provide assistance to the FORESAIL consortium on maturing concept of the FORESAIL-2 mission from level 1 to 3, and partially to 4 of CML framework (Figure 3.1) where the first is derivation of requirements, the second is a study on initial feasibility, the third is a study of trade space, and the fourth is a specification of selected design. Noteworthy, CML framework requires a development from CML 2 to CML 4 to be iterative [15]. Therefore, the scope of this research is instead not to answer all questions for every CML but to produce the first iteration of concept studies.

The CML 1 requires close collaboration between scientists and engineers, and thus, several intensive sessions will be conducted as a part of this research. The expected results from these sessions will be a Science Traceability Matrix (STM), Science Return Diagram (SRD), and Mission Traceability Matrix (MTM).

The research within the framework mentioned above will constitute quantitative, qualitative, and action methods. The former one will include single-subject, correlational and causal-comparative, analytical, and numerical approaches. The later one will include historical and content analysis approaches. The action method will be represented by collaboration with scientists and engineers of FORESAIL-2 project.

The computations in this research will be done with the help of Systems Tool Kit by AGI [88] serving as an accurate orbit propagator. MATLAB [89] will be used in conjunction with the STK to produce additional computation and graphic plots. Furthermore, SPENVIS by ESA [90] will be used to estimate radiation doses at the GTO with different shielding thickness values. Google and Excel spreadsheets will be used to summarise parameters of different spacecraft systems for the link, power, and mass budgets.

4 CONCEPT STUDIES

4.1 CML1: Science

4.1.1 Science Traceability Matrix (STM)

The science traceability matrix (STM) is the first step in mission concept development as it draws a relationship between mission goal, science goals, and mission requirements for the spacecraft [91]. The STM was developed based on science requirements provided by the consortium science team [3]. The STM is available in a table format in Appendix 1 [3].

4.1.2 Science Return Diagram (SRD)

The Science Return Diagram (SRD) allows setting baseline and threshold science goals that will have an impact on mission requirements (Figure 4.1). The SRD will define the sophistication of science instruments in terms of spatial and temporal resolutions within the science bin. The red line is an opportunity cost cap while the green dashed line is the desired threshold science. While green line sets the border between enhancing and enabling levels, the red line indicates that an increase in budget would be required to accommodate science breakthrough level.

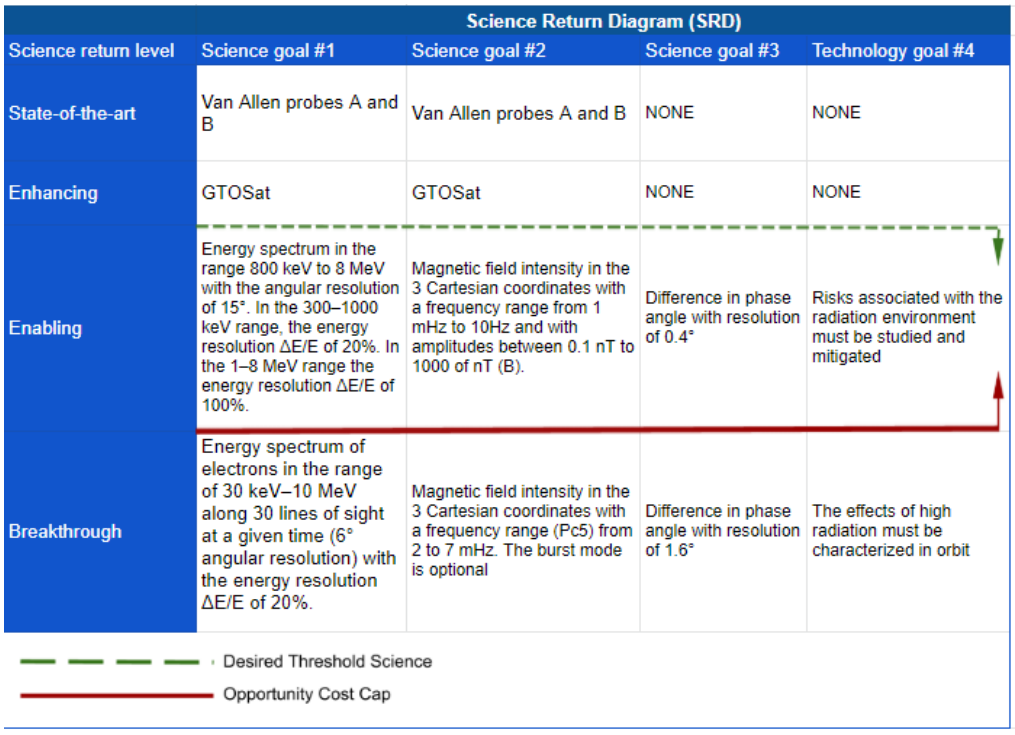

Figure 4.1 Science Return Diagram (SRD) for FORESAIL-2 science goals. The red and green lines encompass sector with a scope of science observations fitting the budget constraints [3].

4.1.3 Mission Traceability Matrix (MTM)

A Mission Traceability Matrix (MTM) was developed based on results of STM as it drew requirements for mission design, spacecraft, ground system, and operations, based on mission requirements set for each science objective. MTM was developed concerning each instrument, and all requirements for the mission were summarised in one row (Table 4.1). Meanwhile, a full MTM is available in Appendix 2 [3].

Table 4.1 Mission Traceability Matrix with requirements derived for mission, spacecraft, ground system, and operations (Appendix 2) [3]

Mission Reqs	Mission Design Reqs	CubeSat Reqs	Ground System Reqs	Operations Reqs
From 01 Science Traceability Matrix [3]	**Launch date:** Launch during forecasted high solar and geomagnetic activities is preferred **Mission length:** Minimum 6 months (> 400 orbits) **Orbit altitude requirement:** Minimum orbit altitude 180 km to ensure minimum mission length Maximum orbit altitude has to be more than 12756 km (> 2 Earth radii) **Geographic coverage:** Daily passes over the region within the latitude of 30 degrees North and South to provide downlink capabilities for science data **Orbit local time:** Wide coverage of Magnetic Local Time (MLT) to meet the science requirement of temporal sampling **Type of orbit:** Highly Elliptical (e > 0,7) Equatorial with i < 45° **Other:** Orbit has to cross Van Allen radiation belts to satisfy science requirement for the high-radiation environment	**Stabilisation:** Spin stabilised with spin axis perpendicular to the magnetic field vector **Mass for payload:** <1530 g (around 1,5 kg) **Power for payload:** >7 W (Highest simultaneous power demand from instruments) **Volume for payload:** 1652,75 cm^3 (around 1.6U) (Sum of volumes of all instruments) Data Rate: 411 bit/s (all instruments producing measurements simultaneously) Temperature Range for operation: - 40°C to 85 °C (smallest range from all instruments) **Attitude knowledge:** > 0,4° (highest accuracy requirement) Position knowledge: 100 - 1000 km **Radiation shielding requirement:** > 10 krad to decrease the rate of degradation of	**Passes per day and duration:** Minimum 1 passes per day with an average 60 minutes **Assumed antenna size:** high-gain (>15 dB) Yagi antenna or 3-meter parabolic antenna **Data volume per day:** 4,44 Mbytes/day (Data storage)	General spacecraft manoeuvre requirements and frequency: De-tumble following orbit insertion to spin rate =< 36°/s. 1 time Spin up spacecraft <180 deg/s. 1 time Deploy tether. 1 time Stabilise spin axis pointed towards the magnetic field vector. 1 time Point solar panels towards the sun. 1 time per orbit Special manoeuvres requirements: None **The rationale for manoeuvres:** Lower spin rate increases sampling rate and allows to scan more extensive areas of the plasmasphere More significant spin rate produces required angular momentum (~20 Nms) and centrifugal force (~0,4 cN) to deploy tether. Pointing solar panels towards the sun ensures that electric power is available for science experiments **Ephemeris requirements:** Position

Mission Reqs	Mission Design Reqs	CubeSat Reqs	Ground System Reqs	Operations Reqs
		electronic components **Other:** Fit within nanosatellite class of spacecraft (1-10 kg)		knowledge of spacecraft within 100 - 1000 km range Changes in viewing modes New view mode per second to cover larger areas of the plasmasphere

Apart from technical requirements, there are non-functional ones such as the cost of the mission. The review of missions in the previous section identified that GTOSat by NASA had the highest cost of mission design and launch equalling to 3,825 million Euro [7].

4.2 CML 2: Feasibility analysis

4.2.1 Mission development

The mission development section will produce a gross characterization of the orbit. Since the requirement is to have HEO, availability of launchers to HEO such as GTO suggests that this orbit should be modelled and analysed (Figure 4.2).

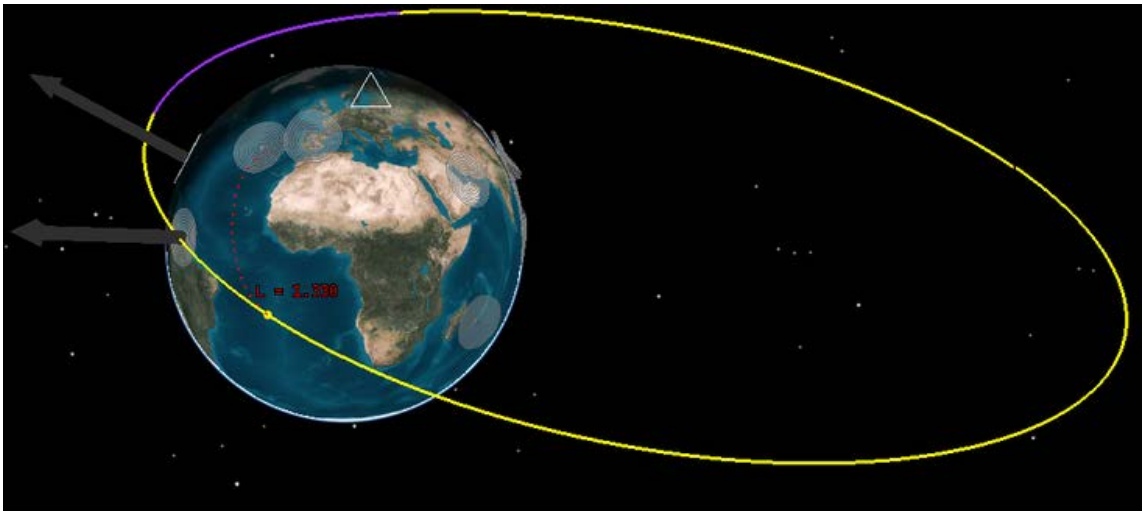

Figure 4.2 An illustration of the modelled orbit with the FORESAIL-2 CubeSat

The orbital propagation and calculation of related to it aspects such velocity of spacecraft, total ionizing dose, thermal balance, communication links, and geomagnetic field intensity, are done with Runge-Kutta-Fehlberg numerical integration methods of the 7th order in the J2000 reference

frame [92] and with constant provided in the Table 4.2. Furthermore, STK was integrated with MATLAB to combine computational tools of both research instruments (Appendix 3).

Table 4.2 Constants employed for numerical analysis in STK

Constant		Value	Units
μ_E	Gravitational Constant of Earth	STK gravity file	m^3/sec^2
R_E	Equatorial Radius of Earth	STK gravity file	m
f_E	Flattening Coefficient of Earth	0,00335281	(dimensionless)
c	Speed of Light	299792,458	km/sec
L_S	Luminosity of Sun	3,823e26	W

The orbit evolution is numerically evaluated with a set of equations (4.1) for acceleration due to drag and solar radiation [93].

Acceleration due to drag is as follows:

$$A_D = (C_D)\left(\frac{A_D}{M}\right)\left(\frac{\rho V^2}{2}\right), \quad (4.1)$$

Acceleration due to solar radiation is as follows:

$$A_R = (K)(C_R)\left(\frac{A_D}{M}\right)\left(\frac{L_S}{4\pi c r^2}\right),$$

where

C_R - coefficient for solar radiation = 1 + η, dimensionless,

where η - the surface reflectivity

C_D - the coefficient for drag, dimensionless,

A_D – spacecraft cross-sectional area along velocity vector, m^2,

A_R – spacecraft cross-sectional area facing the Sun, m^2,

M – spacecraft mass, kg,

ρ - atmosphere density, kg/m^3,

V – spacecraft speed relative to the atmosphere, m/s,

K - a fraction of the solar disk visible at spacecraft location, %,

L_S - the luminosity of the Sun, W,

c - speed of light, km/sec (constant),

r - a distance of the satellite from Sun, m.

The parameters set for orbit propagation are in Table 4.3.

Table 4.3 Initial parameters for the propagation of the orbit of the FORESAIL-2 3U CubeSat

Parameter	Value	Comments
Propagation model	HPOP	This model has been chosen for advanced perturbation modelling. To ensure high accuracy 7th order Runge-Kutta-Fehlberg equations were used for integration and Lagrange interpolation method was used to find missing values.
Orbit Epoch	1 Dec 2021 00:30:00 UTCG	
Start	1 Dec 2021 00:00:00 UTCG	It was assumed that the earliest launch would take place on this date.
End	1 Dec 2023 00:00:00 UTCG	It was assumed that the maximum duration of the mission would be 2 years
Step size	60 seconds	The data points were set to be collected every minute
Apogee	35786 km (Atlas V, Falcon 9)	The furthest point from the Earth as specified in Atlas V specifications for injection orbit
Perigee	185 km (Atlas V, Falcon 9)	The closest to the Earth point as specified in Atlas V specifications for injection orbit
Orbit period	10,5129 hr	The estimated orbit period
Eccentricity	0,73 (Atlas V, Falcon 9)	The orbit was set to be highly elliptical
Semi-major axis	24363,6 km (Atlas V, Falcon 9)	
Inclination	27° (Atlas V, Falcon 9)	This was the lowest possible inclination as Cape Canaveral Air Force Base was located at 27 degrees of North latitude
Argument of Perigee	180° (Atlas V, Falcon 9)	With these values, the ascending node is at the same place as the apogee
RAAN	7,5 deg	Assuming launch took place at 00:30 from Cape Canaveral

The parameters for the CubeSat are defined in Table 4.4.

Table 4.4 Scenario parameters for a 3U FORESAIL-2 CubeSat

Parameters	Value
Mass	5 kg
Drag area	0,01 m^2
The area exposed to Sun	0,09 m^2
Area to mass ratio (exposed to atmospheric drag)	0,002 m^2/kg
Area to mass ratio (exposed to central body radiation pressure)	0,018 m^2/kg (including deployed solar panels)
Cross-sectional area	0,03m^2 (deployment of solar panels was neglected)
Size	3U
Attitude	4 rev/min about the Sun vector
Other	Solar panels deployed on minus and plus Y sides

The calculations of drag force [93] and solar radiation pressure [94] in the STK was done with equations 4.2 and 4.3 respectively .

$$\overline{F_D} = \frac{1}{2} C_D \frac{A}{m} \rho |\bar{V}| \bar{V} , \quad (4.2)$$

where

$\overline{F_D}$ – the drag force, N,

$\bar{V}$ – the velocity of the satellite relative to the atmosphere, m/s,

Cd – drag coefficient, dimensionless,

A - drag area, m^2,

m – a mass of spacecraft, kg.

$$\overrightarrow{f_{solar}} = m\gamma L_S C_r r_{sun}^2 \frac{A}{m} \frac{\vec{r} - r_{sun}^2}{|\vec{r} - r_{sun}^2|^3} , \quad (4.3)$$

where

$\overrightarrow{f_{solar}}$ – solar radiation pressure, N,

m – mass of spacecraft, kg,

γ – shadow factor, 1 – sun, 0 – shadow, 0 < γ < 1 – penumbra phase,

C_r – surface reflectivity, 1 < C_r < 2, dimensionless,

A – cross-section area of spacecraft, m^2

r_{sun} – geocentric distance of the sun, m,

$r\ and\ r_{sun}$ – geocentric vectors of the spacecraft and sun, m,

L_s – luminosity of the sun, W.

$P_s = \frac{E}{c}$,
where

E – solar constant, 1358 W/m^2,

c – speed of light in the vacuum (constant), km/sec.

The parameters set for perturbation forces are listed in Table 4.5.

Table 4.5 Parameters for modelling perturbation forces [92] [129]

Force	Parameter	Value
Central Body Gravity	Gravity model	EGM2008
	Maximum degree	21
	Maximum order	21
	Solid tides	Full tide Truncate to Gravity Field Size Ocean tides: max deg. 4; max order 4; Min: 0m
	Third Body Gravity	Sun: 4,7e+14 km^3/min^2 Moon: 1,76e+07 km^3/min^2
Drag	Model	Type: Spherical Cd: 2,2
	Atmospheric Density	DTM2012
	Low Altitude Density Model	NRLMSISE 2000 Blending range: 30 km
	SolarFlux/GeoMag (Based on Ottawa Observatory values)	Daily F10.7: 150 Average F10.7: 150 Geomagnetic Index (Kp): 3 Approximate Altitude Apparent Sun Position
Central Body Radiation Pressure	General	Albedo Thermal Relativistic Accelerations

Force	Parameter	Value
	Ck	1
	Ground Reflection Model	SimpleReflectionModel.txt (provided by AGI Inc.)

The lifetime of the satellite on orbit. The evaluation of orbital lifetime is required to determine that the CubeSat will not decay prematurely and will decay within 25 years limits to satisfy requirements for mitigation of debris. The aforesaid evaluation was done with the constants provided in Table 4.6.

Table 4.6 Constants for calculations of approximate altitude of the CubeSat

The constants for the nominal shape of the Earth	Value
R_e	6378137 m
$\frac{1}{f}$	298,257223563

The calculation of altitude in the STK was based on the following equation (4.4) for an oblate spheroid [95]:

$$H = R - \frac{R_e(1-f)}{\sqrt{1 - (2f - f^2)cos^2\varphi}}, \quad (4.4)$$

where

H – approximate altitude, m,

R - the distance from the centre of the oblate spheroid, m

R_e - the equatorial radius, m (constant),

f - the flattening factor, dimensionless,

ϕ - the spherical latitude, degrees.

Meanwhile, the relationship of flattening factor to the equatorial and polar radii was defined with the constant for the nominal shape of the Earth (Equation 4.5).

$$f = \frac{R_e - R_p}{R_e}. \quad (4.5)$$

The relationship to the eccentricity of an elliptical cross-section was defined with values of flattening factor (Equation 4.6)

$$e^2 = 2f - f^2 . \quad (4.6)$$

The initial parameters used for the analysis of orbital lifetime are provided in Table 4.7

Table 4.7 Initial parameters for the orbit lifetime analysis

Parameter	Value
Epoch start time	1 Dec 2021 00:30:00 UTCG
Cd	2,2
Cr	1,5
Atmospheric Density model	DTM 2012 (the newest and most accurate model available)
Orbits per Calculation	1 (sampling for the highest accuracy)
Gaussian Quadrature	50 (to provide an adequate number of samples for short passes at regions close to perigee since the orbit is a highly eccentric one)
Decay Altitude	100 km (Karman line)
Solar Flux Sigma Level	2 (to consider possible deviations to the nominal values)
Corrections	2nd Order Oblateness Correction, Rotating Atmosphere (west-to-east winds)

It was estimated that a 3U CubeSat at the GTO would enter the atmosphere in 1 year producing a total of 867 orbits (Table 4.8).

Table 4.8 Results of the orbital lifetime analysis for the FORESAIL-2 3U CubeSat

FORESAIL-2	Parameter	Value
3U	Estimated date of decay	6 Dec 2022 12:40
	Number of orbits	867
	Lifetime	1,0 years

Figure 4.3 shows that eccentricity will be fluctuating due to changes in perigee height, and thus, the semi-minor axis will fluctuate also.

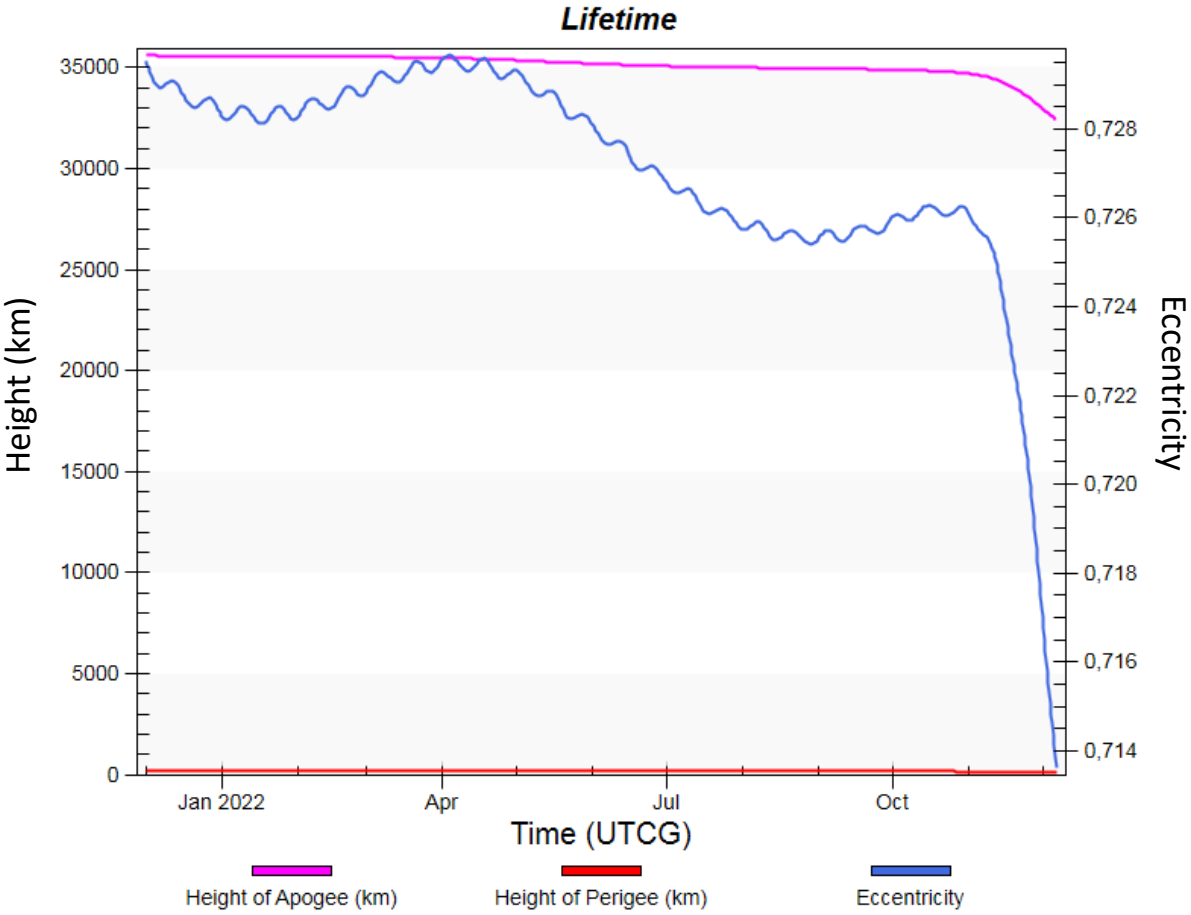

Figure 4.3 Graph of the lifetime of the FORESAIL-2 3U CubeSat with deployed solar panels. Axis on the left provides values in *km* for height of apogee and perigee while axis on the right provides values for eccentricity of the orbit.

The simulation on orbit evolution of 3U FORESAIL-2 CubeSat revealed that while there was a negligible change in the degree of inclination, other orbit parameters steadily went through changes till the full decay (Figure 4.4).

The RAAN was progressing in a retrograde direction and shifted by 147 degrees during a year and by 57,7 degrees for half a year with a rate of 0,4 degrees per day. The change of RAAN was satisfying science requirements to have a wide range of locations in near-earth space such as extensive Magnetic Local Time (MLT) coverage. In the meantime, the argument of perigee rotated by nearly 270 degrees with a rate of 0,65 degrees per day bringing the ascending node to the height of perigee. Finally, the semi-major axis shrank with a rate of 4,6 degrees per day with the same profile as the height of apogee indicating the corresponding decrease in speed at the perigee.

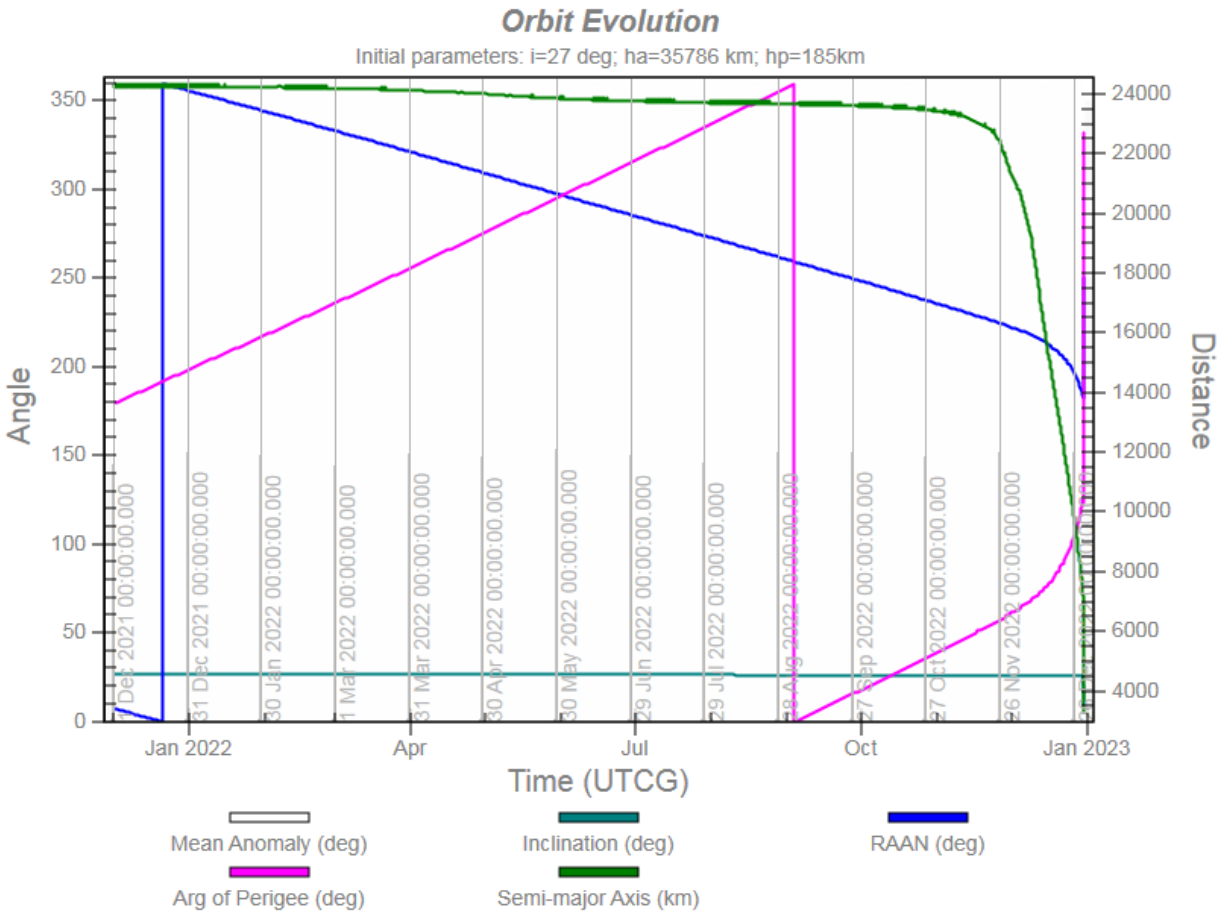

Figure 4.4 Graph of orbit evolution of the FORESAIL-2 3U CubeSat

Nevertheless, the main concern with the orbit evolution was an oscillation of the height of perigee. The oscillation was found to be around 60 km of descension during the first 6 months of mission period followed by the ascension of around 40 km for 3 months (Figure 4.5). The final stage was a decline of the height of perigee to the full decay within the next 3-4 months. These results were found to be in agreement with other researches on the GTO orbit evolution [96]–[98] which reported similar rate and magnitude for perigee height oscillation before the occurrence of solar apsidal resonance.

While launch time which determines if perigee height is to increase or decrease initially is not known yet, it is possible to quickly determine the time when tether should be deployed once launch time is announced.

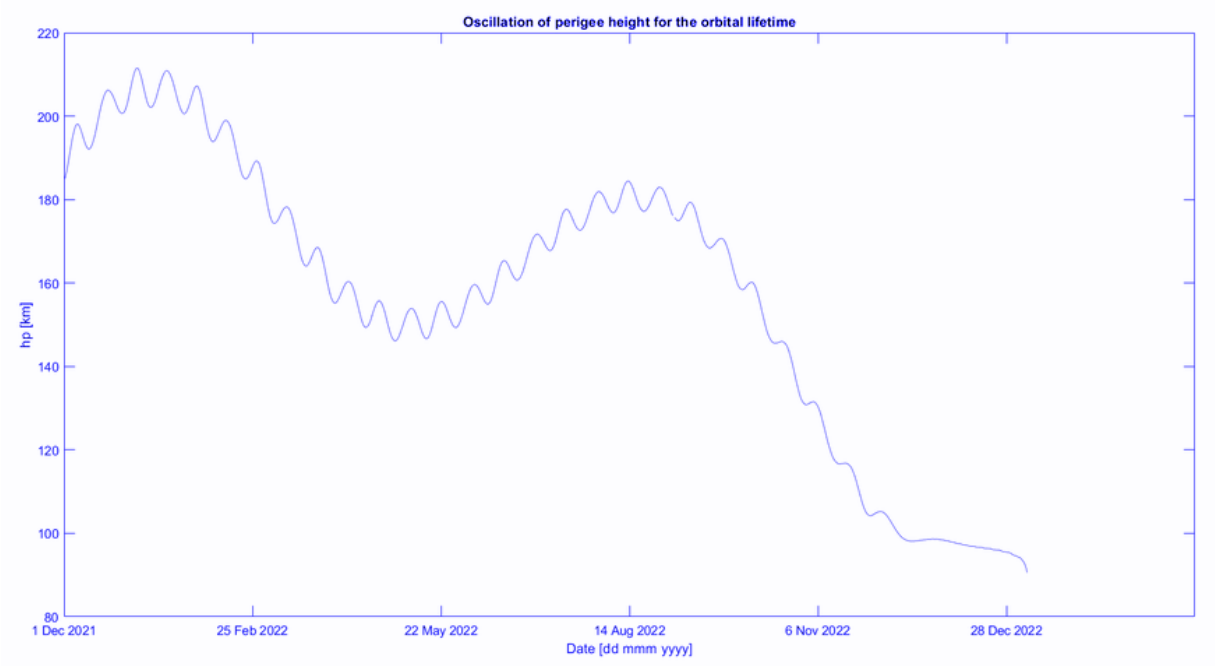

Figure 4.5 Graph demonstrating oscillations of perigee height during the orbital lifetime of the FORESAIL-2 3U CubeSat. Left axis h_p is the height of perigee in km.

4.2.2 Total ionizing doses

The simulation of trapped radiation environment along the propagated orbit for the FORESAIL-2 was done with the help of NASA models as such as AE-8 for the electron-flux model (up to 7 MeV) and AP-8 for the proton-flux model (up to 400 MeV). The selected flux models were used to provide input to the SHIELDOSE-2 radiation-transport model (Figure 3.2.1).

The calculations on trapped electrons were made in the STK and SPENVIS with the help of the Monte Carlo simulations. A number of factors were accounted such as electron energy loss, angular deflections of electrons caused by atomic electrons, and penetration and diffusion of the secondary bremsstrahlung photons and energetic secondary electrons due to delta rays and interaction of bremsstrahlung [99].

$$j\,(T_0,\theta) = \varphi\,(T_0,\theta)cos\;\theta\;, 0\;\leq\theta\;\leq\frac{\pi}{2}, \tag{4.7}$$

where

$\varphi\,(T_0,\theta)$ – incident fluence, cm-2 MeV -1 sr -1,

where T_0 – initial energy, MeV,

θ – angle of incidence with respect to the normal to the plane, sr.

j – current of particles crossing into the medium per unit area of the plane boundary, cm^{-2} MeV^{-1} sr^{-1}.

Therefore, the total incident current J can be found as follows:

$$J = 2\pi \int_0^{\infty} \Delta T_0 \int_0^{\pi/2} sin\theta \, \Delta\theta \, j(T_0, \theta)$$

$$= 2\pi \int_0^{\infty} \Delta T_0 \int_0^{\frac{\pi}{2}} sin\theta \, \Delta\theta \, cos\theta \varphi(T_0, \theta)$$

$$= \pi \int_0^{\infty} \Delta T_0 \varphi(T_0) \, .$$

The initial parameters used for modelling the radiation environment at the GTO are provided in Table 4.9.

Table 4.9 Initial parameters for the radiation environment modelling in STK

Computation mode	NASA Models
Electron and Proton Activity	Solar Max
NASA Energies	Default
Dose channel	Total
Nuclear attenuation	Yes, with neutrons
Detector	Spherical; Silicon
Dose integration step	1 min
Dose report step	10,4 hrs

Table 4.10 provides results on the efficiency of aluminium shielding in protection against ionizing radiation at the GTO.

Table 4.10 Radiation doses for different thickness values of shielding of Aluminium on the decay day (6 Dec 2022) in STK

Shielding (mm)	Max Dose (rad)
3	121400 (88800)
4	47920
5	19900

Shielding (mm)	Max Dose (rad)
6	8758 (most COTS can sustain this TID)
7	3964
8	2145
9	1377
10	997

It was found, that the thickness of 6 mm of shielding of an Aluminium would provide sufficient protection for the onboard electronics components as the tested maximum tolerance for radiation for COTS components was found to be in the range below 10 krad [100] (Table 4.10).

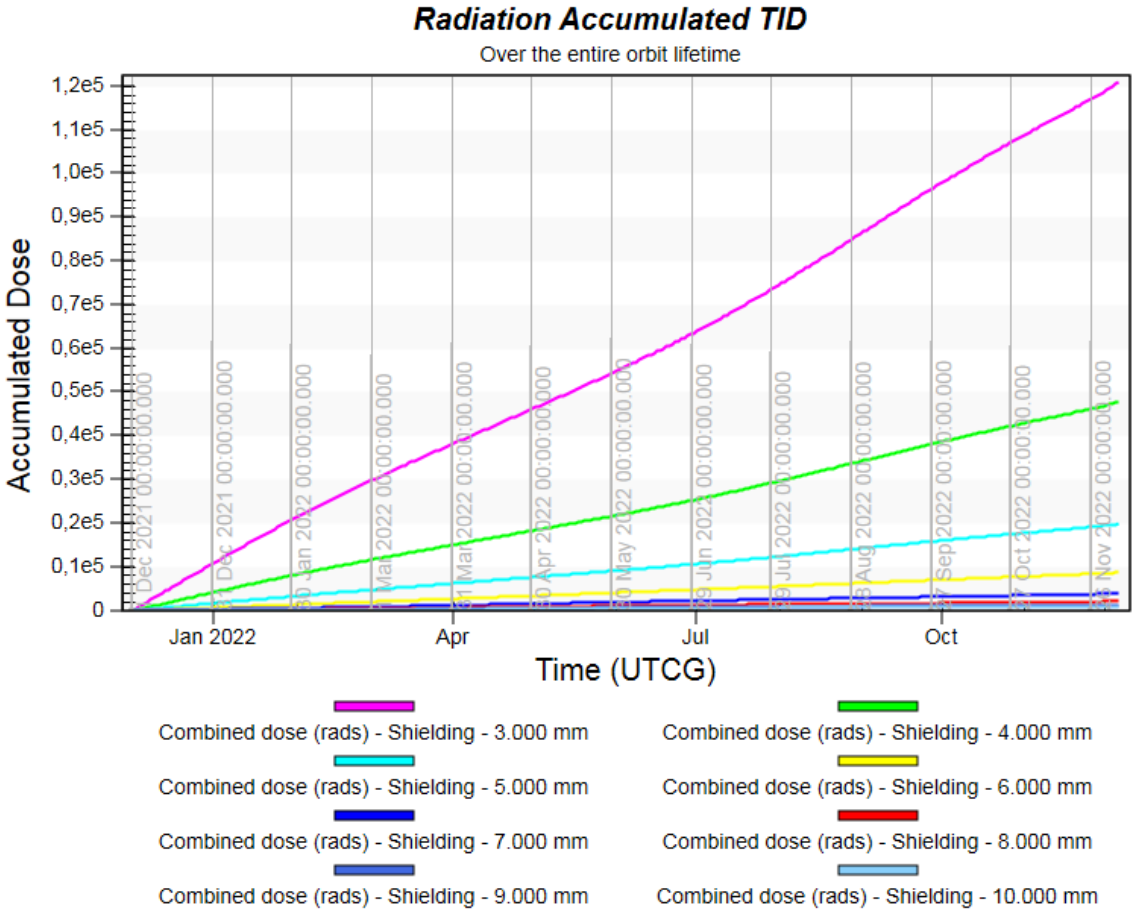

Figure 4.6 An estimate of radiation accumulated TID over the entire mission period for different shielding thickness values of Aluminium for FORESAIL-2 in STK of AGI

The accumulated TID for the entire lifetime of the 6U CubeSat was nearly the same as for the 3U CubeSat (Figure 4.6). It was nearly due to the fact that 6U CubeSat was found to decay one day later than 3U CubeSat, and thus, it would have had a slightly larger period of being exposed to the ionizing radiation.

Nevertheless, there were concerns with the accuracy of radiation environment modelling done in the STK of AGI. The main limitation associated with the modelling of a radioactive environment in the STK was an inability to specify solar minimum for protons and solar maximum for electrons. It was possible to set solar maximum for protons and electrons; however, the worst-case scenario would have included solar minimum for protons while keeping solar maximum for electrons. Thus, the radioactive environment was modelled in SPENVIS with similar initial orbit parameters (Table 4.11).

Table 4.11 Initial parameters for the radiation environment modelling in SPENVIS

Computation mode	NASA Models (AP-8 and AE-8)
Electron and Proton Activity	AP MIN and AE MAX
NASA Energies	Max Proton: 400 MeV; Max Electron: 7 MeV
Internal Magnetic Field for AP	Jensen & Cain 1960
Assumptions	Local time variation is not taken into account
	The probability that fluxes will not be exceeded (AE-4): 50,0%
Nuclear attenuation	No
Detector	Spherical; Silicon
Dose integration step	0,50°
Mean motion	14,35 rad/day

It was found that TID values generated in SPENVIS were around two (2) times larger than the ones produced with STK of AGI. Since 10 krad of TID was assumed to be a threshold value for COTS components [101], shielding of 7 mm would have been required according to the model produced with SPENVIS (Table 4.12).

Table 4.12 Radiation doses for different thickness values of shielding of Aluminium on the decay day (1 Dec 2022) in SPENVIS

Al absorber thickness			Total (rad)	Trapped electrons	Bremsstrahlung	Trapped protons
(mm)	(mils)	(g cm^{-2})				
3.000	118.110	0.810	2.777E+05	2.696E+05	3.407E+03	4.631E+03

Al absorber thickness			Total (rad)	Trapped electrons	Bremsstrahlung	Trapped protons
(mm)	(mils)	(g cm^{-2})				
4.000	157.480	1.080	1.075E+05	1.021E+05	2.495E+03	2.881E+03
5.000	196.850	1.350	4.320E+04	3.921E+04	1.986E+03	2.011E+03
6.000	236.220	1.620	1.799E+04	1.474E+04	1.672E+03	1.581E+03
7.000	275.590	1.890	8.087E+03	5.305E+03	1.458E+03	1.324E+03
8.000	314.960	2.160	4.237E+03	1.776E+03	1.301E+03	1.159E+03
9.000	354.330	2.430	2.774E+03	5.528E+02	1.186E+03	1.035E+03
10.000	393.700	2.700	2.189E+03	1.595E+02	1.097E+03	9.330E+02

The intersection of curves on Figure 4.7 demonstrated that effective shielding of ionizing doses of electron and proton particles occurred for the thickness of Al of 8 and 9 mm. Larger values of thickness of shielding than the ones mentioned above were found to produce negligible changes in TID and thus, were not recommended for use.

The presented in Figure 4.7 curve profile was in agreement with the similar research done by [98]. The only difference was in slightly different parameters for orbit and the orbital lifetime that was 2 years.

[98] claimed that the optimal thickness value for the Al shielding would have been 7,5 mm which was close to the estimate in the current report of 6-9 mm of the thickness of Al shielding to protect COTS components.

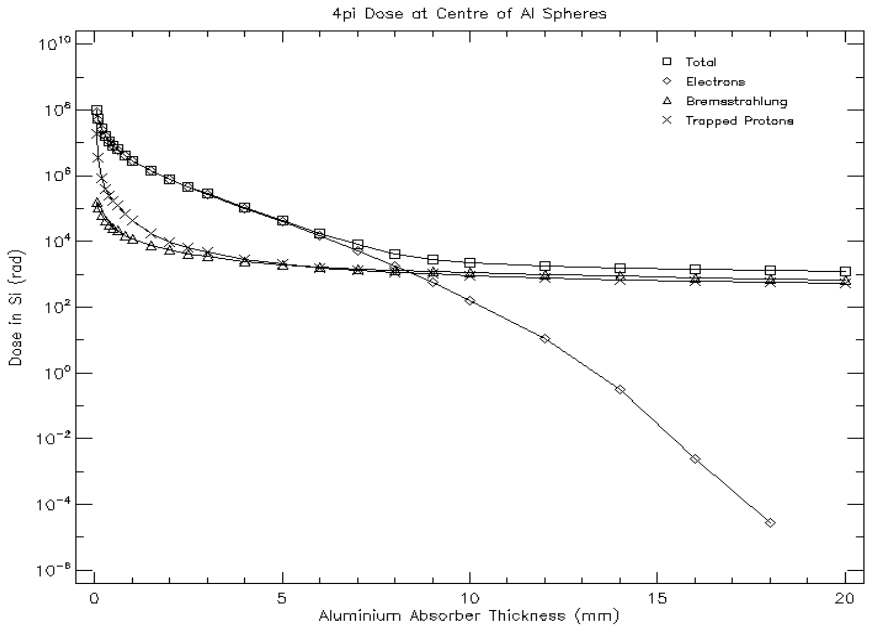

Figure 4.7 An estimate of radiation accumulated TID over the mission lifetime for different shielding thickness values of Aluminium for FORESAIL-2 in SPENVIS

Table 4.13 Mass of inherent shielding for different sizes of CubeSats and thickness values

Aluminium shielding 7075-T6	5 mm m / g	6 mm m / g	7 mm m / g	8 mm m / g	9 mm m / g
1U	562	674,4	786,8	899,2	1011,6
2U	1124	1348,8	1573,6	1798,4	2023,2
3U	1967	2360,4	2753,8	3147,2	3540,6

On the other hand, since a 6-months mission will not exceed the TID of 10 krad as shows simulation, shielding with 5 mm thickness will be enough to protect onboard electronics against ionizing radiation. The shielding thickness was calculated as shown in equation 4.8.

$$m = \rho \sum_{n=6} A \left(\frac{s_t}{10\ cm} \right), \tag{4.8}$$

where

m – mass of shielding, g,

ρ – density of material, g/cm^3,

A – sum of areas of all sides of CubeSat, cm^2,

s_t – required thickness of shielding, mm.

The density of Aluminium 7075-T6 is 2,81 g/cm^3 [102] , while the areas of the long and short sides of a 3U CubeSat are 300 and 200 cm^2 [103] (Table 4.13), respectively. The calculation shown below is done for shielding with 7 mm of thickness.

$$m = 2{,}81\frac{g}{cm^3}(300\ cm^2 + 300\ cm^2 + 300\ cm^2 + \ 300\ cm^2 + \ 200\ cm^2 + 200\ cm^2)\left(\frac{7\ mm}{10\ cm}\right)$$
$$= 2753{,}8\ grams$$

4.2.3 Geomagnetic field conjugation with spacecraft

The geomagnetic field was modelled with International Geomagnetic Reference Field (IGRF) for internal area of magnetosphere [104] and Olson-Pfitzer for the external area of magnetosphere [105] (above 15000 km) (Table 4.14). The multi-pole spherical harmonic expansion [106] was computed with STK using the equation (4.9).

$$V(r,\theta,\lambda,t) = R\sum_{n=1}^{N_{MAX}}\left(\left(\frac{R}{r}\right)^{n+1}\sum_{m=0}^{n}(g_n^m(t)\ cos\ (m\lambda) + h_n^m(t)\ sin\ (m\lambda))\ P_n^m(\theta)\right), \quad (4.9)$$

where

r– distance from the centre of the Earth, km,

θ – geocentric colatitude, degrees,

λ – geocentric longitude,

R – radius for IGRF, km (constant = 6371.2 km,

$g_n^m(t)$ – harmonic coefficients at time t, dimensionless,

$h_n^m(t)$ – harmonic coefficients at time t, dimensionless,

$P_n^m(\theta)$ – Schmidt semi-normalized associated Legendre functions of degree n and order m, dimensionless.

The parameters set for modelling geomagnetic field at the GTO are provided in Table 4.14.

Table 4.14 Parameters for modelling geomagnetic field at the GTO [129]

Parameter	Value
Magnetic Field Model	Fast IGRF
External Field (at higher altitudes; GEO)	Olson-Pfitzer
IGRF Update Rate	1 day
South Atlantic Anomaly (SAA)	Channel > 23 MeV

Parameter	Value
Flux Level	Background + 3 Sigma

The maximum magnetic field intensity Table 4.15 was found to be 51313 nT while the minimum and mean were 101,44 nT and 2411,9 nT, respectively.

Table 4.15 A summary on geomagnetic field intensity at the GTO

Parameter	Value	Date
Max Total intensity	51313 nT	1 May 2022 16:09
Min Total intensity	101,44 nT	3 Dec 2021 19:52
Mean Total intensity	2411,9 nT	-
Max B/Beq	33,78	26 Nov 2022 19:41
Mean B/Beq	1,95	-

The simulation demonstrated that field intensity decreased proportionally to the increase in distance from the Earth (Figure 4.8). On the other hand, the strength of the field was not subject to linear changes in altitude and was varying due to changes in space weather.

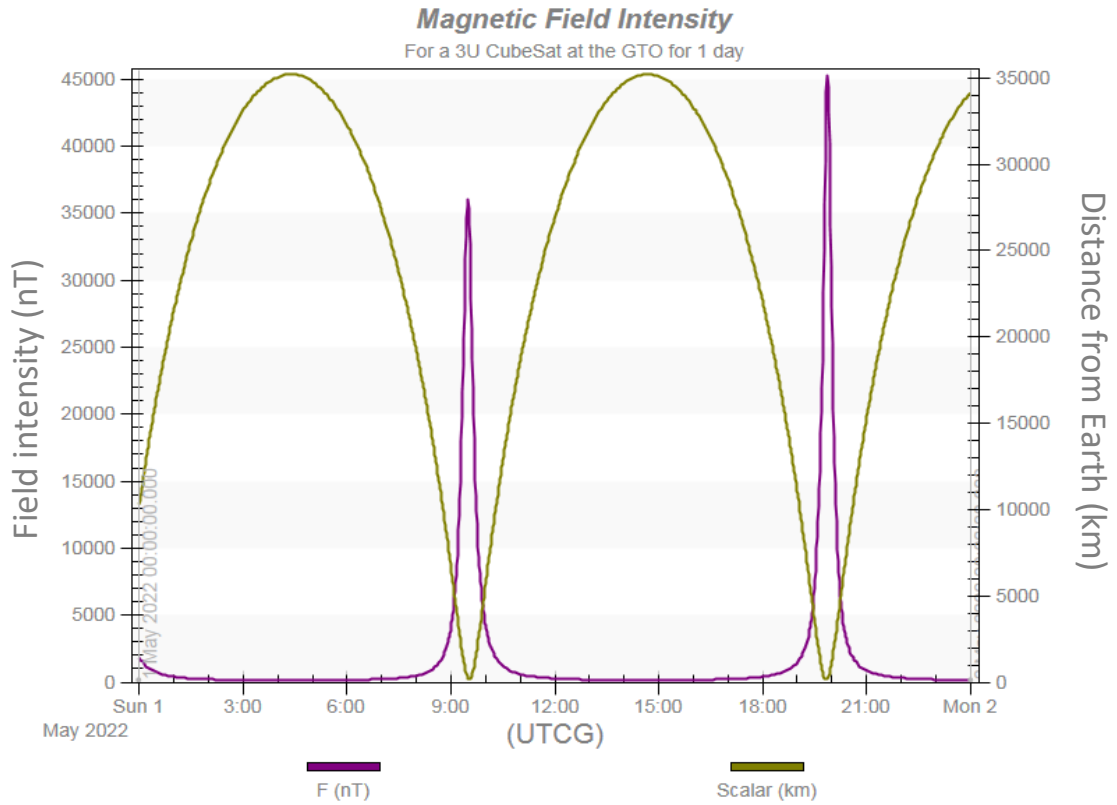

Figure 4.8 Graph with magnetic field intensity in FORESAIL-2 as a function of distance from the centre of the Earth. Axis on the left provides values in nT for magnetic field intensity while axis on the right provides values for distance from the centre of the Earth in km.

It was assumed that the magnetic moment of magnetorquer would be with margin equalling it to 0,5 Am^2 while the typical strength most magnetorquers were capable of providing was around 0,2 Am^2 [107]–[109]. The assumed value was used to estimate generated torque with the mean value of magnetic field intensity along the modelled orbit trajectory of FORESAIL-2. The calculation of the generated torque as a function of magnetic field intensity and magnetic dipole strength [102] is provided with the equation (4.10).

$$T = m \cdot B , \tag{4.10}$$

where

T – magnetic torque vector, Nm,

m – magnetic dipole vector produced by magnetorquer, Am^2,

B – Earth magnetic field vector, T.

The m with a margin to the available for magnetorquer on CubeSats typical dipole strength was 0,5 Am^2 and mean B obtained from simulations in STK was 2411,9 nT.

$T = 0.5\ Am^2 \cdot 2.4119e^{-6}\ T = 1{,}206e^{-6}$ Nm or 0,001 mNm

While the angular momentum required for deployment of aluminium tether was 20,961 Nms, the torque required to desaturate reaction wheels such as RW200 used on Aalto-1 [10] was 0,087 mNm. Therefore, the torque produced with the magnetorquer with the highest available dipole strength would be of no use for FORESAIL-2 mission at the GTO as the minimum required torque was 7 times larger.

On the other hand, it could be useful during perigee passes the mean time of which was 30 minutes as was determined in the section on the power supply. Nevertheless, it must be taken into account that speed at perigee was found to be around 10 km/s as was determined in the CML 3 sections which will affect the ability of the spacecraft to manoeuvre.

4.2.4 Electron and proton fluxes

The analysis of electron and proton fluxes allowed to verify that propagated orbit would potentially traverse through areas of interest to science observations of the electron energy spectrum. The analysis was done for the orbit propagated with the STK and involved numerical approach with the Runge-Kutta-Fehlberg method of 7th order. Initial parameters for modelling particle distribution at the GTO are provided in Table 4.16.

Table 4.16 Initial parameters for modelling fluence of high energy particles at the GTO [129]

Parameter	Value
Galactic Cosmic Rays (GCR)	
Model	BO10 (Based on the NASA Advanced Composition Explorer Cosmic Ray Isotope Spectrometer)
Atomic number	1 (Hydrogen)
Solar Influence	Solar Max
PHI	1100
Sample Time (Fractional Years)	0,25
Solar Energy Particles (SEP)	
Model	ESP (95% confidence level)
Mission Duration	2 years

The proton flux was found to be effective at regions during CubeSat ascension and descension but had no or negligible influence at higher altitudes (Figure 4.9). On the other hand, the electron flux levels were found present at all altitudes with the highest concentration at the region close to apogee (Figure 4.10).

The said confirmed the fact that high energy proton flux was mostly present in the inner region of Van Allen radiation belts while high energy electrons existed at the higher altitudes of Earth's magnetosphere [110].

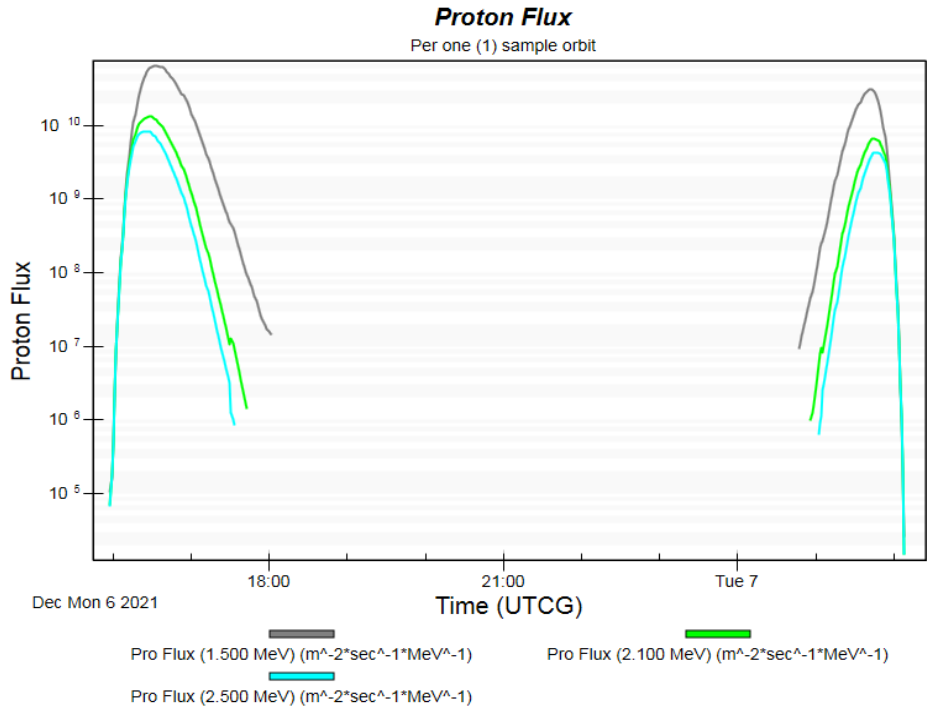

Figure 4.9 Graph with proton flux for different energies with a sample of one (1) orbit period of the FORESAIL-2 CubeSat

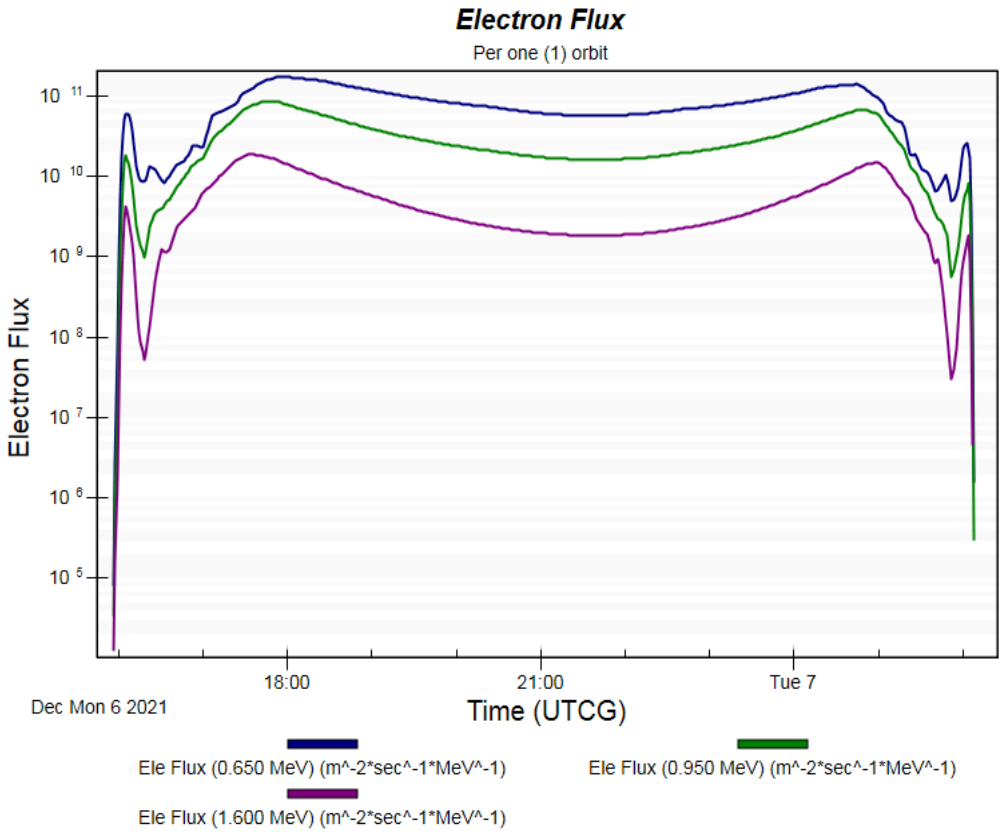

Figure 4.10 Graph with electron flux of different energy levels for the FORESAIL-2 orbit trajectory

The measurement requirements for Relativistic Electron and Proton Experiment (REPE) were to measure the particle energy spectrum in the range of 30 keV - 10 MeV in the breakthrough case and 800 keV - 8 MeV in enabling case. The environmental analysis shows that a large flux of electrons of high energies would be available to the REPE instrument for the most part of the orbit. Meanwhile, a large flux of low energy electrons was expected at the region close to the perigee.

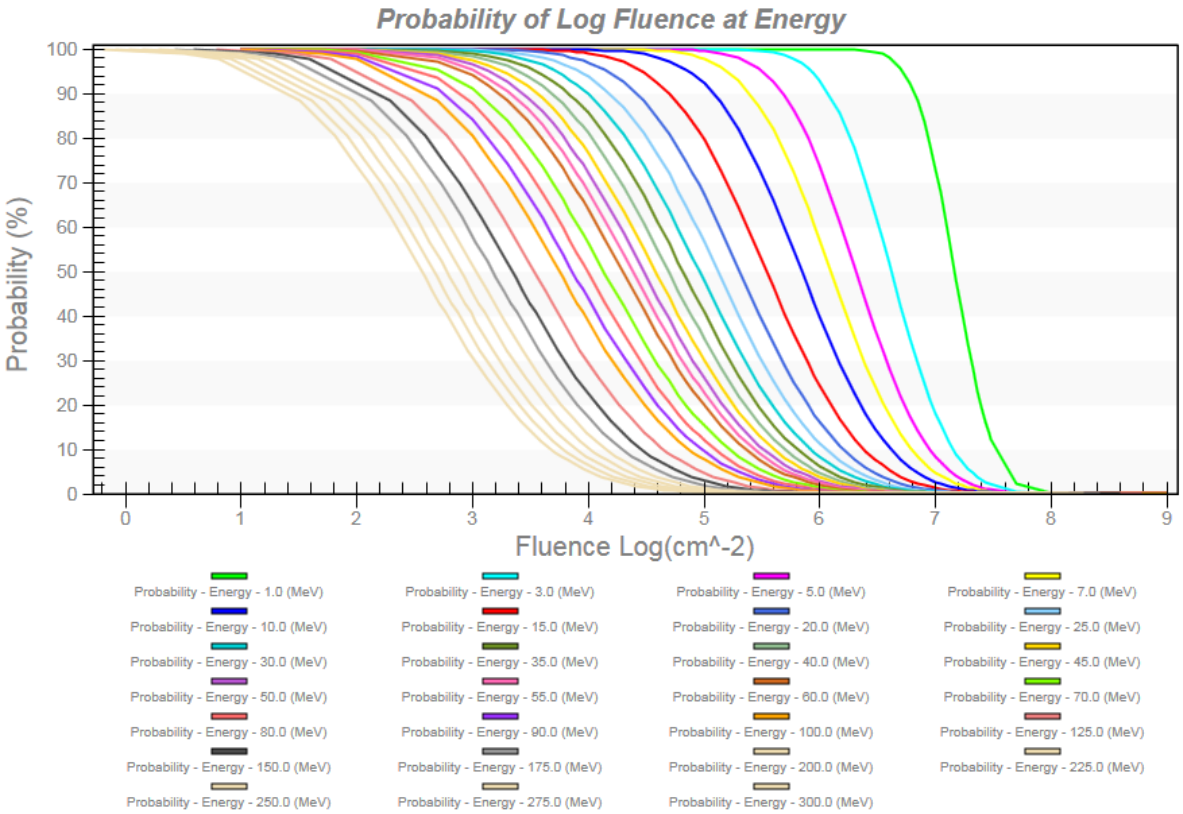

Figure 4.11 Graph showing probability of solar energy particle (SEP) fluence to exceed the specified energy levels

Protons and ions originating from solar winds were predicted in the form of particle fluence with the ESP model [111]. This model accounted for a maximum entropy technique and data from three solar cycles (20-22) of proton observations with Interplanetary Monitoring Platform (IMP) satellite [112] and Geostationary Operational Environmental Satellites (GOES) [113]. The energy levels of interest were in the range above 100 MeV Protons. Figure 4.11 shows that there was a higher probability for exceeded fluence for energy levels from 225 to 300 MeV.

4.2.5 Telemetry and link budgets

The access analysis included ground stations from KSAT [114], SSC [115] and ESTRACK [116] networks located within latitudes from 30 degrees North to 30 degrees South. Nevertheless, although stations in Spain and Portugal were above 30 degrees North, they were included as they

were part of the aforementioned networks and located in the European Union (EU). These networks were assumed to have the highest probability of being utilized for the purposes of the current mission.

The 4/3 Earth Effective Radius method was used in the STK to estimate refracted elevation angle (Equation 4.11) [117].

$$\sin(\theta_{ref}) = \frac{(h_t + r_{eff})^2 - \left(h_{rfo} + r_{eff}\right)^2 - R^2}{2\left(h_{rfo} + r_{eff}\right)R}, \quad (4.11)$$

where

θ_{ref} – refracted elevation angle, degrees,

h_t – altitude of the satellite, km,

r_{eff} – 4/3 earth radius below the radio frequency (RF) satellite, km,

h_{rfo} – altitude of the RF satellite, km

R – range between RF satellite and ground station, km.

Meanwhile, the Line of Sight and the refracted elevation angle of the horizon was computed in the STK with the equation (4.12) based on trigonometry of right angles [117].

$$r_{hor} = \sqrt{h_{rfo}^2 + 2r_{eff}h_{rfo}}, \quad (4.12)$$

where

r_{hor} – horizon, km.

$$\theta_{hor} = \frac{r_{eff}^2 - \left(h_{rfo} + r_{eff}\right)^2 - r_{hor}^2}{2\left(h_{rfo} + r_{eff}\right)R_{hor}},$$

where

$sin\theta_{hor}$ – refracted elevation angle of the horizon, degrees,

R_{hor} – range to horizon, km.

The link would be established if $\theta_{ref} > \theta_{hor}$, otherwise, the computation would be done backwards to find the range from the CubeSat to the ground station [117]. The line of sight between the CubeSat and ground stations located within the required latitude of geographical coverage was compared in terms of mean duration, range, and elevation. The ground station in Singapore was

found to have the smallest mean range, while ground station in Santa Maria, Madrid and Dubai, were found to have the longest mean duration of the communication time window. Nevertheless, the ground station in Espoo where Aalto University was located had 6,6 hours of communication time with the satellite over the mean range of 30926 km Table 4.17 A comparison of access links of different ground stations with the FORESAIL-2.

Table 4.17 A comparison of access links of different ground stations with the FORESAIL-2

Location	Network	Mean Duration / hrs	Mean Range / km	Min Range / km	Mean Elevation / degree
Espoo, Finland	FORESAIL (Finland)	6.6	30926	4233	-79.2
Singapore	KSAT (Norway)	5.8	27828	235	-79.8
Dubai	KSAT (Norway)	7	28531	531	-80.3
Mauritius	KSAT (Norway)	4.7	28211	205	-79.3
Kourou	ESTRACK (ESA)	5.9	27941	198	-79.9
Hawaii	SSC (Sweden)	6.7	28234	409	-80.3
Madrid	SSC (Sweden)	7	29265	1930	-80.2
Santa Maria	ESTRACK (ESA)	7	28993	1534	-80.3
Thailand	SSC (Sweden)	6.5	28079	218	-80.3

Values of elevation angle for antenna were defined as negative values towards the positive y-axis and specified in the range from -180 to +180 degrees (Figure 4.12). Since the ground station at Espoo, Finland was located above 30 degrees of latitude; the elevation angle was the lowest among other ground stations located within the region with -30 to 30 degrees of latitude (Figure 4.13).

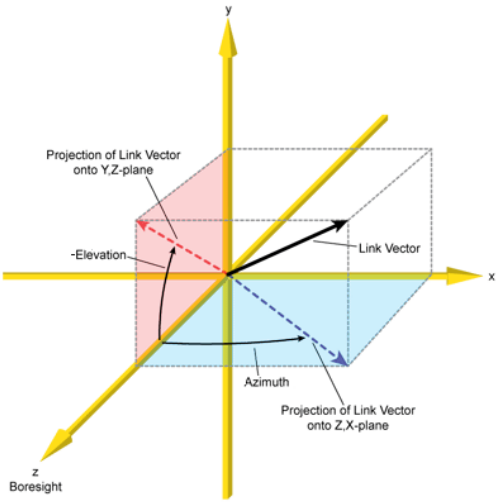

Figure 4.12 An illustration describing elevation and azimuth angles with respect to body axes of the antenna at the ground station [118]

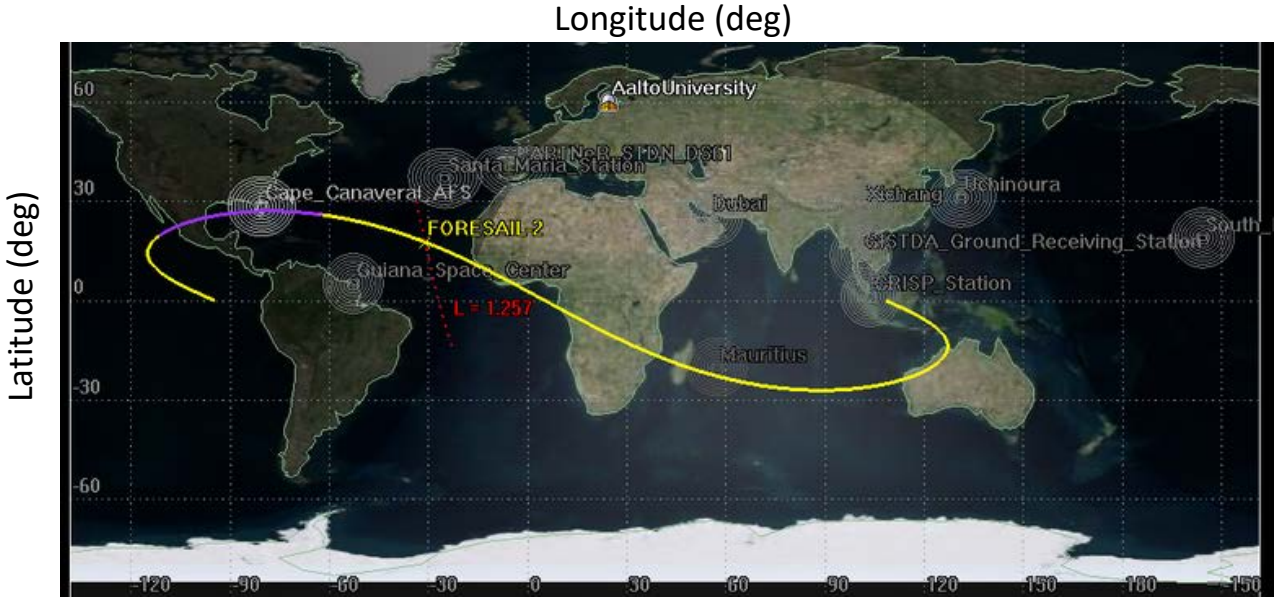

Figure 4.13 A trajectory of the FORESAIL-2 lays within 30 to -30 degrees of latitude. The selected ground control stations are within this area.

The telemetry budget (Appendix 5) was estimated with consideration of compression rate of 21% determined based on evaluations done for Aalto-1 with RADMON data (Equation 4.13).

$$DROS_{day} = \frac{(\sum_{i=1}^{n} DR_{inst} \cdot 3600\ s\ \cdot 24\ hours \div 1 \times 10^{6}\ )}{8\ bits}, \quad (4.13)$$

$$DR_{comp} = DROS_{day} \cdot CR \cdot 1000\ kbytes\ ,$$

$$DR_{time} = DR_{comp} \div \left(\frac{DR_n}{8\ bits}\right) \div 60\ \text{min}\ ,$$

where

$DROS_{day}$ – required onboard storage and dowlink rate for science data, Mbyte/day,

DR_{inst} – data produced by payloads, bit/s,

DR_{comp} – downlink rate with compressed data, kbytes/day,

CR – data compression rate, %,

DR_{time} – required downlink time per day, min/day,

DR_n – minimum or nominal available downlink capacity, Kbit/s.

$$DROS_{day} = \frac{\left(\left(\left(317\frac{bit}{s} + 11\frac{bit}{s} + 100\frac{bit}{s}\right) \cdot 3600\ s \cdot 24\ hours\right) \div 1 \times 10^6\right)}{8\ bits} = 4{,}6\ Mbytes/day$$

$$DR_{comp} = 4{,}6\frac{Mbytes}{day} \cdot 21\% \cdot 1000\ = 971\ kbytes/day$$

$$DR_{time} = DR_{comp} \div \left(\frac{8\ kbit/s}{8\ bits}\right) \div 60\ mins = 16{,}18\ min/day$$

The required on-board storage and downlink rate in science mode was found to be 4,6 Mbytes per day with the required downlink time of 16,18 minutes (Table 4.18). The required time was 0,04% of the mean duration of a communication link which was found previously to be 6,6 hours.

Table 4.18 Results of telemetry budget calculations for FORESAIL-2 (Appendix 5)

Downlink requirements in science mode	Value	Units
On-board storage / Rate with passes	4,6	Mbytes per day
Compressed data	971	Kbytes per day
Downlink data rate	8,0	Kbit/s
Required downlink time	16,18	min per day

It was assumed that downlink data rate would be 8 Kbit/s maximum due to the fact that the set by IARU and ITU requirement [119] for 19,2 Kbit/s (max bandwidth 20 kHz) would be reduced with consideration of protocol overheads, duty cycles and margins. Furthermore, it was assumed that the UHF frequency would be used as there was a higher probability to get a license in this frequency rather than in any other [120]. On the other hand, the ground station at Aalto University has required facilities for communication over S-band frequencies in case better downlink and uplink rates were required [121], [122].

The link budget was developed based on specifications of a 70 cm Yagi antenna [123] installed on the roof of one of Aalto University buildings and UHF transceiver used for Aalto-1 (Table 4.19).

Table 4.19 Parameters of UHF transceivers of Aalto-1 and OH2AGS ground station at Aalto University in Otaniemi Campus [124] [121], [122]

Parameters	Value
Spacecraft	
Frequency	437,220 MHz
Max TX power	1,2 W (dBm 30.8)

Parameters	Value
Modulation	GFSK
Ground station	
Gain	14 dBD
Front/back ratio	>20 dB
Length	70 cm
Uplink	75 W
Tracking	While there is capability for tracking, it was assumed that tracking is off as a worst-case scenario.

The energy-bit to noise density ratio was computed in the STK with equation 4.14 [70].

$$\frac{E_b}{N_o} = \frac{PL_l G_t L_s L_a G_r}{kT_s R}, \tag{4.14}$$

$$\frac{E_b}{N_o} = P + L_l + G_t + L_s + L_a + G_r + 228{,}6 - 10\ log\ T_s - 10\ log\ log\ \ R\ ,$$

where

E_b – Energy per bit, dB,

N_o – Noise spectral density, dB,

P – Transmitter power, dBW,

L_l – Line loss, dB,

G_t – Transmitter antenna gain, dB,

L_s – Space loss, dB,

L_a – Transmission path loss, dB,

G_r – Receiver gain, dB,

k – Boltzmann's constant, dBW/(Hz-K)

T_s – System noise temperature, K,

R – Data rate, bits/s.

The noise would prevail over signal, and thus, more power for signal would be required as can be deduced from Figure 4.14. Another option would be to use Forward Error Correction (FEC) algorithms [60].

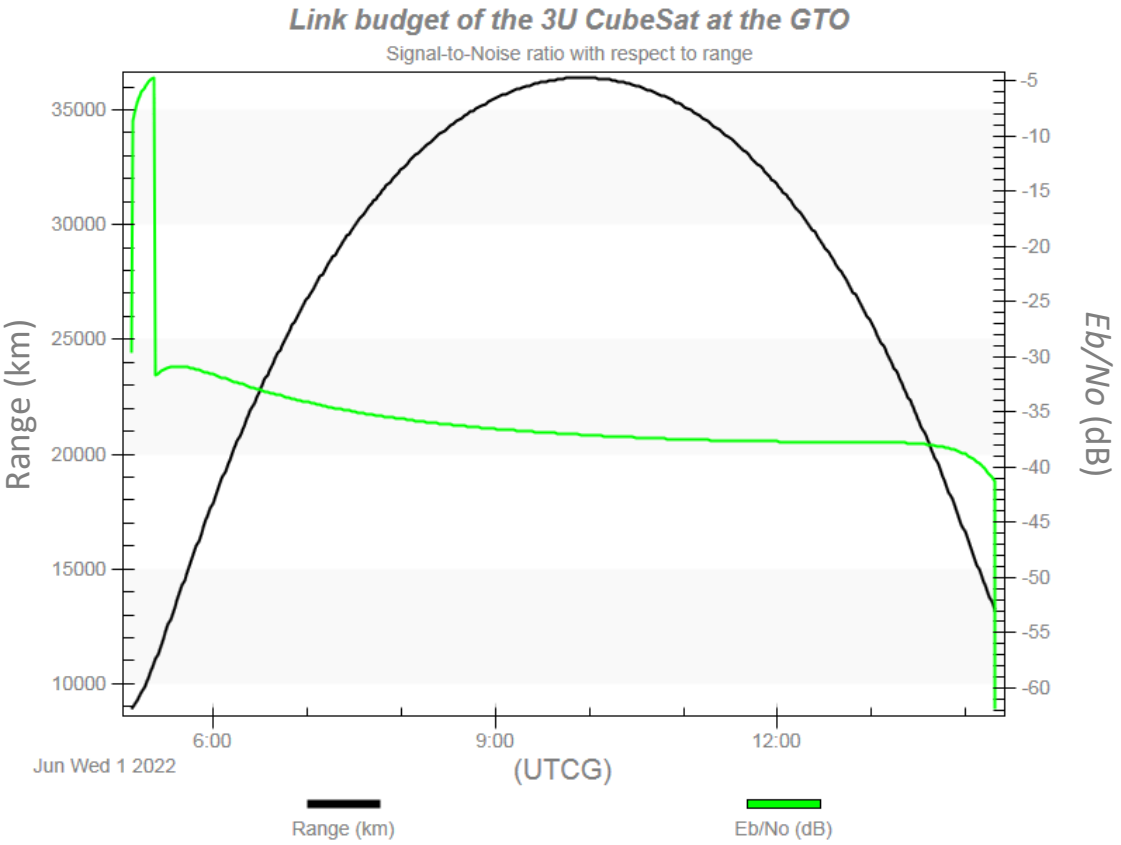

Figure 4.14 Ratio of Energy per Bit (*Eb*) to the Spectral Noise Density (*No*) for the communication link between FORESAIL-2 at the GTO and OH2AGS on the Earth.

The link budget showed that the best time for establishing a link between the ground station at Aalto University and the CubeSat at the GTO was during ascension while the worst was during descension. On the other hand, the evolution of the orbit would change the best time window for each communication session.

4.2.6 Power supply

Continuous power supply is a critical requirement which cannot be compromised and therefore needs to be thoroughly examined. The analysis of power production for the propagated orbit was done for a 3U CubeSat without and with deployed solar panels with assumption with a margin that the maximum efficiency was 28% [125] and based on equation 4.15.

$$P = \mu \cdot Sint \cdot Aeff \cdot SI\,, \tag{4.15}$$

where

P – electrical power produced by solar panels at a given point in time, W,

μ – efficiency of the solar panels, 0 < i < 1,

$Sint$ – solar intensity ranging from 0 (umbra) to 1 (full sunlight), 0 < i < 1,

$Aeff$ – effective area of illumination of solar panels, m^2,

SI – solar irradiance defined as relation of solar flux at 1 AU to relative position of the Sun with respect to the satellite, W/m^2.

Table 4.20 A summary on findings on power generation from solar panels placed on FORESAIL-2 moving on the GTO

Parameter	Value (W)	Date
Max Power (10x30 cm; 28%)	7,34	1 Dec 2021 00:00:06
Mean Power (10x30 cm; 28%)	6,89	-
Max Power (30x30 cm; 28%)	21,85	1 Dec 2021 00:00:06
Mean Power (30x30 cm; 28%)	20,7	-

The mean power produced was found to be 6,89 W for one solar panel and 20,7 W for a deployed configuration with three (3) solar panels exposed to the sun (Table 4.20).

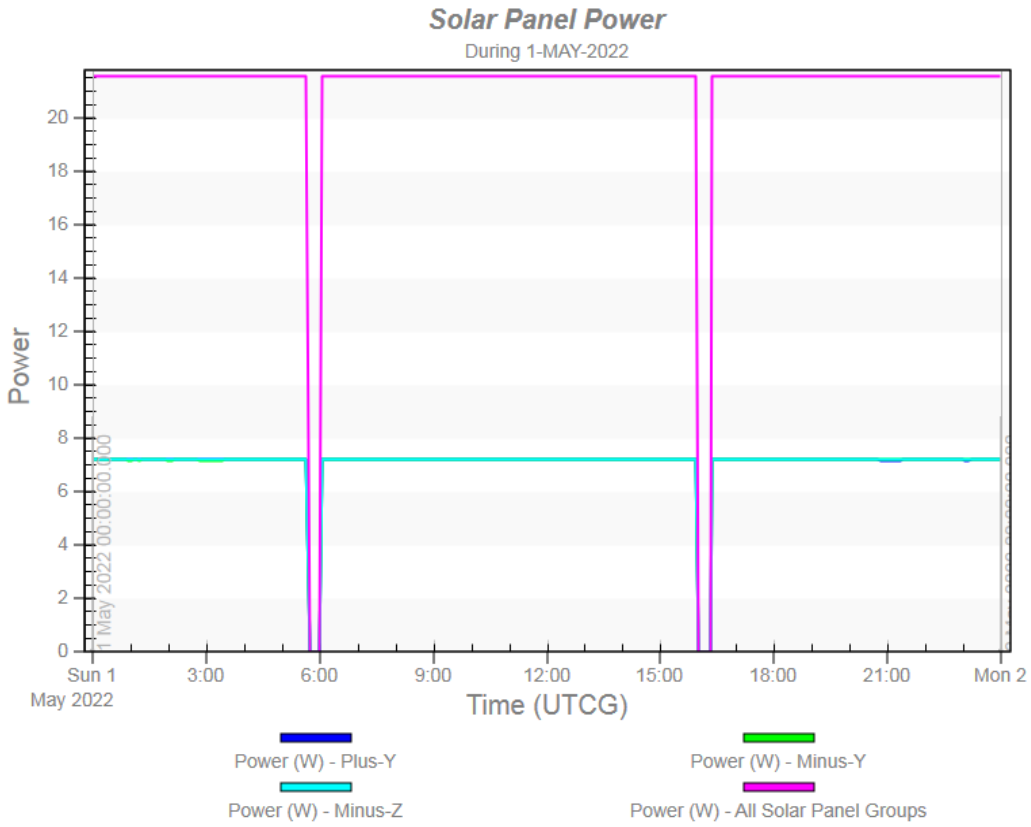

Figure 4.15 Graph of solar panel power generated from deployed and body mounted solar panels on 3U FORESAIL-2 CubeSat with an assumed efficiency of 28%

Figure 4.15 shows that power will be generated for most of the orbit with discharge time during short eclipse periods.

Table 4.21 A summary of findings on the eclipse period and its components for the FORESAIL-2 CubeSat at the GTO

Parameter	Value / minutes	Date / UTCG
Umbra		
Max Duration	56,6	1 Dec 2021 9:11-10:07
Min Duration	6,6	20 Nov 2022 7:39-7:46
Mean Duration	30,4	-
Penumbra		
Max Duration	37,5	30 May 2022 6:37-7:14
2nd after the Max Duration	19,6	25 Oct 2022 12:10-12:29
3rd after the Max Duration	10	20 Nov 2022 17:12-17:22
4th after the Max Duration	9	23 Nov 2022 19:48-19:57
Mean Duration	0,3	-
Sunlight		
Max Duration	51209 (853 hrs)	23 Nov 2022 - 29 Dec 2022
2nd after the Max Duration	4465,5 (74,4 hrs)	20 Nov 2022
Min Duration	27,2	30 May 2022 6:09-6:37
Mean Duration	639 (10,6 hrs)	-
Mean Duration without Max Duration periods	580 (9,6 hrs)	-

The total production of power for one orbital period was estimated based on average time spent in sunlight and shadow (Table 4.21) and nominal power consumption during the science mode (Equation 4.16). The excess production was determined based on selected battery models with a capacity of 30 Wh. These batteries were found to be used in FORESAIL-1 CubeSat mission [126], and thus, there was a high probability to use these model of batteries again.

$$P_{prod} = Ppn \cdot \left(\frac{t_{sun}}{60\ min}\right), \tag{4.16}$$

$$P_{cons} = Pcn \cdot \left(\frac{T}{60\ min}\right),$$

$$P_{ex} = P_{prod} - P_{cons}\,,$$

$$DoD = \left(Pcn \cdot \left(\frac{t_{eclipse}}{60\ min}\right) \div E\right) \cdot 100\ \%\,,$$

where

P_{prod} – total production of electric power from solar panels, Wh,

Ppn – nominal electric power production, W,

t_{sun} – mean time in sunlight, min,

P_{cons} – total consumption of electric power by subsystems and payloads, Wh,

T – orbital period, min,

P_{ex} – excess production of electric power, W,

DoD – depth of discharge of the batteries, %,

E – Battery capacity, Wh.

$$P_{prod} = 6{,}89\ W \cdot \left(\frac{580\ min}{60\ min}\right) = 66{,}6\ Wh$$

$$P_{cons} = 8{,}8\ W \cdot \left(\frac{690\ min}{60\ min}\right) = 101{,}36\ Wh$$

$$P_{ex} = 66{,}6\ Wh - 101{,}36\ Wh = -\,34{,}76\ Wh$$

$$DoD = \left(8{,}8\ W \cdot \left(\frac{31\ min}{60\ min}\right) \div 30\ Wh\right) \cdot 100\% = 15{,}2\ \%$$

The calculations showed that a CubeSat with only one (1) solar panel (10x30cm) exposed to the sun would produce mean power of 6,89 W and cause a deficit in power production for 34,76 W (Table 4.22).

Table 4.22 Results of calculations performed to provide a power budget for FORESAIL-2 without deployed solar panels on the GTO (Appendix 8)

Orbital period	690	min
Avg. time in sunlight	580	min
Avg. time in shadow	31	min
Highest amount of power consumption in science mode	8,8	Watts
Nominal power production in sunlight	6,89	W
Battery Capacity	30	Wh
Total production	66,60	Wh

Total consumption	101,36	Wh
Excess production	−34,76	Wh
Depth of discharge	15,2%	

The EPS of the satellite should be able to produce power continuously for the entire orbit period and ensure the durability of batteries. The durability of batteries can be maintained with relatively constant temperatures while constant charging will heat the batteries. The said can be achieved if batteries are charged during sunlight and discharged during excess production and eclipse periods (Figure 4.16).

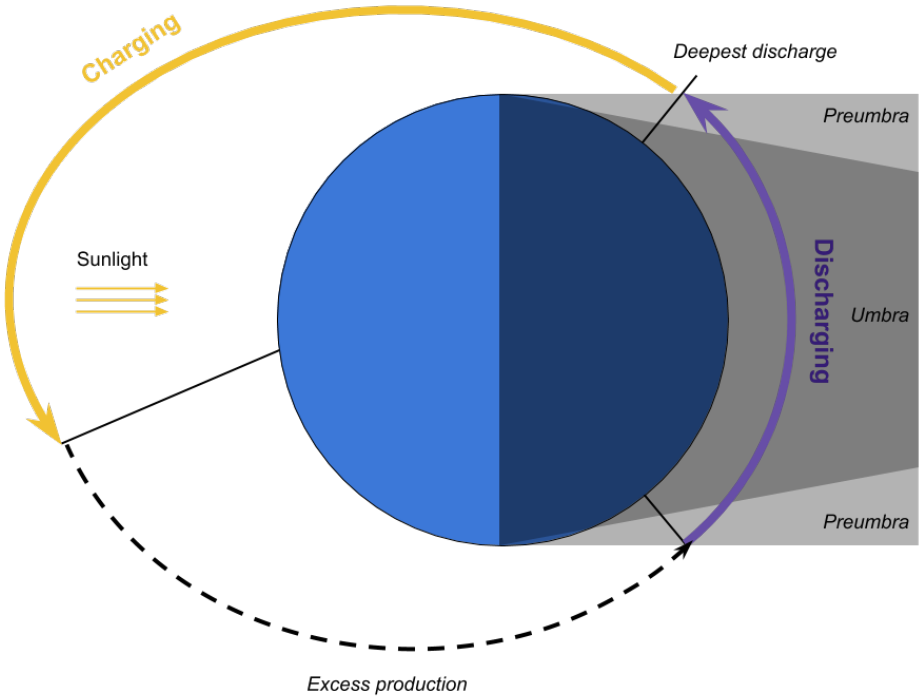

Figure 4.16 Model of power charging and discharging cycles for FORESAIL-2 at the GTO

Meanwhile, the solution to the issue with a lack of power determined in the case with one (1) solar panel facing the sun was to deploy two (2) more solar panels. The deployment of an additional two (2) solar panels increased the active area of illumination to 30x30 cm and mean power to 20,7 W, and generated excess power of 98,74 Wh (Table 4.23).

Table 4.23 Power budget for a FORESAIL-2 with deployed solar panels on the GTO (Appendix 8)

Orbital period	690	min
Avg. time in sunlight	580	min
Avg. time in shadow	31	min
Highest amount of power consumption in science mode	8,8	Watts

Nominal power production in sunlight	20,7	W
Battery Capacity	30	Wh
Total production	200,10	Wh
Total consumption	101,36	Wh
Excess production	98,74	Wh
Depth of discharge	15,2%	

4.2.7 Thermal conditions

The average operating temperature of electronic components was found to be in the range from -15 to +50 degrees Celsius. Meanwhile, rechargeable batteries were found to be operational within a range from 0 to +20 and mechanisms were excellent with 0 to +50 [102].

It was assumed that the internal dissipation of the 3U CubeSat would amount to 1 W produced as heat by onboard systems Table 4.24. The thermal analysis was based on calculations of the steady-state temperature of a single isothermal node with bulk thermal characteristics specified at each time interval of 1 minute. The calculations of mean equilibrium temperature influenced by direct solar and reflected from Earth radiation were produced with the help of thermal balancing equations [127].

Table 4.24 Initial parameters for modelling interaction of aluminium shielded FORESAIL-2 3U CubeSat with the environment at the GTO from the perspective of thermal conditions

Solar Flux at 1AU	1365,078 W/m^2
Earth Albedo	0,30 [128]
Shape	Plate
Cross-section area	3U 0.03 m^2
Material Emissivity	0,80 (assuming the emissivity of triple junction GaAs solar panels)[102]
Material Absorptivity	0,26 (assuming the absorptance of plain anodized aluminium)[102]
Normal vector	Sun
Internal Power Dissipation (Losses)	3U 90% efficient DC-DC converter (1 W)

The reason emissivity coefficient was of solar panel, and absorptance was of anodized aluminium was an assumption that energy solar panel absorbed was converted to electric power and losses were released as heat to space acting as an effective heat sink. On the other hand, aluminium had a negligible value for the coefficient of emissivity compared to its absorptivity [102]. Thus, it was assumed that the primary medium for heat transfer to the CubeSat would be aluminium while solar panel would produce electric power and release heat due to its high emissivity.

The computations for thermal analysis were done analytically with STK and were based on the conservation of energy and Stefan-Boltzmann law [129] (Equation 4.17).

$$E_{emitted} = E_{dissipated} + E_{absorbed}\,, \tag{4.17}$$

where

$E_{emitted}$ – energy emitted by satellite body, W,

$E_{dissipated}$ – energy dissipated internally due to work of satellite subsystems, W,

$E_{absorbed}$ – energy absorbed by satellite body, W.

$$\sigma_B T_0^4 = \left[\left((Q_{sun} + Q_{ER})\mu_0 + \frac{Q_i}{\varepsilon_0}\right) + Q_{IR}\right]\frac{1}{A_0},$$

where

σ_B – the Stefan-Boltzmann constant, 5,670367 x 10^{-8} W m^{-2} K^{-4},

T_0 – average external temperature of the satellite, K,

Q_{sun} – thermal power delivered from the Sun, W.

Q_{ER} – thermal power from the Sun reflected from the Earth, W,

Q_{IR} – radiant infrared power emitted from the Earth, W,

Q_i – power produced by subsystems inside the satellite, W,

μ_0 – absorptivity coefficient of surface materials of the satellite, dimensionless,

ε_0 – emissivity coefficient of surface materials of the satellite, dimensionless,

A_0 – total radiating surface, m^2.

Results of thermal condition analysis (Table 4.25) indicated potential problems with a significant swing in temperature of about 100 degrees per orbit. On the other hand, it must be noted that cold case happened during eclipse period that had the mean time of about 30 minutes while hot case when CubeSat was exposed to sunlight lasted for about 10 hours per orbit. While the heat transfer

with aluminium shielding on CubeSat would reduce the range of temperature swing, a reeled-out tether could act as a radiator.

Table 4.25 A summary of exterior temperature values of FORESAIL-2 CubeSat on the GTO

FORESAIL-2	Parameter	Value	Date / UTCG
3U	Max Temperature	46,9 ℃	17 Dec 2021 12:52
	Min Temperature	-92,5 ℃	1 Dec 2021 09:11
	Mean Temperature	27,3 ℃	-
	Max Solar Flux	1,4117e+03 W/m^2	4 Jan 2022 03:38
	Min Solar Flux	1,3205e+03 W/m^2	4 Jul 2022 08:53
	Mean Solar Flux	1.3656e+03 W/m^2	-

The production of such a giant thermal swing via conduction with aluminium material, 73,8 MJ of energy would be required (Equation 4.18). Furthermore, the spin-stabilized mode of spacecraft would reduce the rate of heat distribution while evenly scattering it over the surface of the CubeSat. Therefore, the internal environment of the CubeSat would not be subjected to significant thermal swings.

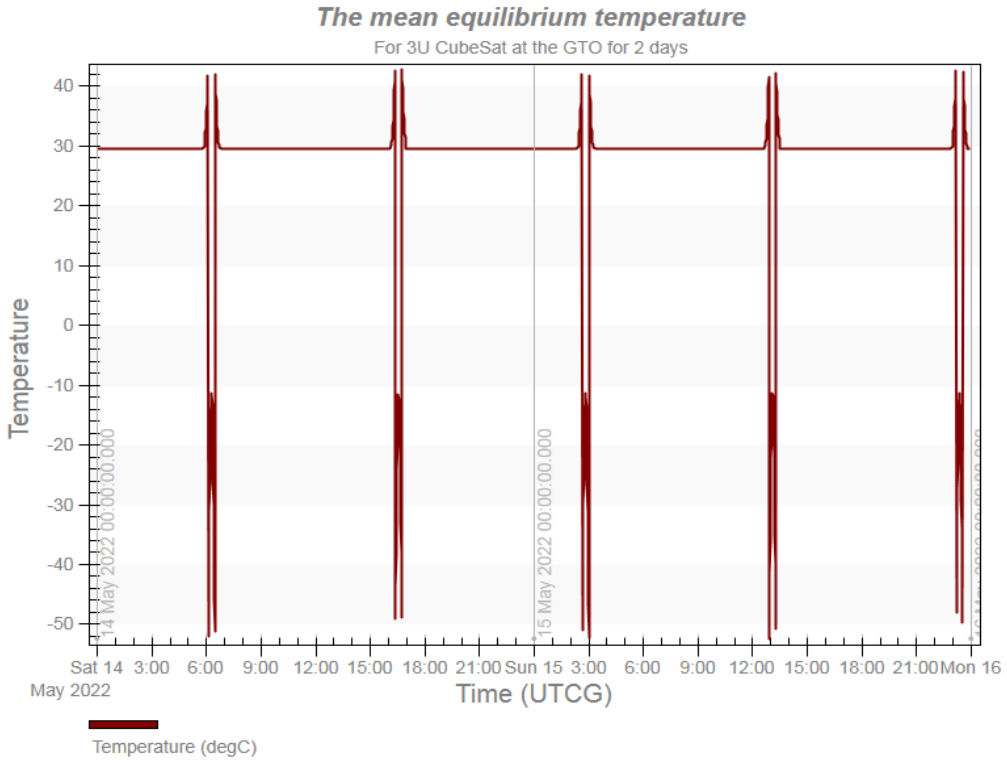

Figure 4.17 Mean equilibrium temperature for a 3U FORESAIL-2 CubeSat at the GTO for a period of 2 days

Figure 4.17 shows that temperature drastically increases when a spacecraft approaches perigee, during perigee, and when it starts ascension. Meanwhile, Figure 4.18 suggests that temperature on the external surface of the satellite would vary according to change in seasons.

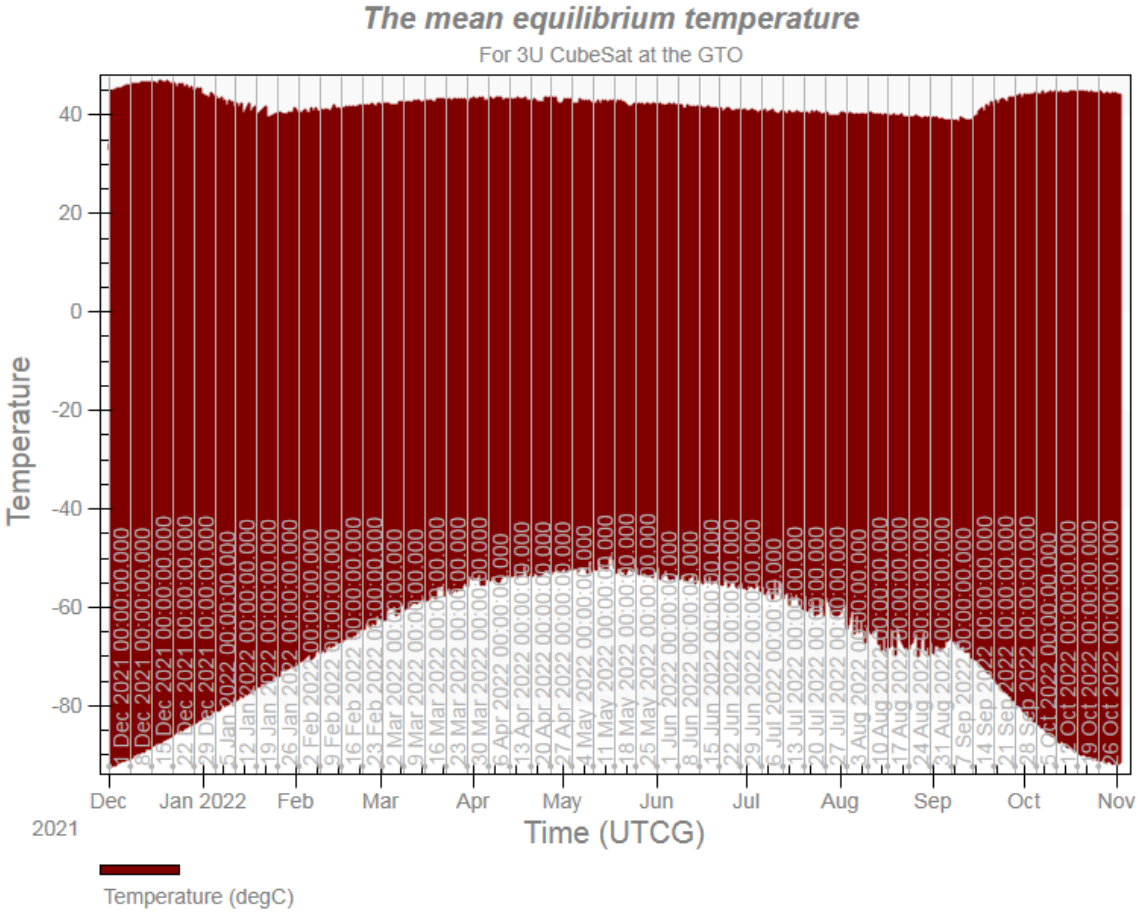

Figure 4.18 The mean equilibrium temperature values for the entire orbital lifetime of FORESAIL-2 at the GTO

While the solar-array temperature would drop quickly, temperature levels of electronic components would not cool rapidly due to the thermal mass presence [130] and would remain within operating temperature. If multi-nodal thermal analysis would show that the cooling rate for some components was too fast, either a finish with lower-emittance coefficient would be required as a passive measure or electric heater as an active measure. Nevertheless, the use of heater should be avoided as it would increase mass, volume, and power required for the CubeSat.

The heat transfer from exterior to the interior of the satellite via aluminium shielding was calculated with the Fourier's Law equation (4.18).

$$q = \frac{k \cdot A \cdot \Delta T}{L} \div 1000\ , \tag{4.18}$$

where

q – conductive heat transfer rate, kW,

k – thermal conductivity of material, W/m °C,

A – area of the shielding, m^2,

ΔT – difference between temperatures a second before eclipse and the lowest one during the eclipse, °C,

L – thickness of the shielding, m.

$$q_{time} = \frac{q \cdot 1000 \cdot t}{1 \times 10^6},$$

where

q_{time} – heat transfer for the duration of eclipse, MJ,

t – duration of the eclipse, s.

The shielding material was selected to be the same as was used for Aalto-1 and FORESAIL-1, Aluminium alloy 7075-T6-T7 [51]. The thermal conductivity of this material was 121,2 W/m °C [51]. Meanwhile, the area of shielding was assumed to be equal to the cross-sectional area of a 3U CubeSat, 0,03 m^2.

The conductive heat transfer analysis was done for the thermal swing during 15 May 2022 lasting 22 minutes or 1320 seconds when the temperature dropped by 92,3 °C. Since the analysis on ionizing radiation showed that one of the optimal shielding thickness values would be 6 mm, this value was used for the following calculation.

$$q = \frac{121.2 \frac{W}{m} °C \cdot 0.03\ m^2 \cdot (42.6\ °C - (-49.7\ °C))}{0.006\ m} \div 1000 = 55{,}9\ kW$$

$$q_{time} = \frac{55.9\ kW \cdot 1000 \cdot 1320\ s}{1 \cdot 10^6} = 73{,}8\ MJ$$

Since the cold case was expected to happen during wintertime and mission was to last not more than 6 months, launching or commissioning satellite at the end of the 1st quarter of a year was suggested to minimize adverse effects of the cold case scenario.

While this analysis did not consider the thermal analysis of the internal environment as it was not possible with the steady-state approach and transient approach would be required instead, it was expected that temperature swing would be slower inside the CubeSat.

On the other hand, it must be noted that frequent temperature cycling could lead to fatigue-related solder joint failures [131]. Nevertheless, the frequency of temperature cycling at the GTO was not more than 2 times per day while it was 15-16 times per day at the Sun Synchronous Orbit (SSO).

4.2.8 Delta-V budget

A rudimentary analysis of the required Delta-v was built based on mission operation requirements and calculations of tether deployment. Required angular velocity was approximated to a linear one and change from current velocity to the required one was calculated (Equation 4.19) [135].

$$v = r \cdot \omega \,, \tag{4.19}$$

$$\omega = \frac{\theta}{s} \cdot \frac{\pi}{180},$$

where

v – linear velocity, m/s,

r – radius taken from the center of spin axis to the wall of the CubeSat, m,

ω – angular speed of the CubeSat, rad/s.

θ – spin rate of the CubeSat, deg/s.

$$\Delta v = I_{sp} g_0 ln \frac{m_0}{m_f},$$

$$m_p = m_0 - m_0 \div e^{\frac{\Delta v}{I_{sp} g_0}},$$

where

ΔV – change of speed of the satellite from a previous one to the desired, m/s,

I_{sp} – specific impulse of the propellant, s,

g_0– gravitational acceleration constant, 9,81 m/s^2,

m_0 – full mass of the satellite, g,

m_f – mass of the satellite after propellant required for dV was expelled, g,

m_p –mass of propellant to required to perform desired dV, g.

It was assumed that once CubeSat would be de-tumbled the first change in spin rate would be to provide 36 deg/s (Table 4.26). This amount of spin rate was defined based on the assumption that with the resolution of 1 degree of phase angle and 10 Hz of sampling rate given in science requirements to this mission magnetometer would be able to sample all 360 degrees of spin. Meanwhile, the spin axis would be perpendicular to the long side of the CubeSat as tether was required to be released along the long side. Therefore, the radius of rotation would be 0,15 m prior to the deployment of the tether. The full mass was assumed to be 5 kg, the maximum allowed mass for a 3U CubeSat, and specific impulses of fully heated butane of 70 s [132], partially heated butane of 43 s [133], and water of 100 s [134], were applied in calculations below.

$$\omega = \frac{36\ deg}{s} \cdot \frac{\pi}{180} = 0{,}628\ rad/s$$

$$v = 0{,}15\ m\ \cdot 0{,}628 \frac{rad}{s} = 0{,}0942\ m/s$$

$$For\ fully\ heated\ butane, m_p = 5000\ g - \ 5000\ g \div e^{\frac{0.0942\ m/s}{70\ s \cdot 9.81\ m/s^2}} = \ 0{,}69\ g$$

$$For\ partially\ heated\ butane, m_p = 5000\ g - \ 5000\ g \div e^{\frac{0.0942\ m/s}{43\ s \cdot 9.81\ m/s^2}} = 1{,}12\ g$$

$$For\ water, m_p = 5000\ g - \ 5000\ g \div e^{\frac{0.0942\ m/s}{100\ s \cdot 9.81\ m/s^2}} = \ 0{,}48\ g$$

Table 4.26 Delta-V budget for the FORESAIL-2 at the GTO

3U and 6U CubeSat with Aluminium tether				
Sequence	Mode	Required spin rate / deg/s	Change in spin rate / deg/s	Delta-v / m/s
1	Initial state	0	0	0,00000
2	Spin stabilized	36	36	0,09425
3	Tether deployment	180	144	0,37699
Spin rate after deployment		6,5394	-173,4606	0,45412
Final state			6,5394	0,92536

The essential estimation of required mass propellant was made with Tsiolkovsky's rocket equation [135]. The propellant mass required to spin a 3U CubeSat from 0 to 36 deg/s was 0,69 g for Butane, 1,12 g for a partially heated Butane with *Isp* of 43 s, and 0,48 g for the selected for FORESAIL-2 water propellant (Table 4.27). The water propellant was found to have higher *Isp* (> 100 s) and energy density compared to Butane [134].

Table 4.27 Required amount of propellant to spin up FORESAIL-2 to 36 deg/s

Butane m_p / g	Partially heated Butane m_p / g	Water (Aurora Propulsion) m_p / g
0,69	1,12	0,48

The spin rate after deployment of the tether and the required mass of propellant were determined by calculating the change in the centre of gravity, angular momentum and impulse. The parameters for tether (Table 4.28) and method of evaluating tether deployment were provided by the inventor of the electric solar wind sail propulsion system [136], Pekka Janhunen of Finnish Meteorological Institute (FMI).

Table 4.28 Parameters for the tether used in measurements of Coulomb Drag force and plasma density

Parameter	Value
Tether tension	1 cN
Endmass	1 g
Tether wire effective multiplicity	4
The radius of a tether wire	17,5e-6 m
Length of a tether	300 m

The analytical estimation of the required final spin rate and propellant mass was produced with the equations from (4.20) to (4.23) [137].

$$\lambda = N_w \pi r_w^2 \rho \,, \tag{4.20}$$

where

λ – linear mass density of the tether, kg·m^{-1},

N_w – wire multiplicity factor, dimensionless,

r_w – tether wire radius, m,

ρ – density of tether material, kg/m^3.

$$m_{tether} = l_{tether}\lambda \,,$$

where

m_{tether} – mass of the tether, kg,

l_{tether} – a full length of the tether, m.

$$x_{cm_{sat}} = -\frac{l_x}{2} \cdot m_{sat} \,,$$

where

$x_{cm_{sat}}$ – center of mass of the satellite, m,

l_x – length of the x-axis of the satellite, m,

m_{sat} – mass of the satellite, kg.

$$x_{cm_{tether}} = \frac{l_{tether}}{2} \cdot m_{tether} \,,$$

where

$x_{cm_{tether}}$ – center of mass of the tether, m,

$$x_{cm_{endmass}} = l_{tether} \cdot m_{endmass} \,,$$

where

$x_{cm_{endmass}}$ – center of mass of the endmass, m,

m_{tether} – mass of the endmass, kg.

$$m_{total} = m_{sat} + m_{tether} + m_{endmass} \,,$$

$$x_{cm} = \frac{x_{cm_{sat}} + x_{cm_{tether}} + x_{cm_{endmass}}}{m_{total}} \,,$$

$$l_{force} = x_{cm} + l_x \,,$$

where

m_{total} – total mass, kg,

x_{cm} – total center of mass, m,

l_{force} – distance of moment arm, m.

$$\omega = \sqrt{\frac{T_{tether}}{0.5\lambda(l_{tether} - x_{cm})^2 + m_{endmass}(l_{tether} - x_{cm})}}, \tag{4.21}$$

where

ω – angular velocity of the satellite after tether deployment, rad/s,

T_{tether} – required tension in the tether, N.

$$L_{final} = \frac{\lambda(l_{tether} - x_{cm}) \cdot 3\omega + m_{endmass}(l_{tether} - x_{cm}) \cdot 2\omega}{3}, \tag{4.22}$$

$$L_{init} = \frac{\lambda(x_{cm}) \cdot 3\omega + m_{sat}\left(x_{cm} + \frac{l_x}{2}\right) \cdot 2\omega}{3},$$

$$L = L_{initial} + L_{final},$$

where

L_{final} – angular momentum for deployed tether, Nms,

$L_{initial}$ – initial angular momentum, Nms,

L – total angular momentum, Nms.

[137]

$$J = \frac{L}{l_{force}}, \tag{4.23}$$

$$m_{prop} = \frac{J}{I_{sp} g_o},$$

where

J – impulse required to change in momentum, Ns,

m_{prop} – mass of propellant required to produce change in momentum, kg,

g_0 – gravitational acceleration constant, 9,81 m/s^2.

$$\lambda = 4\pi \cdot (17.5e^{-6})^2 m \cdot 2.7e^3 \frac{kg}{m^3} = 1{,}04e^{-5}\ kg/m$$

$$m_{tether} = 300\ m \cdot 1.04e^{-5}\frac{kg}{m} = 3{,}1172e^{-3}\ kg$$

$$x_{cm_{sat}} = -\frac{0.34\ m}{2} \cdot 5\ kg = -0{,}85\ m$$

$$x_{cm_{tether}} = \frac{300\ m}{2} \cdot 3.12e^{-3}\ kg = 0{,}4676\ m$$

$$x_{cm_{endmass}} = 300\ m \cdot 1e^{-3} kg = 0{,}3\ m$$

$$m_{total} = 5\ kg + 3.12e^{-3}\ kg + 1e^{-3}\ kg = 5{,}0041\ kg$$

$$x_{cm} = \frac{(-0.85\ m + 0.4676\ m + 0.3m\ )}{5.0041\ kg} = -0{,}01647\ m$$

$$l_{force} = -0.01647\ m + 0.34\ m = 0{,}3235\ m$$

$$\omega = \sqrt{\frac{1e^{-2}\ N}{0.5 \cdot 1.04e^{-5}\frac{kg}{m} \cdot (300\ m\ - x_{cm})^2 + 1e^{-3} \cdot (300\ m - (-0.01647\ m))}}$$

$$= 0{,}1141\frac{rad}{s}\ or\ 6{,}5394\ deg/s$$

$$L_{final} = \frac{\begin{matrix}1.04e^{-5}\frac{kg}{m} \cdot \left(300\ m\ - (-0.01647\ m)\right) \cdot 3\left(01141\frac{rad}{s}\right) \\ + 1e^{-3} \cdot \left(300\ m - (-0.01637)\right) \cdot 2(0.1141\ rad/s)\end{matrix}}{3} = 20{,}9486\ Nms$$

$$L_{init} = \frac{\begin{matrix}1.04e^{-5}\frac{kg}{m}(-0.01647\ m) \cdot 3\left(01141\frac{rad}{s}\right) \\ + 5\ kg\left(-0.01647\ m + \frac{0.34\ m}{2}\right) \cdot 2(0.1141\ rad/s)\end{matrix}}{3} = 0{,}0135\ Nms$$

$$L = 0{,}0135\ Nms + 20{,}9486\ Nms = 20{,}9620\ Nms$$

$$J = \frac{20.9620\ Nms}{0.3235\ m} = 64{,}7914\ Ns$$

$$m_{prop} = \frac{64.7914\ Ns}{70\ s \cdot 9.81\ m/s^2} = 66{,}0462\ g$$

The final spin rate after aluminium tether was deployed was estimated to be 6,5 deg/s and required mass of propulsion in case of water in the resistojet system was 66 grams. The angular momentum and impulse required to deploy tether were 21 Nms and 64,8 Ns, respectively.

4.2.9 Spacecraft System Design

The size of the CubeSat sent to the GTO depends on a volume of payloads, avionics and tank for propellant. Additionally, it must be noted that measures for protection from radiation will require an increase in the thickness of walls, and thus, will lead to increase in the volume required to place avionics and payloads [33]. Finally, the increase to intermediate values such as 4 or 5U between standard 3 and 6U will increase the cost of the launch to 6U due to the standard deployer dimensions [138].

Since the launch of 6U CubeSat will increase costs at least two times as was found in the section on cost estimation, the use of 3U is preferable to satisfy cost budget constraints. On the other hand, the use of 3U increases complexity as the satellite will need higher accuracy and efficiency in its design and fabrication to accommodate all avionics, payloads, and propulsion in a tight space.

The preliminary list of subsystems and associated components for 3U CubeSat was developed based on heritage from FORESAIL-1 mission [126] and the current list of suppliers of payloads and propulsion system (Table 4.29).

Table 4.29 Preliminary list of components to be used in FORESAIL-2 mission

Subsystem	Amount	Model and manufacturer
OBC		
OBC board	1	In-house developed with 2 Texas Instruments Hercules MCUs
EPS		
EPS Board	1	In-house developed with Vorago VA10820 MCU
Solar panels	4	Triple Junction GaAs 30% solar cells mounted on in-house developed panels
Batteries	4	Panasonic 18650 Li-ion cells 2S2P
Battery board	1	In-house developed with MSP430FR
ADCS		
Reaction wheels	3	Hyperion Technologies RW210 3 mNms [139]
Gyroscope	1	New Space stellar gyroscope NSGY-001 [140]
Sun sensors	1	In-house developed
UHF		

Subsystem	Amount	Model and manufacturer
UHF board	1	In-house developed
Antennas	1	In-house developed
Propulsion		
Propellant system	1	Aurora Propulsion
RCS thrusters	8	Aurora Propulsion
Propulsive thrusters	4	Aurora Propulsion
Control board	1	In-house developed
Structure		
Rails	2	In-house developed
Top plate	1	In-house developed
Bottom plate	1	In-house developed
Avionics Shielding	1	In-house developed
Harnessing and integration	1	In-house developed
Payloads		
Relativistic Electron and Proton Experiment (REPE) telescope	1	University of Turku
Magnetometer	1	Aalto University and University of Helsinki
Radiation Mitigation Experiment (RME) board	1	The University of Turku and Aalto University
Coulomb Drag Experiment (CDE) tether	1	FMI
Retroreflectors	1	ETH Zurich and HSLU [141]

The volume estimation (Equation 4.24) was based on actual dimensions of the components available at the moment in FORESAIL-1 [126]. The analysis showed that volume would exceed the limit for a 3U CubeSat by 18%. The most considerable amount of volume consumed was by REPE (40%) followed by CDE tether (22,5%) and avionics stack (28,42%) (Figure 4.19).

$$V_{fraction} = \frac{V_{component}}{V_{3UCubeSat}} \times 100\% , \tag{4.24}$$

where

$V_{fraction}$ – fraction of total volume consumed by the component, %,

$V_{component}$ – volume occupied by the component, cm^3,

$V_{3UCubeSat}$ – the maximum volume allowed for a 3U CubeSat, cm^3.

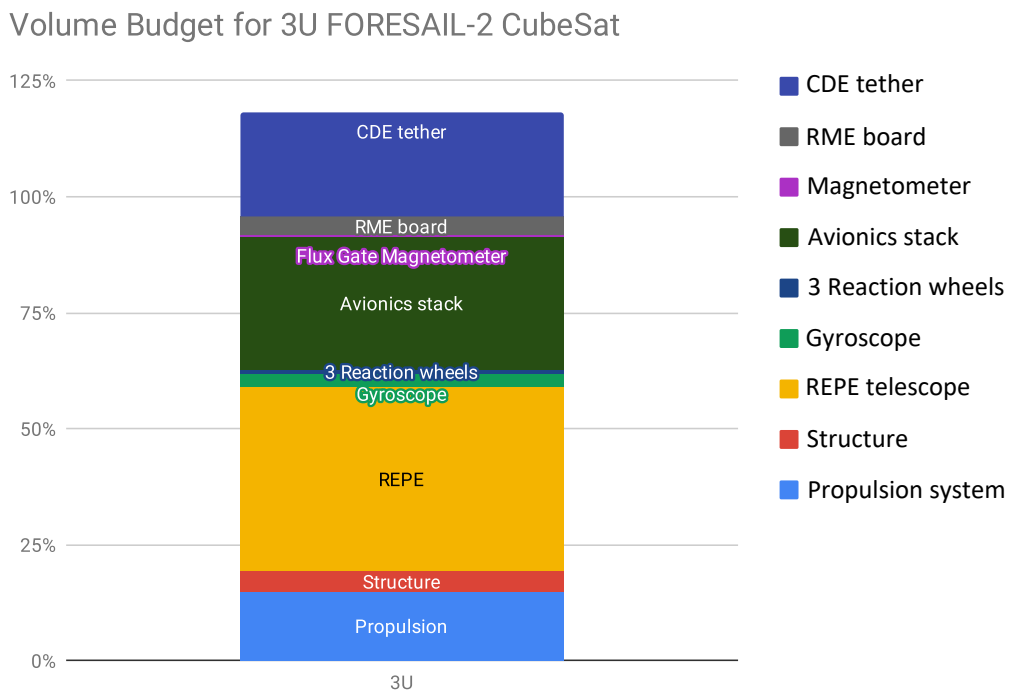

Figure 4.19 Estimation of volume consumption by subsystems and payloads of a 3U FORESAIL-2 CubeSat (Appendix 6). RME board, Flux Gate Magnetometer, reaction wheels, and gyroscope, are positioned off their blocks as their proportion is tiny compared to volume taken by other components.

While the volume was found to exceed the limit with contingencies of 20% for payloads and subsystems and 50% for propulsion, the planned volume without contingencies would have resulted in 140,45 cm^3 of free space. Meanwhile, the mass budget analysis (Equation 4.25) showed that total planned mass of 4860 g would be close to allowed limit of 5000 g for 3U CubeSat [103]. Furthermore, the total mass with contingencies was found to exceed the specified above limit by 800 grams (Appendix 7).

$$m_{fraction} = \frac{m_{component}}{m_{3UCubeSat}} \times 100\% \,, \tag{4.25}$$

where

$m_{fraction}$ – fraction of total mass consumed by the component, %,

$m_{component}$ – mass added by the component, g,

$m_{3UCubeSat}$ – the maximum mass allowed for a 3U CubeSat, g.

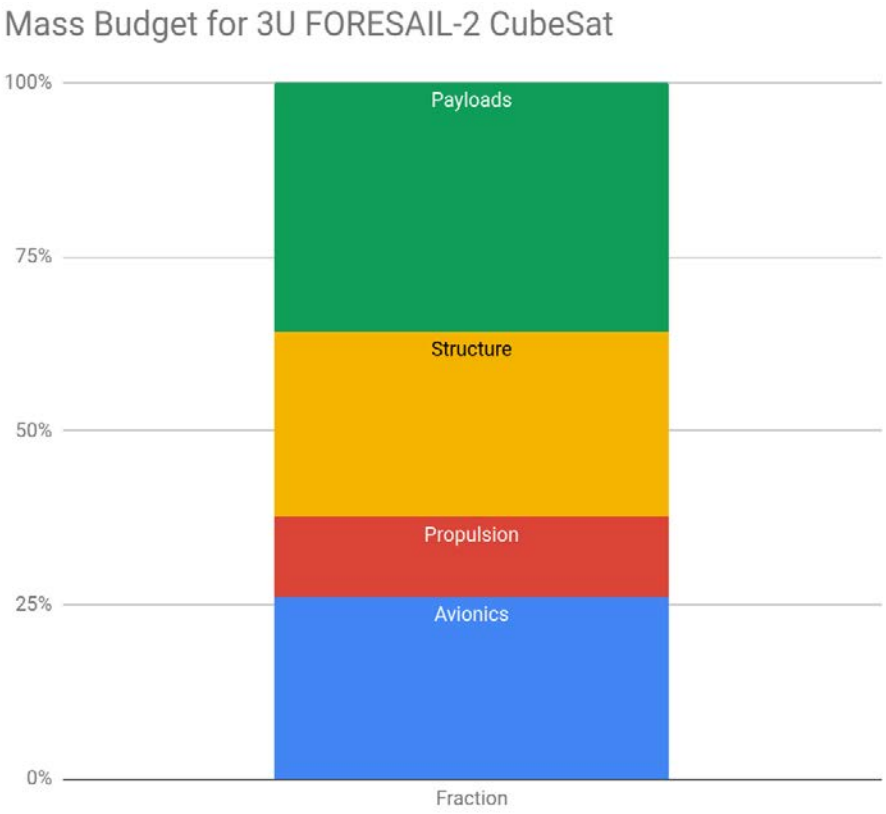

Figure 4.20 Estimation of required total mass for subsystems and payloads onboard of the 3U FORESAIL-2 CubeSat (Appendix 7)

Therefore, FORESAIL-2 has to have a reduced mass and volume or increased engineering effort to ensure that mass stays within planned estimate in order to fit the 3U CubeSat specifications. The most significant contributors to the mass are payloads (35,7%) with REPE leading (20,7%), structure (26,7%) with avionics shielding of 5 mm leading (11,6%), and EPS (16,9%) with solar panels (10,8%) leading.

Deployable on boom magnetometer. Performance of the magnetometer might be affected by magnetic disturbances produced by satellite subsystems such as ADCS [142], and other payloads such as CDE tether deployment mechanism. One of the options to resolve the aforesaid issue is to design subsystems with consideration of return current paths and selection of inductors [143]. Another option is to mount the magnetometer on a deployable boom [142]. Nevertheless, deployed on a boom magnetometer is not protected by spacecraft from harsh radiation environment. The said increases complexity of required design for magnetometer on the boom while leaves the possibility of its implementation within mass and volume constraints.

4.2.10 Technical risk assessment

This section involves technical risk assessment based on comparative analysis, and thus, represents partially an extension of literature review. On the other hand, answers provided in this section complement feasibility analysis of the proposed space mission concept.

The exposure of a CubeSat to high-energy electrons (>100 keV) might lead to internal electrostatic discharge [144]. Furthermore, the exposure of a spacecraft to high-energy protons (>10 MeV) and heavier ions might produce single event effects (SEE). Lastly, the total ionising dose received by a CubeSat at the GTO and region of Van Allen belts, in particular, will lead to degradation of onboard electronics, and thus, shorten a lifetime of a mission [145].

On the other hand, the GTO has its perigee region at altitudes close to the LEO (0 - 2000 km) where low-energy particles are abundant [146]. Therefore, a CubeSat will be exposed to low-energy electrons (<100 keV) which might lead to a surface charging.

During the close pass by of the Earth at the perigee region by a CubeSat, there might be an increased drag applied on the spacecraft due to the thermal expansion of Earth's upper atmosphere during space weather storms [93].

Moreover, communication disruption between a CubeSat and the ground stations is expected due to the possibility of ionospheric irregularities happening in the space [68]. Additionally, attitude determination and control system might be subjected to disruptions due to large storm-time magnetic field fluctuations [144].

The primary mission challenges expected to be at the GTO have been identified and listed in the Risk Assessment Matrix along with an indication of a probability and severity provided risk-wise [144][144], [147].

The most likely hazards to happen are internal and surface ESD and SEE [144] (Table 4.30). Furthermore, the attitude determination might be compromised due to the exposure of star tracker in no small number of protons causing the appearance of false stars.

Table 4.30 List of spacecraft failures with confirmed sources of failure. Noteworthy, not all spacecraft that failed had mission failure since some missions successfully ended before spacecraft failure [144].

Spacecraft	Date	Confirmed cause of failure	Orbit
DSCS II	Feb 1973	Surface ESD	GEO
GOES 4	Nov 1982	Surface ESD	GEO
Feng Yun 1	Jun 1988	ESD	LEO
MARECS A	Mar 1991	Surface ESD	GEO
MSTI	Jan 1993	SEE	SSO
Hipparcos	Aug 1993	Total Radiation Dose	GTO
Olympus	Aug 1993	Micrometeoroid Impact	GEO
SEDS 2	Mar 1994	Micrometeoroid Impact	LEO
MSTI 2	Mar 1994	Micrometeoroid Impact	SSO
IRON 9906	1997	SEE	n/a (Military SAT)
INSAT 2D	Oct 1997	Surface ESD	GEO

Another hazard, surface charging is the largest at the altitude of about 27000 to 29000 km and latitude in the range from 20 to -20 degrees [148]. Since the CubeSat to spend most of its orbit period closer to the apogee region that is above the mentioned altitudes, the risk of surface charging event is low. On the other hand, probability of internal charging was found to be high as the CubeSat will cross areas with orbit altitude higher than 10000 km and inclination less than 45 degrees.

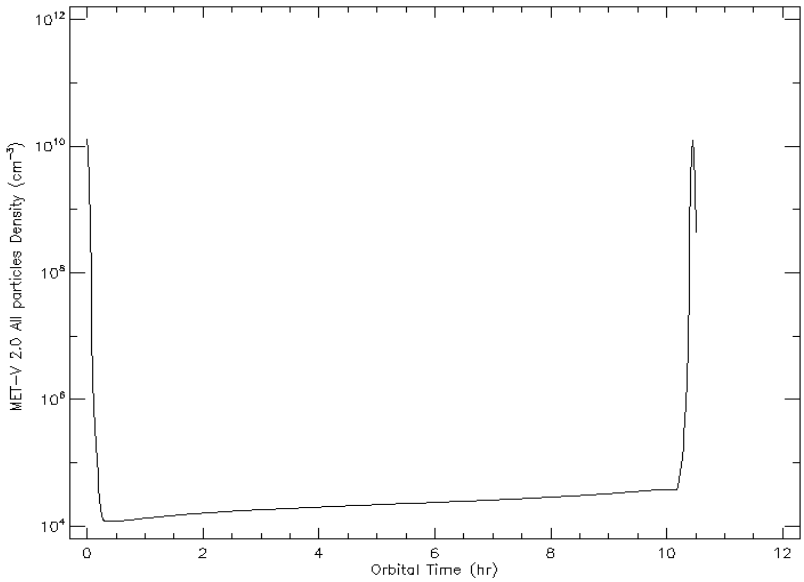

Figure 4.21 Graph shows the density of all particles in the upper layers of atmosphere for the FORESAIL-2 at the GTO modelled in SPENVIS

Atomic oxygen impact on surface erosion was found to be low for most of the orbit period as seen in Figure 4.21. Therefore, the probability of this risk taking place during the mission was concluded to be low.

4.2.11 Technical margins

There are many technical challenges associated with the CubeSat mission to the GTO. Nevertheless, the critical aspects affecting the future of the mission have been identified as the following ones:

Attitude Determination and Control System. The spacecraft will require constant adjustment of its pointing to ensure that the spin axis is perpendicular to the magnetic field vector. Furthermore, science observations will require ADS to provide minimum pointing knowledge of 0,6° of phase angle. Moreover, the analysis of geomagnetic conjugacy demonstrated that CubeSat will be deprived of magnetorquers and have only reaction wheels and propulsion system. Besides, a number of CubeSat missions in the past such as Dellinger had experienced problems with ADS sensors which were solved by having a redundant sensor onboard. Therefore, a margin in the form redundancy must be provided.

Thermal Control System. The surface of the spacecraft will be subjected to temperature swings in the order of 100° C. This will produce stress on the structure of the satellite and will degrade performance and lifetime of batteries. Therefore, margin must be provided in terms of the power required for heating.

Protection from radiation. The spacecraft will be subjected to high doses of radiation. While the minimum most COTS are able to withstand is 10 krad, margin must be given in terms of smaller ratings for screened packages and higher required thickness for shielding. Furthermore, it must be noted that shielding was found to be non-efficient against protons.

Communication system. While the link with the ground station at Otaniemi is maintained for a mean time of 6,5 hours, the vast distances between spacecraft and ground station lead to an increase in signal-to-noise ratio. The disturbed downlink might reduce science return from the mission. The said must be considered, and margins must be added to the power for transmission.

Propulsion system. The propulsion system is required to provide enough angular momentum for tether deployment and dumping momentum produced by reaction wheels. Mishandling the propulsion system might lead to the failure of the mission. The propulsion system will require power for heating to increase specific impulse of stored liquid and enough mass and volume available for propellant. Therefore, margin must be given to power required for heating and mass of propellant.

The technology challenges must address mission challenges to ensure the success of the mission. Noteworthy, technology challenges must be taken into account not only by engineers working on a satellite platform but by scientists as science payloads are to be subjected to the same environmental hazards.

The surface charging was found to be the most probable and most fatal risk for spacecraft in the GTO. The internal ESD was found to be present due to high geomagnetic activities, while surface ESD was believed to be a cause of rapid transition through cold and hot plasma. Therefore, properties of resistivity of materials must be given a margin [149] [150].

4.2.12 CML Review

The analysis of available launchers and orbit lifetime and evolution showed that mission requirements were feasible to fulfil. On the other hand, spacecraft requirements were possible to fulfil with certain conditions being satisfied only (Table 4.31).

Table 4.31 Feasibility assessment based on the results of concept studies at CML 2

Requirement	Value	Feasibility assessment
Mission length	> 6 months	Feasible for 6 months only, with rad-tolerant components and shielding with 5 mm of thickness minimum.
Orbit altitude	Perigee > 180 and apogee > 12756 km	Feasible due to availability of launchers and orbit evolution
Geographic coverage	Latitude within 30° N and 30° S	Feasible due to availability of launchers within the region
Orbit local time	Wide coverage of MLT	RAAN drifts by 57,7° for 6 months with a rate of 0,4 °/day. Feasible.
Type of orbit	HEO with i < 45°	Launchers are available to the GTO. Feasible.
Other mission requirements	Must cross Van Allen belts	Launchers available to the GTO which traverses through GTO

Requirement	Value	Feasibility assessment
Stabilization	Spin stabilized with spin axis pointing perpendicular to the magnetic field vector	Feasible with a magnetometer, reaction wheels and thrusters
Volume	Not more than 3000 cm^3	Volume with contingencies does not satisfy this requirement. Planned volume is within limits
Mass	Around 1.5 kg for payload	Mass with contingencies does not satisfy this requirement. Planned mass is within limits
Power	> 7 W	Feasible only with deployed solar panels (30x30 cm).
Data rate	441 bit/s (4,44 Mbytes/day)	Feasible. Required downlink time is 16,2 mins, while the mean communication time window is 6,5 h
Temperature range	- 40 °C to 85 °C	Feasible with a battery heating. The mean temperature is 27,3 °C
Position knowledge	100 - 1000 km	Feasible. Tracked with reflectors at perigee and spacecraft orbit is propagated.
Radiation shielding	> 10 krad	Feasible with a minimum of 5 mm of shielding thickness for 6 months and 7 mm for 1 year
Other spacecraft requirements	Fit within nanosatellite class of spacecraft	Partially feasible. Occupies 85% of the 3U volume but has issues with requirements for total mass.

While link budget was within constraints of available technology and 3U CubeSat standard specifications, volume, mass and power budgets were in a risk category. The planned total mass was estimated to be 4860 grams while the mass with contingencies exceeded the maximum allowed for 3U CubeSats total mass by 800 grams. Meanwhile, the planned total volume was estimated to be 2859,6 cm^3 while the volume with contingencies exceeded the maximum allowed for 3U CubeSats total volume by 547,83 cm^3. It means that mission with 3U is possible only if the volume and mass budget is within planned total mass and volume or mass and volume with contingencies reduces below 5 kg and 3000 cm^3 limit, respectively.

Furthermore, power consumption for the 2nd observation phase where all science instruments except RME board were producing measurements simultaneously was found to be 8,8 W. Meanwhile one solar panel was able to produce mean power of 6,89 W while at the GTO.

A 3U CubeSat was found to be capable of having four (4) solar panels attached to its sides. On the other hand, the power generated in this configuration would be effectively of one panel only as with spinning CubeSat only one side will be oriented towards the sun with 34,76 Wh of the deficit. Therefore, the risk associated with a low power availability must be addressed to ensure flawless execution of mission operations. One of the ways to resolve the issue with low power is to deploy solar panels and orient that side of the CubeSat perpendicular to sun vector.

The mean power produced with deployed solar panels on the 3U CubeSat was 20,7 W with an excess of 98,74 Wh. While the amount of excess power is relatively large, it must be taken into consideration that displacement damage dose (DDD) will cause degradation of solar cells leading to a drop in the amount of energy produced.

The mentioned above situation with power consumption was related to breakthrough science case where REPE, magnetometer and CD tether were employed simultaneously. If only REPE and magnetometer used, then power consumption would fall to 6,9 W.

Therefore, a 3U CubeSat must have deployable solar panels and planned total mass without contingencies regardless of science case being breakthrough or enabling. If the mission lifetime exceeds six months, a more significant thickness of shielding would be required such as 6 to 8 mm. If the thickness of shielding for avionics increases to 6 or 7 mm, the mass would increase to 670 and 780 grams, respectively. The FORESAIL-2 mission 3U CubeSat is conditionally feasible, and thus, trade space analysis can be performed for this concept.

Since the 3U CubeSat was found to be close to limits in total planned mass and volume and exceeded allowed total mass and volume with contingencies by 800 grams and 423,2 cm^3 respectively, the next possible CubeSat configuration was considered. The next to 3U standard size allowed for launches to space is 6U.

Therefore, the baseline mission for FORESAIL-2 is a flight with a 3U CubeSat with deployed solar panels and a mission duration of 6 months, while the threshold one is a flight with a 6U CubeSat with a mission lifetime of 1 year. The next section will compare 3U and 6U and provide other related trade space studies.

4.3 CML 3: Trade space analysis

The trade space analysis will be built upon results of CML 2 where the baseline was defined as 3U CubeSat and threshold as 6U CubeSat. Therefore, trade space analysis will be produced to explore opportunities for launches with a 6U CubeSat.

4.3.1 Launch services

The previous section explored opportunities with launches from Cape Canaveral with either Atlas V or Falcon 9 for a 3U CubeSat. The orbit evolution for launches from Kourou with Ariane 5 and Satish Dhawan Space Centre with GSLV II for 3U and 6U CubeSats will be explored in this section with the STK utilizing equations from (4.1) to (4.6).

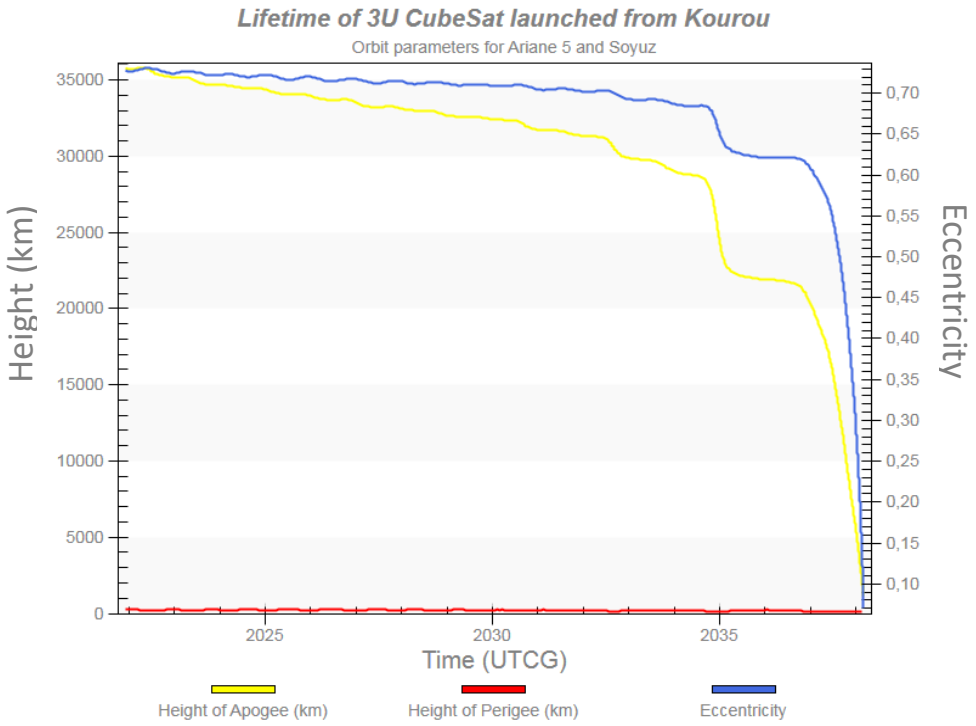

Figure 4.24 Orbital lifetime of a 3U CubeSat launched to the GTO from Guiana Space Centre with Ariane 5 and Soyuz rockets. Left axis represents values in *km* for heights of apogee and perigee while right axis provides values for eccentricity.

The launch from Kourou was found to increase lifetime to 16,2 years with 17711 orbits (Figure 4.24) for a 3U CubeSat while the lifetime of a 6U CubeSat was found to be 15,5 years with 16280 orbits Figure 4.25.

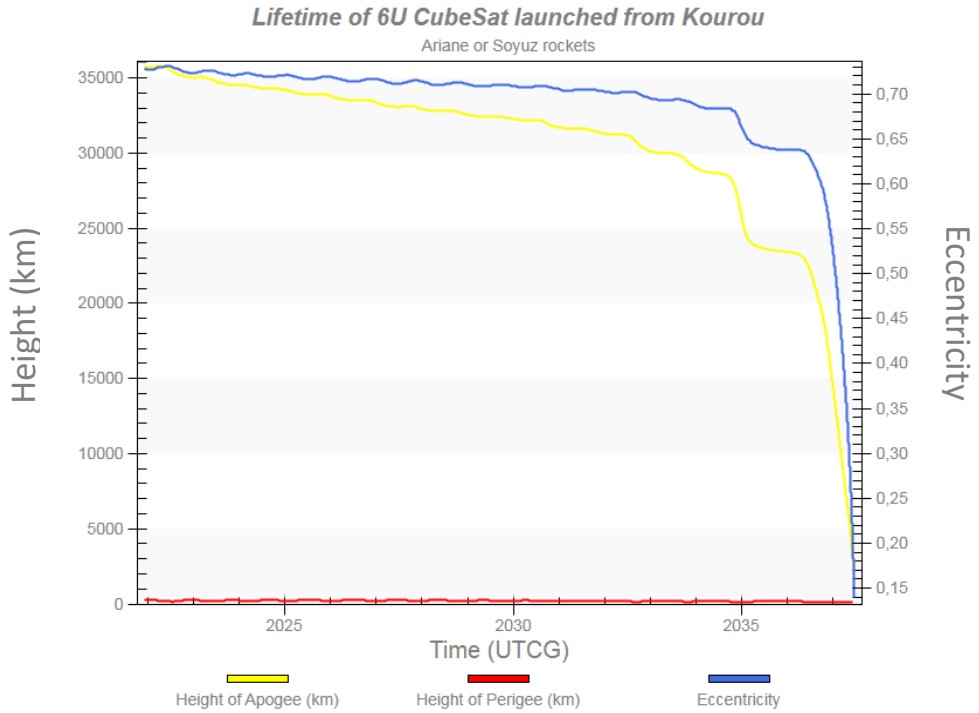

Figure 4.25 Orbital lifetime of a 6U CubeSat launched to the GTO from Guiana Space Centre with Ariane 5 and Soyuz rockets. Left axis represents values in *km* for heights of apogee and perigee while right axis provides values for eccentricity.

Since orbit evolution of GTO was found to be predictable before solar apsidal resonance takes place, it is desirable that orbit decays in a span of the first five (5) years [96]. Nevertheless, if FORESAIL-2 is launched from Kourou with either Ariane or Soyuz rocket, there is a reasonable probability that this CubeSat will not decay within 25 years as chance is that the solar apsidal resonance will happen [96].

Launch of a 3U CubeSat from Satish Dhawan Space Centre in India was found to increase orbital lifetime to 3.6 years with a total of 4269 orbits (Figure 4.26). While this option is suitable for the launch of FORESAIL-2, it must be taken into account that primary payloads are communication satellites which do manoeuvres to transfer to GEO and thus, the standard perigee height for launches of GSLV II is 170 km. This low height of perigee together with known fluctuations might lead to premature decay of the spacecraft, and thus, propulsion might be required to increase the height of perigee if this option for launch is selected.

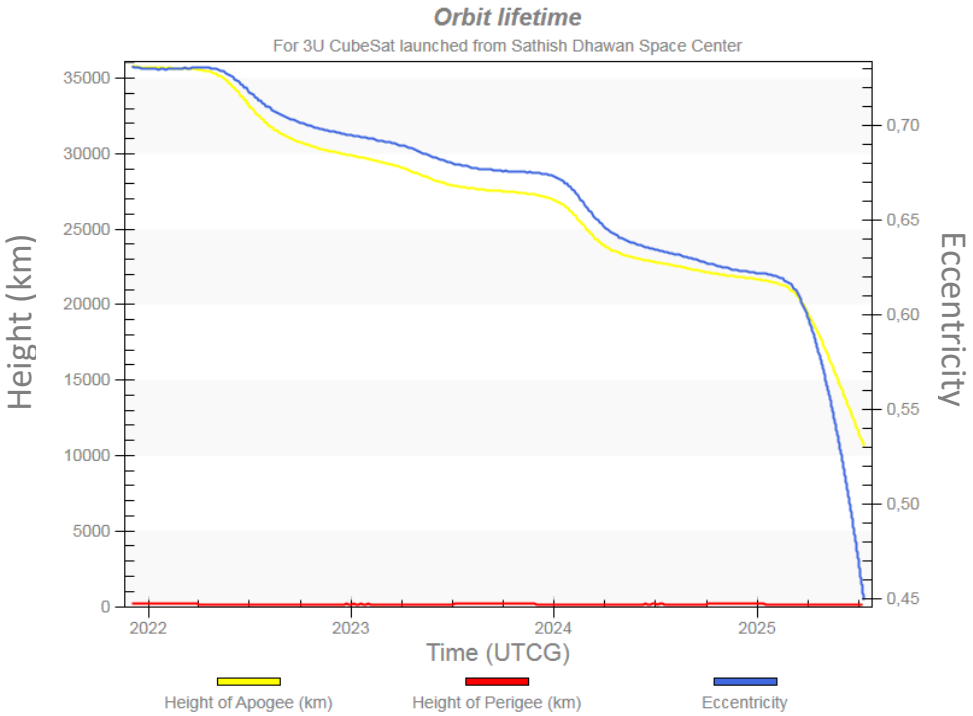

Figure 4.26 Orbital lifetime of a 3U CubeSat launched to the GTO from the Satish Dhawan Space Centre with GSLV II. Left axis represents values in *km* for heights of apogee and perigee while right axis provides values for eccentricity.

Finally, a 6U CubeSat launched from Cape Canaveral with Atlas V or Falcon 9 was found to have nearly the same orbital lifetime as the 3U CubeSat with a total of 871 orbits (Figure 4.27). Therefore, the most suitable for FORESAIL-2 launch site and rockets would be Cape Canaveral US Air Force Base and Atlas V or Falcon 9, respectively.

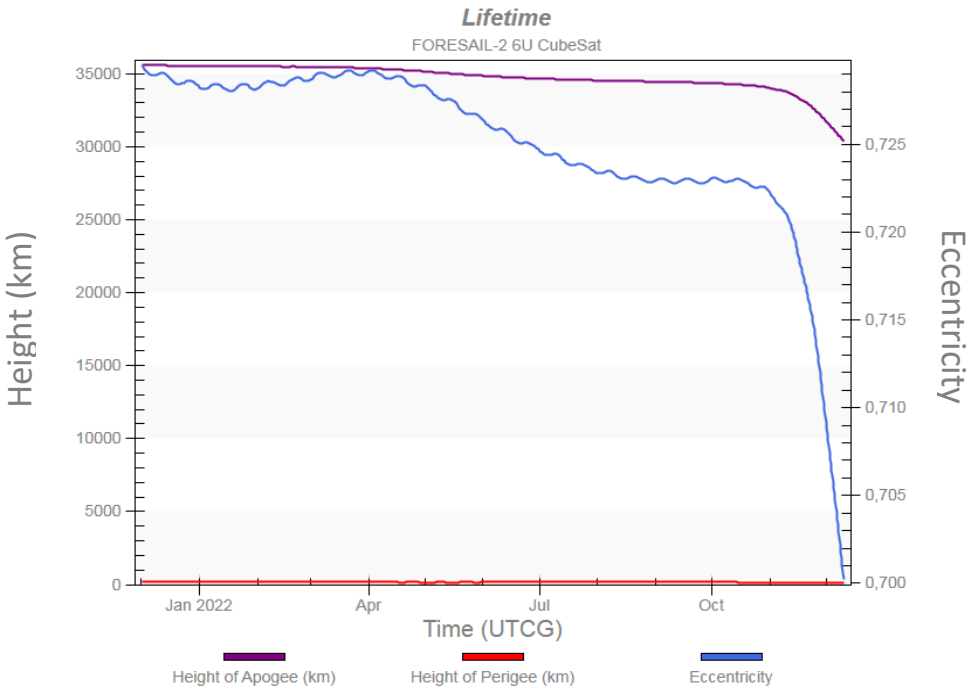

Figure 4.27 Orbital lifetime of a 6U CubeSat launched to the GTO from Cape Canaveral US Air Force Base with Atlas V or Falcon 9 rockets. Left axis represents values in *km* for heights of apogee and perigee while right axis provides values for eccentricity.

4.3.2 Science observation scenarios

Different science observation scenarios were produced to evaluate the impact of different orbit evolutions and system design configurations towards the operation of science instruments.

Science scenario 1: Mission reduced to 6 months period. The previous section discussed properties of the orbit for one (1) year lifetime while another scenario could be that mission lasts six (6) months only. The effect of reduced mission lifetime is investigated in relation to orbital mechanics and science goals, and according to equations (4.4 – 4.6).

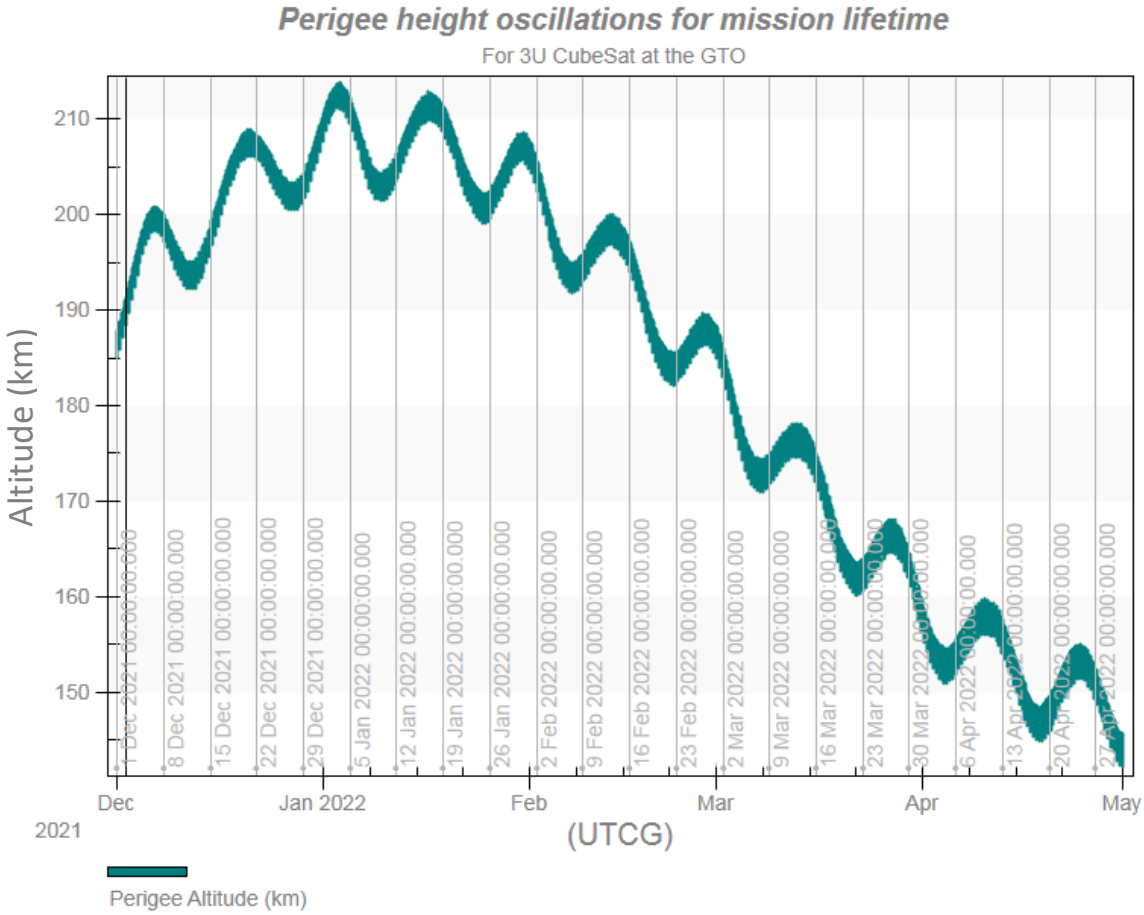

Figure 4.28 Fluctuation in the height of perigee for the 3U CubeSat mission to the GTO with the lifetime of six month. Left axis represents values in *km* for height of perigee.

The perigee height for a 6-month mission will have small oscillations and one (1) significant fluctuation going first upwards and then reducing to less than 150 km (Figure 4.28). These oscillations were found to have no positive or negative contribution to the science goals fulfilled with REPE telescope and magnetometer since ranges of interest were more than 2 Earth radii.

On the other hand, CDE tether might benefit from fluctuations of perigee height since the requirement for CDE force measurements specifies a range of up to 2 Earth radii. Meanwhile, released tether at low altitudes might contribute to faster decay due to interaction with Earth atmosphere.

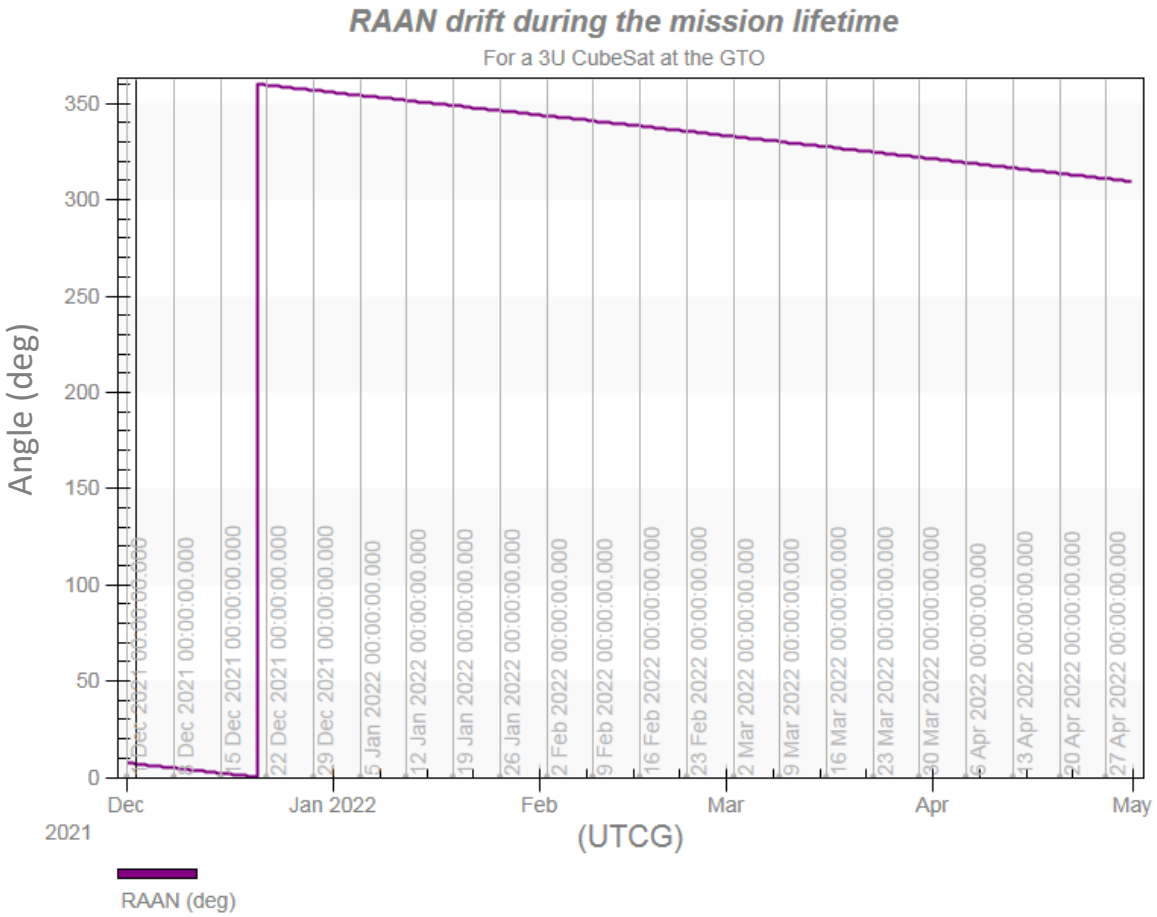

Figure 4.29 Drift rate of RAAN for the 3U CubeSat mission at the GTO with a lifetime of six months. Left axis represents values in *degrees* for RAAN.

The RAAN was found to drift by a total of 57,7 degrees during 6 months with a mean rate of 0,4 degrees per day (Figure 4.29). While 6 months mission produces 89,3 degrees less of RAAN drift than a 1-year mission, it provides relatively comprehensive coverage of MLT to satisfy measurement goals for REPE and magnetometer. Noteworthy, it was found from these simulations that the rate of RAAN drift was accelerating proportionally with the orbital lifetime.

Science scenario: changes in speed and speed rate. The REPE, magnetometer and CDE tether will benefit from lower speeds which will allow for better accuracy of mapping electron and plasma densities in the plasmasphere. Therefore, the propagated GTO was evaluated in terms of the speed at different segments and compared between 3U and 6U CubeSats.

Table 4.34 A summary on findings on speed and speed rate of 3U and 6U CubeSats at the GTO

FORESAIL-2	Parameter	Value	Date
3U	Max Speed	10,28 km/sec	1 May 2022 16:10
	Mean Speed	3,48 km/sec	-
	Min Speed	1,6 km/sec	1 Dec 2021 05:13
	Max Speed Rate	9,01 km/sec^2	13 Nov 2022 20:05
6U	Max Speed	10,28 km/sec	12 Nov 2022 04:45
	Mean Speed	3,48 km/sec	-
	Min Speed	1,6 km/sec	1 Dec 2021 05:13
	Max Speed Rate	9,02 km/ sec^2	13 Nov 2022 19:55

While the science requirement is to have measurements in all regions with a focus on areas close to plasmapause which are near to the apogee of the GTO, the minimum speed of 1,6 km/sec would allow for a better accuracy of mapping at apogee where speed would be the slowest (Table 4.34). The reason for that are sampling rate constraints of science instruments. The speed at the perigee is estimated to be around 10 km/sec according to the conservation of energy [49] equation (4.26) used in the STK along with equation (4.1).

$$\frac{v^2}{2} - \frac{\mu}{r} = -\frac{\mu}{2a}, \tag{4.26}$$

where

v – velocity relative to Earth atmosphere, m/s,

μ – standard gravitational parameter, $m^3\ s^{-2}$,

r – position relative to the center of the Earth, m,

a – semimajor axis, m.

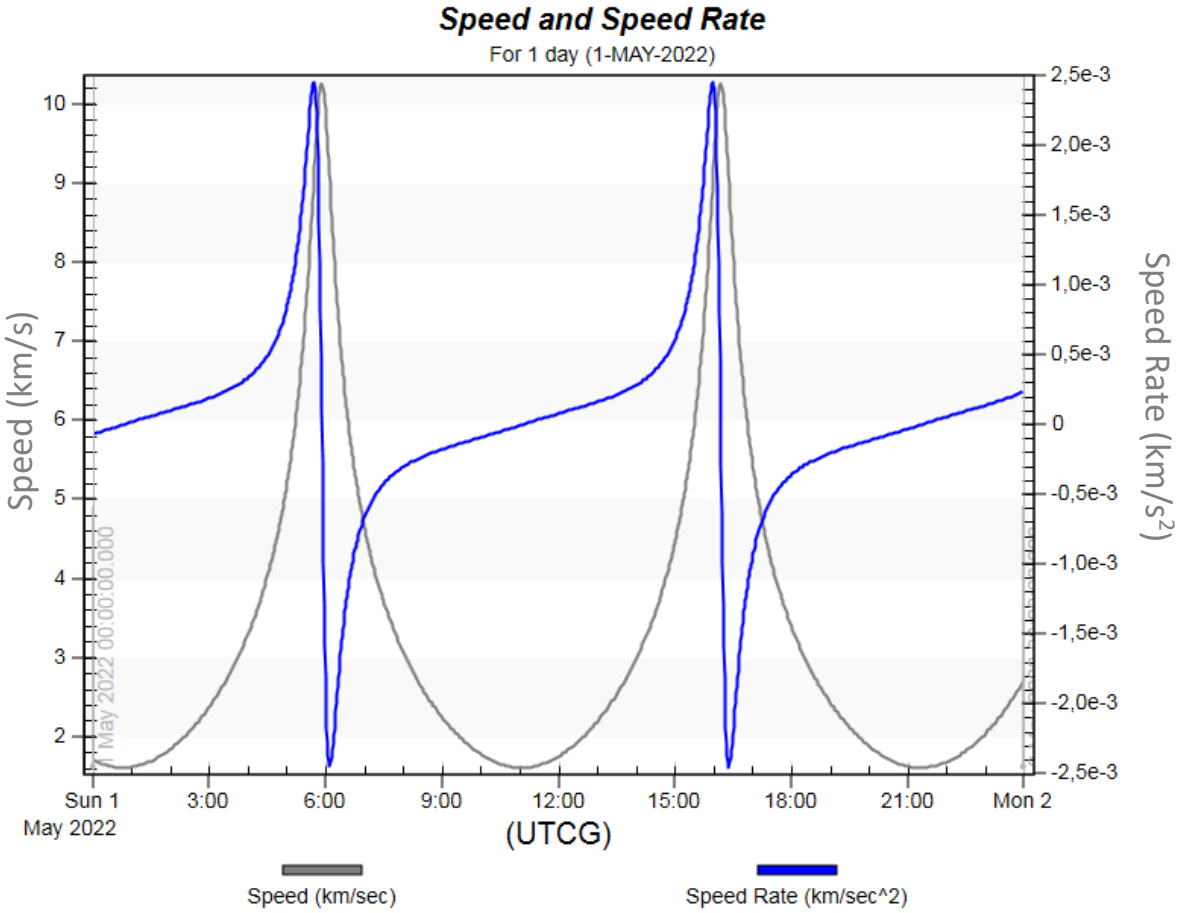

Figure 4.30 Graph of speed and speed rate of the 3U FORESAIL-2 CubeSat at the GTO. Left axis represents speed in km/sec while the right axis provides speed rate in km/sec^2

The speed and speed rate of 3U and 6U CubeSat were found to be the same (Figure 4.30). Thus, the change in dimensions and mass was negligible to produce a change in momentum.

Science scenario: Different tether materials for CDE. There are two science scenarios for Coulomb Drag Experiment (CDE) suggested by the Principal Investigator (PI) of this experiment, Pekka Janhunen [137]. The first science seed in CDE is the use of aluminium tether while the second science seed deals gold tether. The evaluation of these seeds was based on equations (4.20 – 4.23). Aluminium tether of 300 m length will require less angular momentum, but more significant impulse will be needed for reeling out as compared to gold tether.

On the other hand, since gold tether will need lower impulse than aluminium one, the required propellant mass of cold gas would be less. Therefore, the gold tether would be preferred if the aim is to use less propellant mass. On the other hand, gold tether weighs 7,15 times more than aluminium, while the difference in propellant mass consumption between aluminium and gold is in the order of 1,5 or 29,7 grams.

While the difference between the mass of tethers of different materials is only 19,2 grams, the more substantial weight of tether would be preferred as it gives less uncertainty to successful deployment than the presence of a larger mass of propellant. It must be noted that calculation assumes particular *Isp* which depends on a degree of heating; thus, the risk is higher to have less Isp than that larger mass of tether would have different requirement for impulse.

Furthermore, the initial assumption of the specific impulse being 70 s might be idealistic in case of butane as it would require pressure in tank maintained at a certain level [133]. Frequent heating would be required to keep pressure in the tank high enough to have required specific impulse. Heating of the tank would draw current and reduce available for payloads electric power.

Therefore, the assumption was made based on the performance of SNAP-1 propulsion system where *Isp* was expected to be 70 s but turned out to be 43 s only, that CubeSat with butane based cold gas propulsion system at the GTO would have *Isp* of 43 s [133] instead. The lower *Isp* would require 137 grams of propellant for aluminium tether and 87,5 grams for a gold one. Another option would be to use water-based resistojet propulsion system such as developed by a potential partner of FORESAIL project, Aurora Propulsion company. It is estimated that this propulsion system would be able to give a minimum *Isp* of 100 s consuming nearly two and three (2,3) times less propellant mass needed to reel out a tether (Table 4.35). All calculations done below utilized equations (4.19) provided in the previous section where the delta-v budget was estimated.

Table 4.35 Trade space on tether materials, propellants, and sizes of CubeSat

Type of CubeSat	Tether material	Propellant mass / *Isp* / 70 s	Propellant mass / *Isp* / 43 s	Propellant mass / *Isp* / 100 s [134]
3U	**Aluminium** Spin period 55,0507 s Angular momentum 20,962 Nms Impulse 64,7914 Ns	94,3 grams	154 grams	66 grams
	Gold Spin period 119,7583 s Angular momentum 39,7561 Nms Impulse 44,3423 Ns	64,6 grams	105,1 grams	45,2 grams
6U	**Aluminium** Spin period 55,065 s	125,1 grams	203,7 grams	87,6 grams

Type of CubeSat	Tether material	Propellant mass / *Isp* / 70 s	Propellant mass / *Isp* / 43 s	Propellant mass / *Isp* / 100 s [134]
	Angular momentum 20,966 Nms Impulse 85,9244 Ns			
	Gold Spin period 119,92 s Angular momentum 39,8 Nms Impulse 82,2734 Ns	119,8 grams	195 grams	83,9 grams

The final spin rate after deployment of aluminium tether was found to be 6,5 deg/s and 3 deg/s for gold, respectively, regardless of the size of a CubeSat.

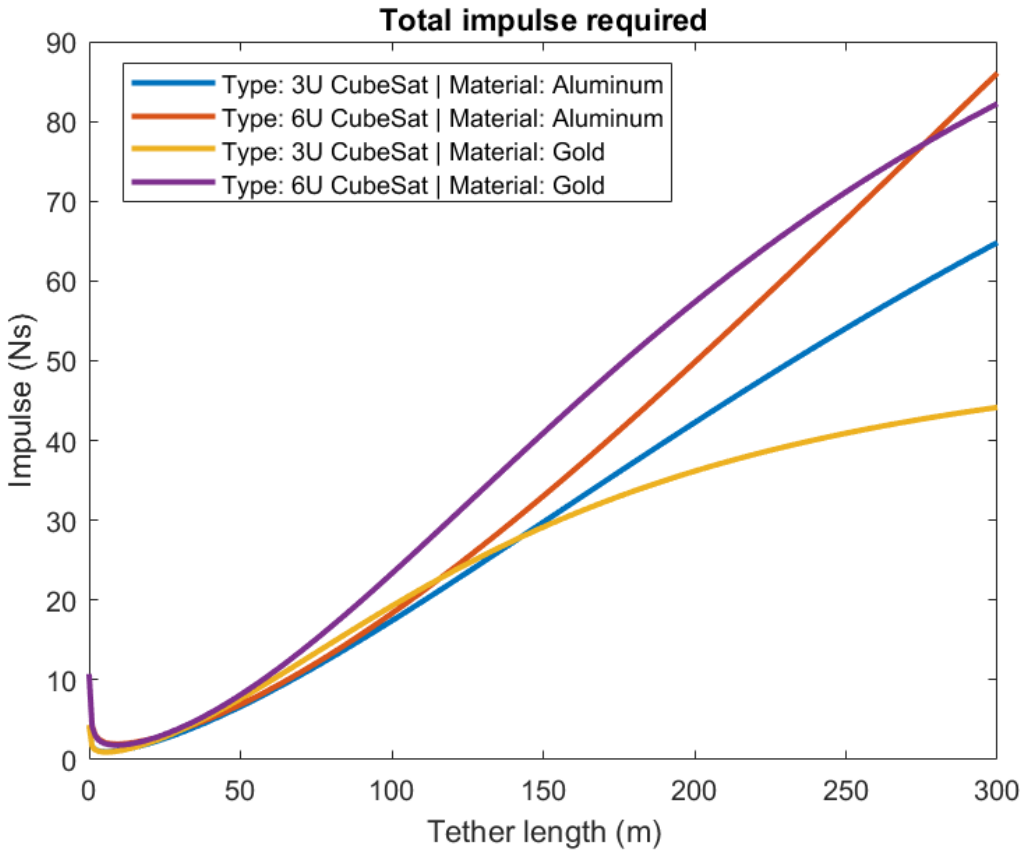

Figure 4.31 Total impulse required to deploy aluminium and gold tether from a 3U and 6U CubeSat (Appendix 9)

The total impulse required to deploy the full length of aluminium tether in case of a 3U CubeSat was 64,8 Ns (Figure 4.31). On the other hand, a 6U CubeSat with the same type of tether material required more significant impulse amounting to 85,9 Ns due increase in mass and volume as

compared to 3U CubeSat. Meanwhile, the total impulse required to deploy the full length of gold tether in case of a 3U CubeSat was 44,3 Ns which was 1,5 times less than in case of the aluminium tether.

Finally, a 6U CubeSat required for deployment of gold tether 82,3 Ns of impulse which was smaller only by 3,6 Ns when compared to the requirement of aluminium tether deployment. Therefore, since there is a significant difference between required impulses for 3U CubeSat with different tether materials, more effort must be given to compare and evaluate different possible tether materials. On the other hand, if a 6U CubeSat to be launched, the selection of tether material does not play a significant role and can be ignored.

The change in the delta-v budget in case gold tether is used would be 0,00926 m/s more compared to the delta-v budget for 3U CubeSat with aluminium tether (Table 4.36).

Table 4.36 Delta-V budget with deployment of gold tether from the body of 3U and 6U CubeSats

Sequence	Mode	Required spin rate / deg/s	Change in spin rate / deg/s	Delta-v / m/s
1	Initial state	0	0	0,00000
2	Spin stabilized	36	36	0,09425
3	Tether deployment	180	144	0,37699
Spin rate after deployment		3,0019	-176,9981	0,46338
Final state			3,0019	0,93462

4.3.3 Power supply

A 6U CubeSat on GTO was found to produce more than 19 W of power (Figure 4.32) without deploying any solar panels according to equation (4.15). Since 3U CubeSat will have to deploy solar panel to satisfy requirements for power, 6U is a better option in this case as it has no risk of deployment mechanism failing to deploy panels.

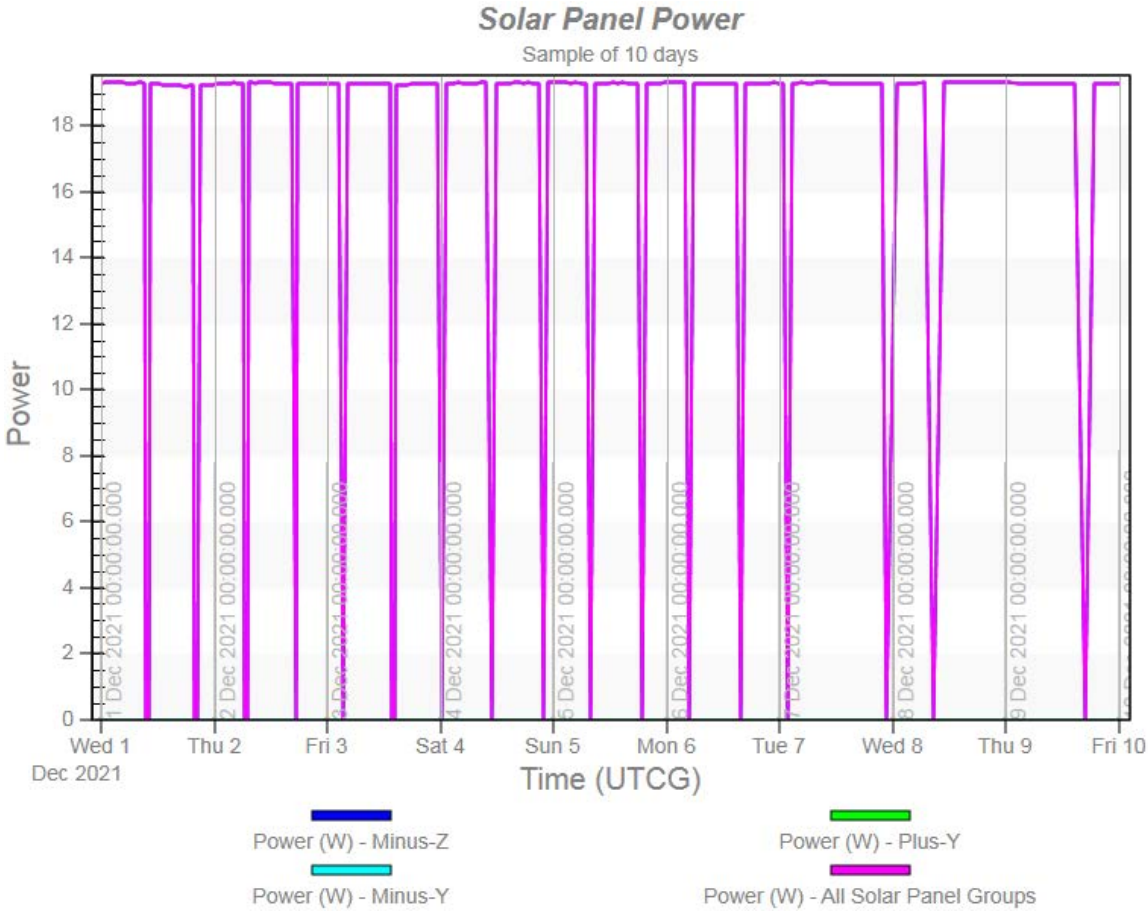

Figure 4.32 Graph with solar panel power production for the 6U CubeSat with the sun vector perpendicular to Minus-Z side

4.3.4 Thermal conditions

The initial parameters for thermal modelling were set the same as for the 3U CubeSat with only difference in cross-section area of the plate (Table 4.37). Meanwhile, the same equation (4.17) as in the previous section was used in this case.

Table 4.37 Initial parameters for temperature modelling of FORESAIL-2 6U CubeSat

Solar Flux at 1AU	1365.078 W/m^2
Earth Albedo	0,30
Shape	Plate
Cross-section area	6U 0,06 m^2
Material Emissivity	0,80 (assuming the emissivity of triple junction GaAs solar panels) [102]
Material Absorptivity	0,26 (assuming absorptivity of plain anodized aluminium) [102]

Normal vector	Sun
Internal Power Dissipation (Losses)	6U 90% efficient DC-DC converter (1 W)

The plot for the mean equilibrium temperature for 6U CubeSat shows the same pattern as for 3U CubeSat. The minimum temperature for a 6U CubeSat was found to be -110,6 degrees ℃, while maximum and mean were 44 ℃ and 23,7 ℃, respectively.

Thermal condition analysis in the previous section was done for the orbital period until its decay amounting to nearly one (1) year. Nevertheless, it was hypothesized that if the same CubeSat was launched for a period of six (6) months as required by the scientists of the mission and avoiding winter, the thermal swing would be reduced. Therefore, the isothermal node model was created for a 3U CubeSat launched on the 21st of March 2022 with a period of six (6) months (Figure 4.35).

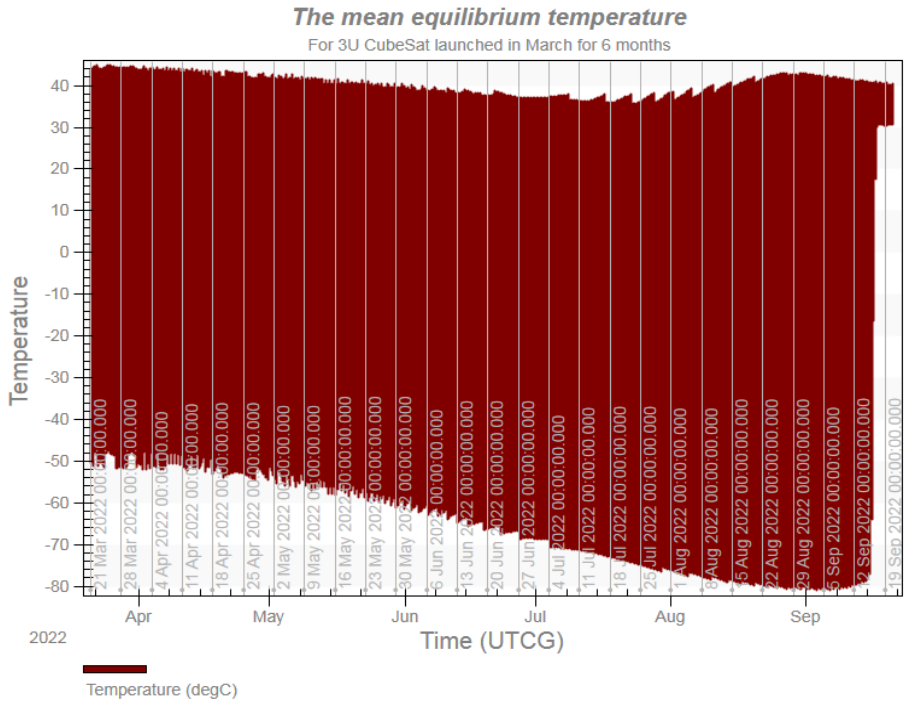

Figure 4.35 Mean equilibrium temperature of the 3U CubeSat launched in March 2022 to the GTO for a mission lifetime of six months

While the thermal swing was reduced to 139 ℃, the mean temperature increased to 28,3 ℃ with 46,9 ℃ as maximum and -92,5 ℃ as minimum temperatures (Table 4.38).

Table 4.38 Summary of thermal condition analysis for the 3U CubeSat launched from Cape Canaveral with Atlas V or Falcon 9 rockets

	Max Temperature	46,9 ℃	17 Dec 2021 12:51

3U (<6 months)	Min Temperature	-92,5 ℃	1 Dec 2021 09:11
	Mean Temperature	28,3 ℃	-

Furthermore, the same 3U CubeSat was modelled for launch from Kourou for a period of 6 months. Noteworthy, the launch from Kourou produced lower mean temperature and thermal swing compared to the launch from Cape Canaveral. The change of inclination is believed to cause this difference between initial orbits of rockets launched from these launch sites.

While thermal swing was reduced by putting all mission phases from April to October and avoiding winter, the orbital lifetime increased to 54,6 years (Figure 4.36). This meant that the de-orbiting mechanism would have been required and there was a high likelihood to have a solar apsidal resonance.

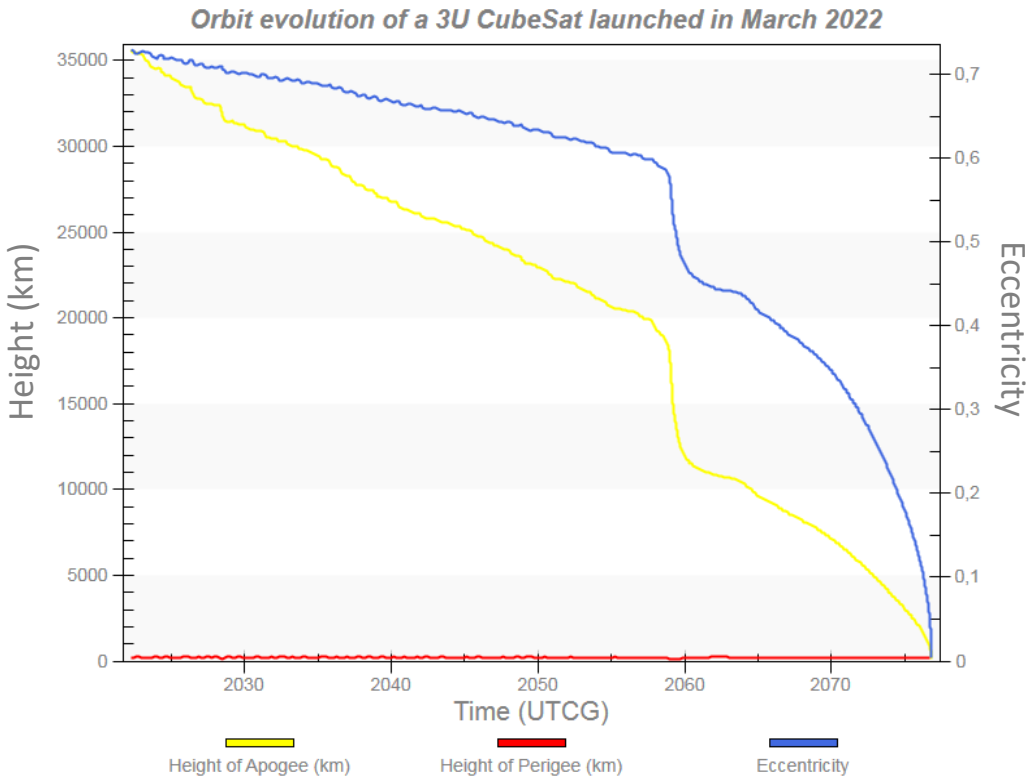

Figure 4.36 Orbital lifetime of the 3U CubeSat launched to the GTO in March 2022. Left axis represents values in *km* for heights of apogee and perigee while right axis provides values for eccentricity.

Table 4.39 Summary of thermal condition analysis for the 3U CubeSat launched from Kourou with Ariane 5 or Soyuz rockets

3U (<6 months launched from Kourou)	Max Temperature	41,4 ℃	23 Dec 2021 08:42
	Min Temperature	-89,3 ℃	1 Dec 2021 09:31

	Mean Temperature	23,217 ℃	-

4.3.5 Technical risk assessment

The worst-case scenarios were developed based on the assessment of environmental and technical risks during the CML 2 concept development (Table 4.40).

Table 4.40 Worst case scenarios for the FORESAIL-2 at the GTO and mitigation measures

Worst case	Description	Solution
Cold case	This is the case when spacecraft will be subjected to the lowest temperatures such < - 80 °C	Use the heater to maintain the temperature of batteries within the operating range
Hot case	This is the case when spacecraft will be subjected to the highest temperatures such < - °40 °C	Use solar panels as radiators and coating with low absorptivity
Lack of power	This is the case when solar panels degrade, or one of the panels fails	Use three (3) solar panels to provide redundancy where two panels still would be enough (~14 W) to keep the mission intact
Low data rate	This is the case when the surface of antenna degrades due to radiation	Use several antennas deployed on different sides to provide redundancy
Extra mass	This is the case when the mass of flight model exceeds the limits	Reduce planned mass to fit into a mass with contingencies.
Geomagnetic storm	This the case when geomagnetic storm activity disturbs the operation of ADCS	Interpolate gaps in pointing knowledge during post-processing of science data
Launch delay	This is the case when delivered to launcher CubeSat has been put on hold.	To avoid degradation of battery performance, set automatic turning on and off once a month.
SEE effect	This is the case when data gets corrupted.	Use the forward error correction method and watchdog for rebooting

4.3.6 Spacecraft system design

The spacecraft system design in the previous section evaluated volume, mass, and power budgets for a 3U CubeSat. Therefore, trade space analysis for spacecraft system design will be performed for a 6U CubeSat in this section.

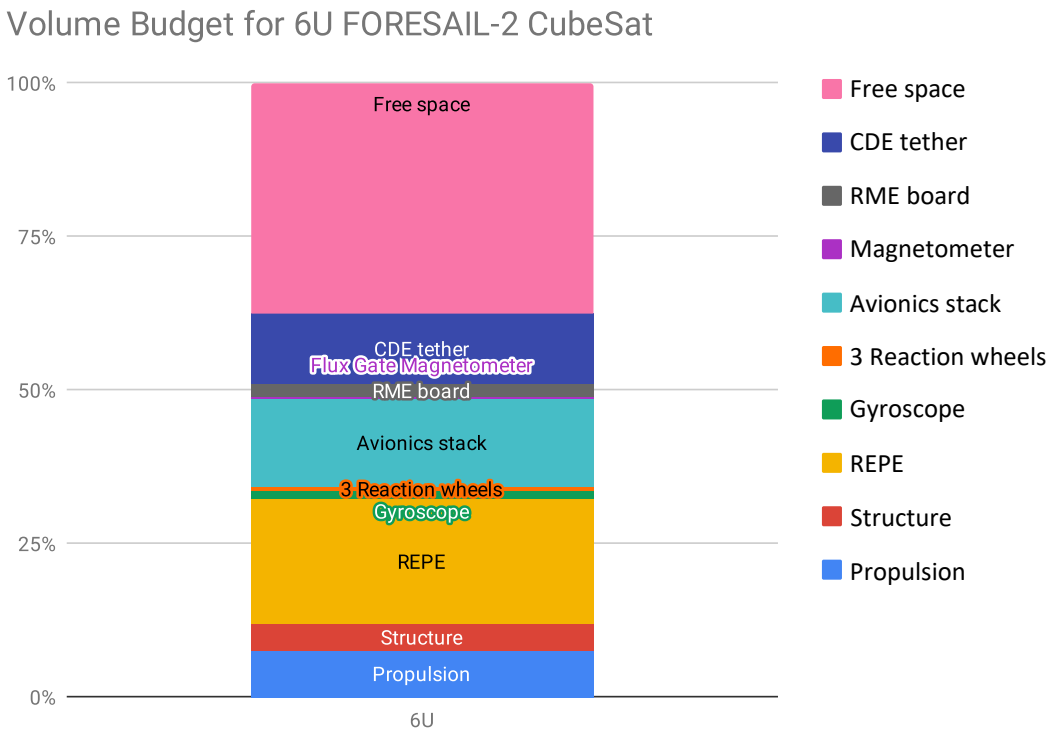

Figure 4.37 Volume budget for the 6U CubeSat with the same set of subsystems and payloads as were used for 3U CubeSat analysis. RME board, Flux Gate Magnetometer, reaction wheels, and gyroscope, are positioned off their blocks as their proportion is tiny compared to volume taken by other components.

If the same subsystems and payloads as was defined for a 3U CubeSat are to be used in a 6U CubeSat form factor, the amount of free space will increase to 37% (Figure 4.37) according to equation (4.24). The newly available space might be used to enhance science instruments to pursue breakthrough science as was defined in the SRD. Furthermore, more space will be required for the propulsion system to store a more significant amount of propellant. Moreover, the redundancy of subsystems can be improved by putting redundant components into the available space.

Spacecraft systems configurations were developed based on studies of available technology, spacecraft requirements, heritage from Aalto-1 [10] and FORESAIL-1 [126], and industry standard practices (Table 4.41).

Table 4.41 A matrix with different configurations for each subsystem of the FORESAIL-2 CubeSat launched to the GTO

Subsystem	Configuration 1	Configuration 2	Configuration 3
ADCS	2 Digital Sun Sensors 1 Star tracker 1 Coarse 3-axis gyro 3-axis Reaction Wheel Package	2 Coarse Sun Sensors 1 Fine 3-axis gyro 3 Reaction Wheels 8 Thrusters	2 Fine Sun Sensors 1 Fine 3-axis gyro 3 Reaction Wheels 3-axis Magnetorquer

Subsystem	Configuration 1	Configuration 2	Configuration 3
	3-axis Magnetorquer 3 Thrusters Onboard magnetic field model propagator		1 Onboard magnetic field model propagator
Protection from radiation	AdHoc Shielding Inherent Mass Shielding	Inherent Mass Shielding	Radiation tolerant components (10 krad<) AdHoc Mass Shielding
Thermal control system	1 MLI Blankets 3 Heat pipes 1 Heater line (2 heaters + 1 sensor) Black paint	Black and white paint 1 MLI Blankets	External plain anodizing Internal black paint Silvered tape Battery heater Screened packages for electronics Temperature sensors
Communication system	1 DHU modem 1 S-band UP/DW converter 4W 2 S-band LGA	1 UHF transceiver 1 Class 1 SD storage Software Defined Radio (SDR)	1 UHF transceiver 1 beacon
Propulsion system	Chemical: Cold gas (Butane)	Electric propulsion: RF generated ions	Resistojet: Water

The configuration 2 was selected for ADCS where magnetorquers were removed as they were found to have no use at the GTO with respect to given mission and spacecraft requirements. Therefore, thrusters and reaction wheels would be required to produce pointing. The pointing knowledge would be produced with one (1) fine gyroscope to measure the change in phase angle with a resolution of 0,6 degrees and two (2) coarse sun sensors assisted with a maximum power point tracking (MPPT) for sun pointing. The reason coarse sensors are suggested is the fact that sun pointing is not required to be accurate while having two instead of one ensures redundancy.

Protection from radiation can be ensured with radiation tolerant components with tolerance higher than 10 krad. The Ad Hoc shielding would be preferred over inherent mass shielding since the later was found to produce larger mass values according to equation (4.8) (Table 4.42).

Table 4.42 Trade space for different thickness values of aluminium shielding and sizes of CubeSat

Shielding material Al 7075 T-6	5 mm m / g	6 mm m / g	7 mm m / g	8 mm m / g	9 mm m / g
3U	1967	2360,4	2753,8	3147,2	3540,6
6U	3091	3709,2	4327,4	4945,6	5563,8

The configuration 3 was selected for thermal control system where battery heater, external plain anodizing, internal black paint, silvered tape, and screened packages for electronics were included. Battery heater would be needed to counter thermal swings and keep the battery at operating temperature. External plain anodizing would be required to produce a surface with low absorptivity and emissivity to counter thermal swings. Internal black paint and the silvered tape would be needed to remove heat dissipated by internal components to space. Finally, screened packages would provide a broader range of operating temperatures for sensitive electronics.

The communication system is suggested to be realized with UHF transceiver, SDR, and Class 1 SD storage. The reason this configuration was selected was the finding that the downlink rate would be only 4,6 Mbytes per day while the required downlink time would be only 16 minutes out of 6,5 hours of communication window availability.

Finally, the resistojet with water as a propellant was selected since it was found to have a high specific impulse (> 100 s) to generate required angular momentum of 20 Nms with a smaller amount of propellant. Meanwhile, cold gas propulsion with butane was found to have less of specific impulse while electric propulsion with RF generated ions was not able to produce the required amount of angular momentum and would have required more time to accelerate.

4.3.7 SWOT: 3U vs 6U

The comparison of 3U (Figure 4.38) and 6U (Figure 4.39) with the help of SWOT method (Table 4.43) demonstrates that the pivot point between the two is the cost (Table 4.44). The cost difference between the two was estimated to be of a factor of 2 based on cost estimation during the CML 2 concept maturing. The research proposal to the Finnish Academy of Science for which funds were allocated included only measurements on magnetic field intensity in the range of Pc5 waves and energy spectrum of electrons at a range from 800 keV [3].

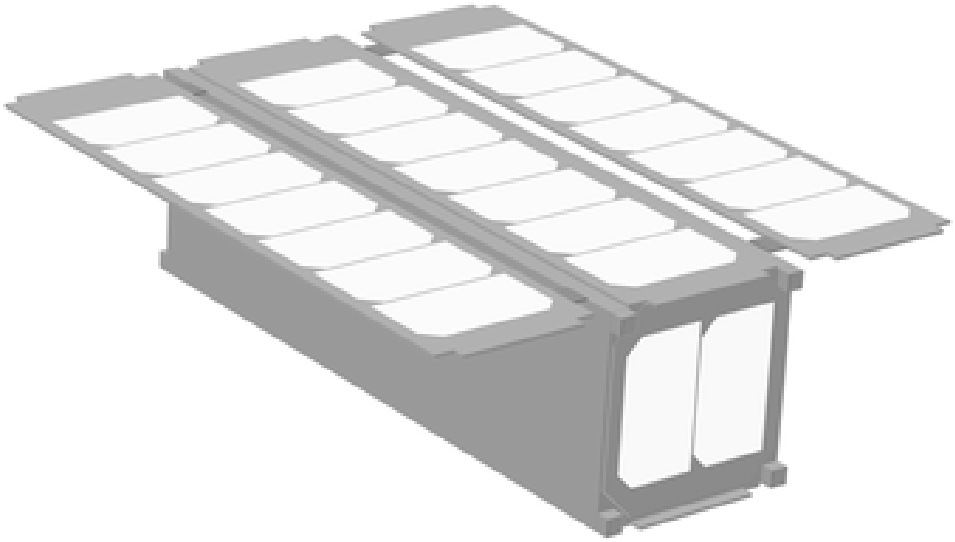

Figure 4.38 A 3D model of a 3U CubeSat implemented in simulations

The said science goals can be achieved with two instruments only such as the REPE telescope and fluxgate magnetometer. While other instruments can be removed without compromising goals declared in the proposal, the mission driver to maintain active collaboration within the FORESAIL consortium would be severely affected. Furthermore, it is expected that the investments made into the current mission, in case of mission success, will be returned with significant dividends in terms of science and technology recognition. This recognition will ensure more substantial funding for science and better partnering conditions for technology.

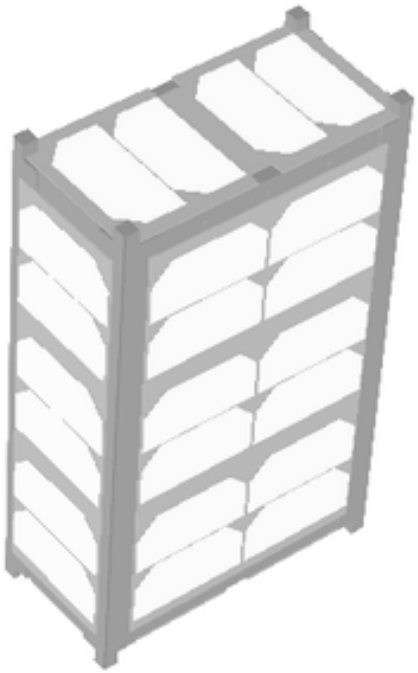

Figure 4.39 A 3D model of a 6U CubeSat implemented in simulations

NASA concluded that 6U was the minimum size CubeSat would need to provide reliable performance and advanced science observations. Currently, the Goddard Space Flight Centre of NASA envisioned the use of 6U CubeSats for science missions beyond the LEO and 12U CubeSats for interplanetary missions [18].

Table 4.43 Strengths, Weaknesses, Opportunities, and Threats (SWOT) of launching the FORESAIL-2 mission with a 3U CubeSat

3U CubeSat	Useful to mission goals	Harmful to mission goals
Internal origin	Strengths Cheaper to build than 6U Cheaper to launch than 6U Experience in building 3U platforms The legacy mission with similar instruments and subsystems (FS-1)	Weaknesses Lower volume and mass availability than 6U Lower power availability than 6U No flight proven components for the GTO
External origin	Opportunities To be the first 3U nanosatellite science mission to the GTO To prove the feasibility of a 3U mission in a high radiation environment To introduce know-how into miniaturization of components	Threats Failure to accommodate all payloads and thus, downgrading the science value of the mission. Failure to meet requirements for maximum mass. Failure to get enough power for components. Failure to implement measures for active thermal control Failure to implement radiation mitigation measures

Since the GTOSat sets as one of its goals to replace Van Allen probes which were classified as the state-of-the-art for science, the cost of this 6U nanosatellite of 3,8 million Euro sets the threshold. Furthermore, the main reason developers of GTOSat decided to build 6U instead of 3U was to accommodate all their science instruments. The same question arises for FORESAIL-2. FORESAIL-2 and GTOSat pursue similar science goals in measurements of the energy spectrum of electrons and magnetic field intensity, while CDE tether and RME board are used for measurements that have a chance to become state-of-the-art in science in case of success of these measurements. The reason these instruments can become state-of-the-art in science is the fact that there were no Coulomb Drag and Radiation Mitigation experiments done at the GTO with nanosatellites.

Table 4.44 Strengths, Weaknesses, Opportunities, and Threats (SWOT) of launching the FORESAIL-2 mission with a 6U CubeSat

6U CubeSat	Useful to mission goals	Harmful to mission goals
Internal origin	Strengths Higher volume and mass availability than 3U	Weaknesses Higher cost to build than 3U

	Higher power availability than 3U Easier to maintain a temperature level	Higher cost to launch than 3U Lack of experience in building 6U Not many legacy 6U missions compared to 3U No flight proven components for the GTO
External origin	Opportunities To improve science return level to enhancing and complement the GTOSat by NASA To prove the feasibility of a 6U mission in a high radiation environment To introduce know-how into miniaturization of components	Threats Failure to deliver FQM in time due to the lack of experience with 6U configuration.

Furthermore, GTOSat aims to pave the way for deploying a constellation of satellites producing similar measurements. Thus, if FORESAIL-2 proves to be a success, platform and instruments used on board have the potential to be commissioned by NASA to be a part of this constellation.

4.3.8 Master and Power Equipment Lists

The Master Equipment List (MEL) provides the mass of all significant components and systems selected for a 3U FORESAIL-2 CubeSat. The total planned mass is 4860 grams and 5979,4 grams with contingencies included (Appendix 7).

The Power Equipment List (PEL) provides power consumption of major components and systems selected for a 3U FORESAIL-2 CubeSat (Appendix 8). The power consumption in nominal mode is estimated to be 3,3W while for safe mode it is 2,3 W. The first observation phase will need 6,9 W while the second and third ones 8,8 W and 5,8 W, respectively. The reeling of the tether will consume 7 W while propulsion will need up to 1,5 W. Finally, subsystems and payloads are estimated to consume 5,4 W in the telemetry mode.

4.4 CML 4: Point design

The concept will require further development at the CML 3 to produce more inputs to the CML 4. Nevertheless, the first iteration with CML 2 and CML 3 allows introducing certain point design elements in CML 4 now.

4.4.1 Operating phases

The design of operation phases is produced based on requirements laid out in MTM and planned mission lifetime of six (6) months minimum (Appendix 10). The first phase lasting 2 weeks is a launch and commissioning. All subsystems will be verified for standard functionality during the commissioning. The next phase is a REPE demonstration lasting for another 2 weeks and where the full functionality of the mentioned instrument will be tested and verified, and thus potentially increase its TRL to the highest level.

The following phase is the 1st observation phase where magnetometer will be deployed, and measurements on magnetic field intensity and electrons energy spectrum will commence. The said phase will last 2 months while the following phase where tether will be deployment and CDE demonstrated will take only 2 weeks once CDE demonstration is over, the second observation where REPE, CDE tether, and magnetometer producing measurements simultaneously will commence. This phase will be the most important one in terms of overall mission success and will last 4 months. Once the 2nd observation phase is over, the 3rd observation phase with the RME will commence and last till the full decay or failure of all subsystems.

4.4.2 Point design of a system

Since the MEL and PEL were defined in the previous section, it was possible to produce a point design of a system for a 3U FORESAIL-2 CubeSat (Figure 4.40) showing how different subsystems and payloads would be integrated into one system.

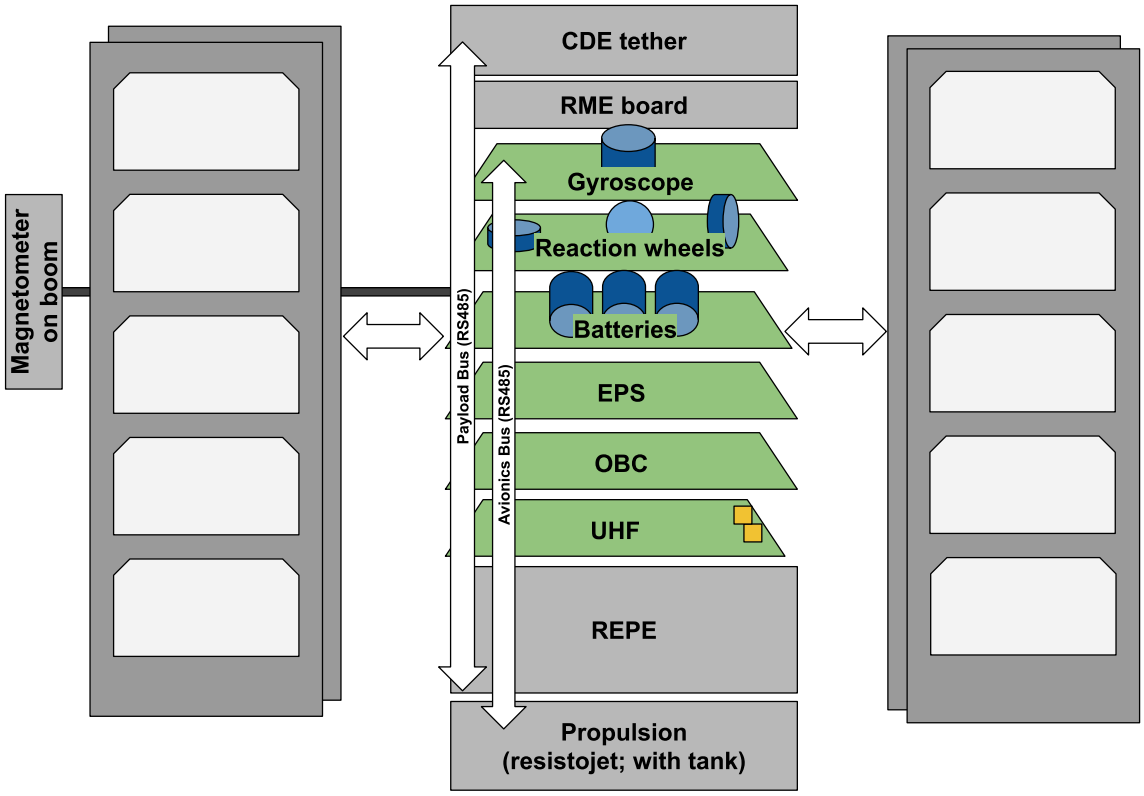

Figure 4.40 Point design of FORESAIL-2 system. Science instruments are CDE tether, REPE telescope, RME board, and flux gate magnetometer on boom while the rest are onboard avionics and propulsion system.

The system design includes deployable solar panels, payloads and subsystems, and illustrates payload and avionics buses separated and communicating over RS485 interface.

The propulsion system and CDE tether are placed at different ends of the CubeSat to balance change of centre of mass and provide non constrained areas for release of tether and exhaust of propellant, respectively.

4.4.3 Product tree

The product tree provides a breakdown of the integrated 3U CubeSat into a subsystem, ground segment and payloads. There are six subsystems, four payloads, and at least one ground station for the ground segment.

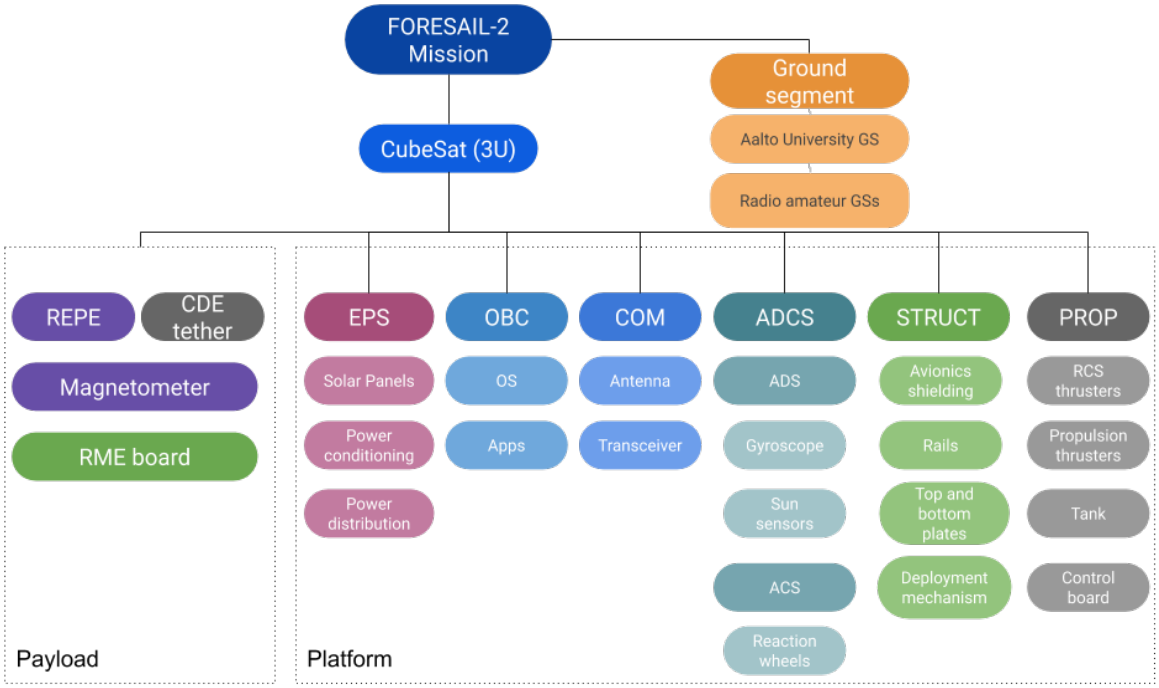

Figure 4.41 Product tree showing a breakdown of deliverables and dependencies for each subsystem and payload

The subsystems included are Radiation Mitigation Experiment (RME) board, electric power system (EPS), onboard computer (OBC), communication (COM), attitude determination and control system (ADCS) comprising attitude determination system (ADS) and attitude control system (ACS), structure (STRUCT), and propulsion (PROP). Meanwhile, the ground segment will include Aalto University ground station and radio amateur global network of ground stations.

4.5 Discussion

According to [96], prediction of orbital lifetime and evolution in the case of GTO was possible only prior to the occurrence of solar apsidal resonance which was the U-turn of the solar azimuth. Furthermore, these researchers found that the height of perigee would oscillate by 50-60 km before the occurrence of solar apsidal resonance.

Moreover, three types of resonance events in the GTO were identified where it was concluded that resonance would lead to re-entry in most cases rather than to increase of orbital lifetime. Additionally, it was found that resonance occurred not earlier than 8-9 years from the launch date in different scenarios reported in that research.

In another paper [97] on the evolution of the GTO, it was found that STK-HPOP orbit propagator used for the current research had a good agreement with other propagators before the occurrence of the solar apsidal resonance. Nevertheless, the solar apsidal resonance occurred not earlier than the 9th year.

Moreover, [98] utilized HPOP propagator in STK to account for aerodynamic drag, solar radiation pressure, J2 effect, gravitational effects of the Moon and the Sun, the Earth's gravitational harmonics up to the 21st order and thermal radiation effects. The researchers found that HPOP was sufficient to produce an accurate orbital evolution geometry which agrees with the statement in the previously reviewed paper that orbital evolution could be predicted prior to the occurrence of solar apsidal resonance. [98] found that the height of perigee oscillated by 50 km in the period of 600 days.

Since the mission lifetime is planned to last less than 1 year, the orbital lifetime should not affect the objectives of the mission. On the other hand, oscillations of the height of perigee prior to the resonance should be taken into account. While the oscillations of the height of perigee are essential for determining orbital lifetime, time for tether deployment, and a need for orbit correction, it must be noted that all the reviewed above papers reported oscillations progressing at the rate of every six (6) months nearly.

Therefore, it would be suggested that once CubeSat has been launched and exact launch time is known, or satellite has been tracked with lasers to propagate the orbit trajectory once again with HPOP to determine the period of perigee height increase and decrease. It is crucial to consider perigee fluctuations as the release of a tether during the decrease of a height of perigee might lead to the pre-emptive end of the mission due to the risk of interaction with atmospheric drag forces. On the other hand, since perigee height mostly increases for the first 6 months, it might not be required to track perigee fluctuations to select a time to release tether.

Meanwhile, the ADCS of the CubeSat at the GTO needs to account for the weak magnetic field of Earth due to the remoteness of its apogee and impact of the Kepler's 3rd Law [102]. Therefore, a common practice for the CubeSat at the LEO using magnetorquer should be either dismissed entirely or used at regions close to perigee where magnetic field intensity is higher than at apogee.

The use of reaction wheels is around 81% [155] on all CubeSat missions employing ADCS, and thus, magnetorquers or thrusters are added as secondary tools for attitude control as their role is

minimized to damping the momentum or desaturating the reaction wheels. The popularity of reaction wheels is explained by their compactness, fine precision and low energy demand. Furthermore, there is a large number of control algorithms employed together with Kalman Filters tailored for use with reaction wheels [45]. The Kalman Filters do not directly affect the operation of reaction wheels but ensure accuracy of input from attitude determination components such as sun sensors.

Nevertheless, since the use of magnetorquers to compensate for the momentum produced by reaction wheels is only efficient at regions close to perigee, thrusters must be employed for this purpose at altitudes, close to apogee, where the magnetic field would be weak [37].

If the attitude configuration requires reaction wheels and thrusters with or without magnetorquers, the use of sun sensors is paramount for attitude determination. Whether the sun sensor should be fine or coarse depends on needed accuracy and presence of star tracker. The implementation of star tracker gives the highest possible pointing accuracy, and thus, it would not require fine sun sensors. On the other hand, sun sensors whether they are fine or coarse are always needed to ensure maximum power is produced from solar cells. Furthermore, since sun sensors directly affect the performance of EPS, one of the most crucial to the resilience of the mission subsystem, redundancy must be provided. The story of anomalies with Dellingr mission in 2018 showed a situation where in-house fine sun sensor failed, and the mission was saved thanks to the additional coarse sun sensor [45]. Finally, the use of star tracker in the GTO possesses high risks of getting false stars due to the presence of high-energy protons. Meanwhile, the use of gyroscope is necessary to provide feedback on the operation of reaction wheels, and its resolution has to be fine to ensure attitude knowledge of 0,6 ° of phase angle as a minimum.

Existing technologies for protection from radiation at the GTO do not offer many solutions for CubeSat. There are either inherent mass shielding that is an increase of thickness of walls of CubeSat structure or AdHoc Shielding that is the same as previous one but requires to increase vault thickness only at regions with sensitive electronics. The most preferable but the most expensive solution is to use radiation tolerant components. While the cheapest but less efficient one is to use inherent mass shielding. On the other hand, the use of inherent mass shielding for all sides of the CubeSat dramatically increases the total mass of the spacecraft according to equation (4.8).

Most of the CubeSat missions at the LEO that were concerned with protection from radiation relied solely on increasing thickness of aluminium structure walls for avionics vault, using voting and redundancy, and changing the scale of etching and materials used in electronics [156].

It must be noted that most of the COTS components are designed to sustain the radiation environment at GTO for three (3) months maximum [157]. Some missions to the GTO such as M-BARC is planned to stay on the GTO for 3 months only [32]. Other missions such as ADE [26], Orbital Factory II [23] and MarCO [6] are designed to be short term also. Meanwhile, the FORESAIL-2 mission is assumed to last six (6) months minimum before it is decommissioned.

The only CubeSat mission known to conduct radiation mitigation experiments was Shields-1. Noteworthy, the goal of Shields-1 CubeSat mission was to test different type of materials including novel Atomic Z-grade shielding in a harsh radiation environment. Another key takeaway is the need to use charge dissipation film due to the presence of extreme charging environment at the GTO [33].

Therefore, the minimum set of mitigation measures against high doses of radiation and SEE at the GTO for FORESAIL-2 include use of radiation tolerant components (> 10 krad), shielding of sensitive electronics, redundancy of electronic components, and software techniques for error correction and detection of SEEs.

While there are several solutions provided for the thermal control system (TCS), careful approach to the selection of components for the TCS must be taken as with a lack of specific requirements and a presence of a great variety of technology, design cannot be well optimized. Meanwhile, one of the most efficient and simplest ways to ensure low emissivity insulation is to apply black paint internally and on nadir facing surface, and white paint or silvered tape externally on sun pointing surface [51]. It must be noted that insulation is the essential part of the thermal control system for the CubeSat at the GTO since large temperature swings are expected to happen during the transition to and from eclipse region. Therefore, Kapton tapes [51] are proposed to provide additional thermal stability, and thus, ensuring that thermal strain for the structure is minimized and batteries and electronics are kept within operational temperature regions. Special attention must be given to the thermal protection of batteries as large temperature swings will cause fast degradation of internal contents of batteries, and thus, shorten their capacity and lifetime [40]. The solution could be the implementation of a battery heater to maintain an optimal temperature of batteries.

The main challenge with the communication system is defined by short passes over ground stations during transition via perigee region and remoteness of the CubeSat during its transition at the apogee region. This results in increased noise level produced against the signal, and thus, requires higher power and time for downlink. It must be noted that according to the Kepler's 2nd Law [49], the CubeSat will be the longest at the apogee region potentially adding to the latency of communication channel [49].

Therefore, while the slot at the UHF band is the most affordable and most comfortable to obtain a license for, the S-band would be preferred for its high downlink rate and lower risk of EMI. On the other hand, the requirement for low data rate per each pass validated the use of the UHF, while downplaying the need for uplink required for troubleshooting. The anomalies with Dellingr mission in 2018 [45] showed the need for redundant uplinks of software updates and larger systems health telemetry volume that would require more significant downlink rate.

Finally, the propulsion system required to ensure full attitude control of the CubeSat was suggested to be of a liquid type such as resistojet with water as a propellant. There are two primary implementations for the thruster, - desaturation of reaction wheels and producing the impulse to spin the CubeSat up to required angular momentum to release the tether with required tension in it. Since the mission would not require the application of a propulsion system for orbit correction; there is no necessity for a high specific impulse but a need for a high thrust. On the other hand, high specific impulse could have ensured the smaller size of the tank. Nevertheless, trade-offs should be made with respect to the size of the tank to accommodate for the reliability of the technology. The best suited for CubeSat mission with TRL of 9 propulsion system is a cold gas with butane [72] as a propellant. While there are developments in RF ion propulsion systems, they are yet to be tested in the space environment. The attractiveness of RF ion propulsion systems is in the fact that it has 100 times larger specific impulse [132] with the same thrust capability as a cold gas propulsion system.

On the other hand, the proposed water-based resistojet propulsion system has a higher specific impulse than the butane based cold gas propulsion system [134]. While the TRL of the proposed system is not even five (5), the promised performance, lower cost, high degree of customization, and close proximity of developers, make it an attractive candidate to become a propulsion system for FORESAIL-2.

5 SUMMARY

5.1 Conclusion

The current research produced the concept studies of a CubeSat mission to the Highly Elliptical Orbit (HEO). The research work was done for a FORESAIL-2 CubeSat mission concept proposed by the Finnish Centre of Excellence in Research of Sustainable Space and funded by the Academy of Finland.

The goal of the research was to verify that the proposed CubeSat mission concept was feasible and to produce trade space studies. The framework used to develop the CubeSat mission concept to the HEO was a Concept Maturity Level (CML) framework introduced by the Jet Propulsion Laboratory of NASA. The software used to produce computations and simulations were Systems Tool Kit (STK), MATLAB, and SPENVIS.

The CML 1 chapter developed the science case into the mission, spacecraft and operation requirements. The output from research at the CML 1 was Science Traceability Matrix (STM), Mission Traceability Matrix (MTM), and Science Return Diagram (SRD).

The CML 2 chapter provided with a mission feasibility analysis where different aspects of the mission concept were studied with respect to the requirements specified in the CML 1. The first question studied within CML 2 was the availability of launchers to the desired orbit. It was found that there were three (3) potential launchers available with the main one being Atlas V 401 and Falcon 9 launched from the Cape Canaveral US Air Force base. The launch was provided to the orbit of HEO type known as Geostationary Transfer Orbit (GTO).

Consequently, the space technology available for nanosatellites for use at the GTO was scrutinized. It was found that while space technology for most of the spacecraft subsystems was successfully miniaturized for CubeSat scale, none had technology readiness level (TRL) qualified for use at the GTO since there were no nanosatellite missions done at the GTO.

Another part of CML 2 was the analysis of orbital lifetime and evolution. It was found that the satellite would decay in one (1) year after the launch with the right ascension of the ascending node (RAAN) drifting with a rate of 0,4 degrees per day. While the drift rate provided essential coverage of Magnetic Local Time (MLT), further studies showed that the height of perigee would fluctuate

by 60 km for every 6 months and would increase if solar apsidal resonance takes place leading to increase in orbital lifetime. Nevertheless, the minimum requirement for the mission was to last six (6) months which was within the estimated orbital lifetime.

The study of radiation environment at the GTO and risks associated with it led to the conclusion that onboard electronics would require aluminium shielding with a thickness of 5 mm for a six (6) month mission lifetime. Nevertheless, the minimum thickness of shielding for one (1) year was found to be 6 to 8 mm.

The study of geomagnetic field conjugacy showed that the mean magnetic field intensity would be around 2000 nT which would not be enough to produce torque with magnetorquers for desaturation of reaction wheels. The resistojet propulsion systems with water as a propellant was selected to mitigate the aforesaid problem and provide required angular momentum to deploy tether for Coulomb Drag Experiment (CDE).

The studies on communication links showed that a mean time window available per day for communication with the primary ground station located at the Aalto University was 6,5 hours with required 16 minutes for the downlink of science data.

The thermal analysis of the exterior of CubeSat moving along the GTO trajectory showed that there would be temperature swings in the order of 100 degrees Celsius. Nevertheless, it was found that the thermal mass of components within the CubeSat and thermal conductivity of the aluminium structure would not facilitate fast heat transfer during eclipse periods. The mean time of eclipse periods was found to be 30 minutes while 10 hours of the orbital period would be spent under sunlight.

Subsequently, risk analysis determined that the highest risks for the spacecraft at the GTO were surface Electrostatic Discharge (ESD), Single Event Effects (SEE), and Total Ionizing Dose (TID).

The studies in the CML 2 chapter concluded that mission was feasible with a 3U CubeSat with the condition that volume and mass kept as planned or reduced, and solar panel deployed pointed to the sun. These conclusions were drawn based on the finding that planned volume and mass of the FORESAIL-2 CubeSat was close to the limit specified for 3U CubeSats while volume and mass with contingencies were exceeding the limit by 423 cm^3 and 800 grams, respectively.

Furthermore, the analysis of power budget showed that the highest demand for power for science mode would be equal to 8,8 W while one solar panel was able to produce a mean power of 6,89 W only. Nevertheless, it was found that power production would increase to around 20 W if solar panels were deployed such that the total illumination area would increase to 900 cm^2.

The CML 2 studies concluded that a 3U CubeSat could be used as a baseline for a six-month mission while the 6U CubeSat was set as a threshold nanosatellite subclass for a one-year mission. Therefore, CML 3 studies were focused on comparing 3U and 6U CubeSats for different aspects related to science goals, mission requirements, and spacecraft design.

The studies in the CML 3 chapter showed that a 6U CubeSat would have the same orbital lifetime and evolution as 3U CubeSat. Nevertheless, the simulation of launches with Ariane 5 and GLSV II rockets showed that the orbital lifetime would be around 16 years for the former and 3,5 years for the later.

Furthermore, it was found that different impulse and thus, the propellant mass was required for deployed tether depending on its material. The deployment of 300 meters of a gold tether would require less mass of propellant than deployment with aluminium tether.

The study on different spacecraft system configurations showed that to satisfy the science requirement of pointing knowledge of 0,6 degrees of phase angle, a fine gyroscope would be needed. Meanwhile, two coarse sun sensors along with maximum power point tracking were found to be sufficient to provide the location of sun vector for solar panels. Furthermore, it was found that a heater would be required for a battery to minimize thermal swing while exterior could have a plain non-black anodized surface.

While CML 3 could have had more studies conducted, some elements of the mission concept were matured to CML 4. The CML 4 produced point designs for operation phases, spacecraft system design, and product tree with all subsystems defined for the FORESAIL-2 CubeSat mission. Meanwhile, the output from CML 3 was Master Equipment List (MEL), Power Equipment List (PEL), volume budget, and telemetry budget.

5.2 Future developments

The concept studies were conducted when requirements from scientists were being formulated. The formulation of these requirements is not over and might change in the course of project development. Furthermore, this research produced the first iteration of concept studies and laid a fundament for further studies.

It would be suggested that the thermal analysis be enhanced with a multi-nodal analysis of the interior of a spacecraft. Meanwhile, it would be advised to test the radiation shielding of the selected thickness on a radiation test bench with preliminary selected components.

Moreover, it would be recommended to produce a link budget of higher fidelity than the one made in this research. The limitation with the current evaluation of link budget lies in a fact that the concept is in its early stages, and not all parameters of the ground station and onboard communication system are available at the moment.

Furthermore, it would be suggested that a more significant number of spacecraft system design configurations be produced for trade space studies. The said can be achieved with deep integration of STK with external algorithms developed in any of supported interfaces such as MATLAB, C#, Java, Visual.Net, and Python. Additionally, it would be suggested to integrate all tools for mission concept development such as commercial computation engines, scripts, spreadsheets, and other items, into a single software web application to provide remote access members of the FORESAIL consortium.

LIST OF REFERENCES

[1] E. Kulu and Others, “Database,” *nanosats.eu*, 2017. [Online]. Available: https://airtable.com/shrafcwXODMMKeRgU. [Accessed: 15-Dec-2018]

[2] B. Young and T. Martin-Mur, “Using telemetry to navigate the MarCO cubesats to mars,” in *AIAC 2018: 18th Australian International Aerospace Congress: HUMS-11th Defence Science and Technology (DST) International Conference on Health and Usage Monitoring (HUMS 2019): ISSFD-27th International Symposium on Space Flight Dynamics (ISSFD)*, Melbourne, 2019, pp. 1516–1531.

[3] Finnish Centre of Excellence in Research of Sustainable Space, “FS2 Mission Objectives and Requirements.” May-2019.

[4] T. Schildknecht *et al.*, “Optical observations of space debris in GEO and in highly-eccentric orbits,” *Adv. Space Res.*, vol. 34, no. 5, pp. 901–911, Jan. 2004.

[5] C. E. Mowry, C. B. Christensen, and P. Smith, “The Global Launch Industry: Progress and Evolution,” in *Recent Successful Satellite Systems: Visions of the Future*, K. D. Sachdev, Ed. AIAA American Institute of Aeronautics and Astronautics, Inc., 2017, p. 405.

[6] A. Klesh *et al.*, “MarCO: Early Operations of the First CubeSats to Mars,” presented at the 32nd Annual AIAA/USU Conference on Small Satellites, Logan, UT, USA, 2018 [Online]. Available: https://digitalcommons.usu.edu/cgi/viewcontent.cgi?article=4286&context=smallsat

[7] L. Keesey, “New Spacecraft Baselined for Small Satellite Bound for Van Allen Belts,” *NASA*, 01-May-2018. [Online]. Available: http://www.nasa.gov/feature/goddard/2018/nasa-s-new-dellingr-spacecraft-baselined-for-pathfinding-cubesat-mission-to-van-allen-belts. [Accessed: 18-Oct-2018]

[8] N. Fox and J. L. Burch, *The Van Allen Probes Mission*. Springer Science & Business Media, 2014.

[9] C. Y. Chiang *et al.*, “Comparison of the Earth’s high-latitude disturbances with energetic electrons measured by the ERG/Arase satellite,” in *2017 AGU Fall Meeting*, New Orleans, 2017, vol. 2017 [Online]. Available: https://ui.adsabs.harvard.edu/abs/2017AGUFMSM21A2564C

[10] H. J. Kramer and ESA, “Aalto-1,” *eoPortal Directory - Satellite Missions*. [Online]. Available: https://directory.eoportal.org/web/eoportal/satellite-missions/a/aalto-1. [Accessed: 28-Jan-2019]

[11] Finnish Centre of Excellence in Research of Sustainable Space, “FS1 Mission paper.” 10-Mar-2019.

[12] A. Slavinskis and et al., “ESTCube-1 in-orbit experience and lessons learned,” *IEEE Aerospace and Electronic Systems Magazine*, vol. 30, no. 8, pp. 12–22, Aug. 2015.

[13] I. Iakubivskyi *et al.*, “ESTCube-2 plasma brake payload for effective deorbiting,” in *7th European Conference on Space Debris, T. Flohrer and F. Schmitz, Eds. Darmstadt, Germany: ESA Space Debris Office*, 2017.

[14] M. Palmroth *et al.*, “ULF foreshock under radial IMF: THEMIS observations and global kinetic simulation Vlasiator results compared,” *J. Geophys. Res. [Space Phys]*, vol. 120, no. 10, pp. 8782–8798, 2015.

[15] R. Wessen, C. S. Borden, J. K. Ziemer, R. C. Moeller, J. Ervin, and J. Lang, “Space Mission Concept Development using Concept Maturity Levels,” in *AIAA SPACE 2013 Conference and Exposition*, San Diego, 2013 [Online]. Available: https://doi.org/10.2514/6.2013-5454

[16] A. Good and J. Wendel, “NASA’s First Deep-Space CubeSats Say: ‘Polo!,’” *NASA Mars News*, 05-May-2018. [Online]. Available: https://mars.nasa.gov/news/8334/nasas-first-deep-space-cubesats-say-polo. [Accessed: 14-Oct-2018]

[17] N. Paschalidis, “Recent CubeSat Missions at NASA/GSFC,” in *7th European CubeSat Symposium*, Liege, Belgium, 2015.

[18] C. Goodloe, “SmallSat Architecture and Platform Enabling Planetary Science,” NASA Goddard Space Flight Center, 16-Aug-2018 [Online]. Available: https://cubesats.gsfc.nasa.gov/symposiums/2018/presentations/Day2/0915_Goodloe.pdf

[19] L. W. Blum, “E-mail,” 19-Sep-2018.

[20] L. J. Keesey, “NASA Prepares ‘Dellingr’ CubeSat to Begin Science Operations,” *NASA*, 28-Nov-2017. [Online]. Available: https://www.nasa.gov/feature/goddard/2017/nasa-begins-checkout-of-dellingr-spacecraft-designed-to-improve-robustness-of-cubesat. [Accessed: 14-Oct-2018]
[21] L. Keesey, “NASA Team Pursues Blobs and Bubbles with New PetitSat Mission,” *NASA*, 09-May-2017. [Online]. Available: https://www.nasa.gov/feature/goddard/2017/nasa-team-pursues-blobs-and-bubbles-with-new-petitsat-mission. [Accessed: 14-Oct-2018]
[22] F. Ongaro, “Keynote Address,” Logan, Utah, USA, 08-Aug-2016 [Online]. Available: https://digitalcommons.usu.edu/cgi/viewcontent.cgi?referer=&httpsredir=1&article=3476&context=smallsat
[23] M. Everett, A. F. Abad, A. R. Khan, K. M. M. Billah, and A. R. Choudhuri, “Orbital Factory II: a 3D Printer CubeSat with Self-repairing Purposes,” in *2018 AIAA SPACE and Astronautics Forum and Exposition*, 2018.
[24] University of Louisiana at Lafayette Physics Department, “UL Lafayette Professors’ Proposed Satellite Awarded Launch Provision,” *Department of Physics*, 22-Sep-2016. [Online]. Available: https://physics.louisiana.edu/news-events/news/20160922/ul-lafayette-professors-proposed-satellite-awarded-launch-provision. [Accessed: 14-Oct-2018]
[25] University of Louisiana at Lafayette, “LACCE-1,” *Department of Electrical & Computer Engineering*, 12-May-2017. [Online]. Available: https://ee.louisiana.edu/research/cape/satellite-missions/lacce-1. [Accessed: 14-Oct-2018]
[26] Purdue University, “ADE (Aerodynamic Deorbit Experiment),” *Purdue University*. [Online]. Available: https://engineering.purdue.edu/CubeSat/missions/ade. [Accessed: 18-Oct-2018]
[27] A. C. Long and D. A. Spencer, “A Passively Stable Pyramid Sail for the Deorbit of Small Satellite Constellations,” in *68th International Astronautical Congress: Unlocking Imagination, Fostering Innovation and Strengthening Security, IAC 2017*, Adelaide, 2017, pp. 3690–3700.
[28] M-BARC Team, “Our Story,” *M-BARC*. [Online]. Available: http://m-barc.com/our-story/. [Accessed: 14-Oct-2018]
[29] A. Liszewski, “Does a Time Capsule Blasted Into Space Have a Better Chance at Surviving 100 Years? (Updated),” *Gizmodo*, 07-Mar-2017. [Online]. Available: https://gizmodo.com/does-a-time-capsule-blasted-into-space-have-a-better-ch-1793043110. [Accessed: 14-Oct-2018]
[30] C. Gonzalez, “Students embark on 100-year space mission,” *Michigan Engineering*, 27-Feb-2017. [Online]. Available: https://news.engin.umich.edu/2017/02/space-time-capsule/. [Accessed: 14-Oct-2018]
[31] Staff Writers, “Time capsule satellite will carry stories to space,” *Space Daily*, 09-Mar-2017. [Online]. Available: http://www.spacedaily.com/reports/Time_capsule_satellite_will_carry_stories_to_space_999.html. [Accessed: 14-Oct-2018]
[32] L. H. Regoli, M. B. Moldwin, J. Thoma, M. Pellioni, and B. Bronner, “Four-Magnetometer Board for CubeSat Applications,” in *32nd Annual AIAA/USU Conference on Small Satellites*, Logan, UT, USA, 2018 [Online]. Available: https://digitalcommons.usu.edu/cgi/viewcontent.cgi?article=4082&context=smallsat
[33] L. Thomsen, “NASA Shields-1, A CubeSat Platform for Testing the Effects of Space Radiation on Materials,” Woodlands Conference Center, 13-Jun-2018 [Online]. Available: https://indico.cern.ch/event/543031/contributions/2987732/attachments/1666755/2672364/NASA_Shields-1_A_CubeSat_Platform_for_Testing_the_Effects_of_Space_Radiation_on_Materials_13JUNE18_Thomsen.pdf
[34] Langley Research Center, “Shields-1 brochure (Part 1).” Luna Inc., May-2015 [Online]. Available: http://lunainc.com/wp-content/uploads/2015/05/Shields_brochure1.png
[35] Langley Research Center, “Shields-1 brochure (Part 2).” Luna Inc., May-2015 [Online]. Available: http://lunainc.com/wp-content/uploads/2015/05/Shields_brochure2.png

[36] B. Segret *et al.*, “BIRDY: an interplanetary CubeSat to collect radiation data on the way to Mars and back to prepare the future manned missions,” in *Modeling, Systems Engineering, and Project Management for Astronomy VI*, Montréal, 2014, vol. 9150, p. 91501N.
[37] J. Kolmas, P. Banazadeh, A. W. Koenig, B. Macintosh, and S. D’Amico, “System design of a miniaturized distributed occulter/telescope for direct imaging of star vicinity,” in *2016 IEEE Aerospace Conference*, Big Sky, MT, USA, 2016, pp. 1–11.
[38] S. D’amico, “mDOT concept.” Universe Today, Aug-2017 [Online]. Available: https://www.universetoday.com/wp-content/uploads/2017/08/mDOT_concept_new.jpg
[39] S. D’Amico, “mDOT Factsheet.” Stanford University, 12-Jul-2018 [Online]. Available: https://people.stanford.edu/damicos/sites/default/files/mdot_factsheet_7-12-18.pdf. [Accessed: 14-Oct-2018]
[40] H. J. Kramer and ESA, “MarCO,” *eoPortal Directory - Satellite Missions*. [Online]. Available: https://directory.eoportal.org/web/eoportal/satellite-missions/m/marco. [Accessed: 14-Oct-2018]
[41] S. W. Asmar and S. Matousek, “Mars Cube One (MarCO) Shifting the Paradigm in Relay Deep Space Operation,” in *14th International Conference on Space Operations*, Daejeon, Korea, 2016, p. 2483.
[42] P. Blau, “Dellingr,” *Spaceflight101*. [Online]. Available: http://spaceflight101.com/dragon-spx12/dellingr/. [Accessed: 14-Oct-2018]
[43] H. J. Kramer and ESA, “Dellingr,” *eoPortal Directory - Satellite Missions*. [Online]. Available: https://directory.eoportal.org/web/eoportal/satellite-missions/d/dellingr. [Accessed: 14-Oct-2018]
[44] C. Clagett *et al.*, “Dellingr: NASA Goddard Space Flight Center’s First 6U Spacecraft,” in *AIAA/USU Conference on Small Satellites*, Logan, Utah, USA, 2017 [Online]. Available: https://digitalcommons.usu.edu/smallsat/2017/all2017/83/. [Accessed: 12-May-2019]
[45] L. Kepko *et al.*, “Dellingr: Reliability Lessons Learned from On-Orbit,” in *32nd Annual AIAA/USU Conference on Small Satellites*, Logan, Utah, USA, 2018 [Online]. Available: https://digitalcommons.usu.edu/smallsat/2018/all2018/250/. [Accessed: 12-May-2019]
[46] S. Bourdarie and M. Xapsos, “The Near-Earth Space Radiation Environment,” *IEEE Trans. Nucl. Sci.*, vol. 55, no. 4, pp. 1810–1832, Aug. 2008.
[47] C. Beierle, A. Norton, B. Macintosh, and S. D’Amico, “Two-stage attitude control for direct imaging of exoplanets with a CubeSat telescope,” in *Proceedings Volume 10698, Space Telescopes and Instrumentation 2018: Optical, Infrared, and Millimeter Wave*, Austin, 2018, vol. 10698 [Online]. Available: https://www.spiedigitallibrary.org/conference-proceedings-of-spie/10698/2314233/Two-stage-attitude-control-for-direct-imaging-of-exoplanets-with/10.1117/12.2314233.short?SSO=1. [Accessed: 12-Apr-2019]
[48] Ö. Z. İbrahim, “Comparative Analysis of Sub GTO, GTO and Super GTO in Orbit Raising for All Electric Satellites,” *Sakarya University Journal of Computer and Information Sciences*, vol. 1, no. 1, pp. 58–64, 2018.
[49] H. D. Curtis, *Orbital Mechanics for Engineering Students*. Butterworth-Heinemann, 2013.
[50] ESA Space Debris Office, “ESA’s Annual Space Environment Report,” European Space Operations Centre, 2, May 2018 [Online]. Available: https://www.sdo.esoc.esa.int/environment_report/Space_Environment_Report_latest.pdf
[51] D. G. Gilmore, *Spacecraft Thermal Control Handbook. Volume1: Fundamental technologies*. AIAA, 2002.
[52] B. Johnston, “The AE9/AP9 Radiation and Plasma Environment Models,” Kirtland AFB, NM, 04-May-2017 [Online]. Available: https://www.swpc.noaa.gov/sites/default/files/images/u33/%281420%29%20AE9AP9_SWW2017_Johnston.pdf
[53] J. A. Van Allen, C. E. McIlwain, and G. H. Ludwig, “Radiation observations with satellite 1958 ε,” *J. Geophys. Res.*, vol. 64, no. 3, pp. 271–286, Mar. 1959.

[54] W. R. Johnston, “60 years of radiation belt science,” Kirtland AFB, USA, 18-Sep-2017 [Online]. Available: https://www.vdl.afrl.af.mil/programs/ae9ap9/files/other/20170918_AFRL_Johnston_RBrefchart.pdf
[55] R. H. Maurer, M. E. Fraeman, M. N. Martin, and D. R. Roth, “Harsh Environments: Space Radiation Environment, Effects, and Mitigation,” *Johns Hopkins APL Tech. Dig.*, vol. 28, no. 1, pp. 17–29, 2008.
[56] B. Yost, “Executive Summaries,” *State of the Art of Small Spacecraft Technology*, 2018. [Online]. Available: https://sst-soa.arc.nasa.gov/executive-summary. [Accessed: 18-Oct-2018]
[57] A. Pickering, “CDF Study Report: NanoSat Development of a Highly-Capable, Modular Miniaturized Platform,” ESTEC Concurrent Design Facility (CDF), CDF-84(A), Feb. 2009.
[58] Elwood Agasid, Roland Burton, Roberto Carlino, et al, “02. Integrated Spacecraft Platforms,” *State of the Art of Small Spacecraft Technology*, 10-Sep-2018. [Online]. Available: https://sst-soa.arc.nasa.gov/02-integrated-spacecraft-platforms. [Accessed: 18-Oct-2018]
[59] Elwood Agasid, Roland Burton, Roberto Carlino, et al, “05. Guidance, Navigation and Control,” *State of the Art of Small Spacecraft Technology*, 10-Sep-2018. [Online]. Available: https://sst-soa.arc.nasa.gov/05-guidance-navigation-and-control. [Accessed: 18-Oct-2018]
[60] J. R. Wertz and W. J. Larson, *Space Mission Analysis and Design, 3rd edition*, vol. 8. Microcosm, 1999.
[61] E. Agasid, R. Burton, R. Carlino, and et al, “07. Thermal Control,” *State of the Art of Small Spacecraft Technology*, 10-Sep-2018. [Online]. Available: https://sst-soa.arc.nasa.gov/07-thermal. [Accessed: 18-Oct-2018]
[62] Elwood Agasid, Roland Burton, Roberto Carlino, et al, “07. Thermal Control – State of the Art of Small Spacecraft Technology,” *State of the Art of Small Spacecraft Technology*, 10-Sep-2018. [Online]. Available: https://sst-soa.arc.nasa.gov/07-thermal. [Accessed: 18-Oct-2018]
[63] Luna Inc., “Luna coating provides radiation protection in space,” *Luna*, 13-Feb-2018. [Online]. Available: http://lunainc.com/luna-coating-radiation-protection-space-2/. [Accessed: 14-Oct-2018]
[64] L. Jenner, “NASA-Developed Technologies Showcased on Dellingr’s Debut Flight,” *NASA*, 02-Aug-2017. [Online]. Available: https://www.nasa.gov/feature/goddard/2017/nasa-developed-technologies-showcased-on-dellingr-s-debut-flight-0. [Accessed: 14-Oct-2018]
[65] D. Sinclair and J. Dyer, “Radiation Effects and COTS Parts in SmallSats,” in *27th Annual AIAA/USU Conference on Small Satellites*, Logan, Utah, 2013 [Online]. Available: https://digitalcommons.usu.edu/smallsat/2013/all2013/69/. [Accessed: 12-May-2019]
[66] Elwood Agasid, Roland Burton, Roberto Carlino, et al, “06. Structures, Materials and Mechanisms,” *State of the Art of Small Spacecraft Technology*, 10-Sep-2018. [Online]. Available: https://sst-soa.arc.nasa.gov/06-structures-materials-and-mechanisms. [Accessed: 18-Oct-2018]
[67] Elwood Agasid, Roland Burton, Roberto Carlino, et al, “08. Command and Data Handling,” *State of the Art of Small Spacecraft Technology*, 10-Sep-2018. [Online]. Available: https://sst-soa.arc.nasa.gov/08-command-and-data-handling. [Accessed: 18-Oct-2018]
[68] M. R. Chartrand, *Satellite Communications for the Nonspecialist*. SPIE Press, 2004.
[69] Elwood Agasid, Roland Burton, Roberto Carlino, et al, “09. Communications,” *State of the Art of Small Spacecraft Technology*, 10-Sep-2018. [Online]. Available: https://sst-soa.arc.nasa.gov/09-communications. [Accessed: 18-Oct-2018]
[70] W. L. Morgan and G. D. Gordon, *Communications satellite handbook*. Wiley-Interscience, 1989.
[71] Australian Space Academy, “Radio Frequencies for Space Communication,” *Radio Space*. [Online]. Available: https://www.spaceacademy.net.au/spacelink/radiospace.htm. [Accessed: 14-Oct-2018]
[72] Elwood Agasid, Roland Burton, Roberto Carlino, et al, “04. Propulsion,” *State of the Art of Small Spacecraft Technology*, 10-Sep-2018. [Online]. Available: https://sst-soa.arc.nasa.gov/04-propulsion. [Accessed: 18-Oct-2018]

[73] M. Tsay and J. Frongillo, “Lunar Cube: A Deep Space 6U Cube Sat with Mission Enabling Ion Propulsion Technology,” in *29th Annual AIAA/USU Conference on Small Satellites*, Logan, UT, USA, 2015, pp. 508–655.
[74] E. F. Agasid *et al.*, “Integration of a MicroCAT Propulsion System and a PhoneSat Bus into a 1.5U CubeSat,” presented at the 4S Symposium Small Satellites Systems and Services Symposium, Porto Petro, Majorca; Spain, 2014 [Online]. Available: https://ntrs.nasa.gov/search.jsp?R=20140008601. [Accessed: 15-Oct-2018]
[75] G. A. Landis *et al.*, “A Cubesat Asteroid Mission: Propulsion Trade-offs,” in *50th AIAA/ASME/SAE/ASEE Joint Propulsion Conference*, Cleveland, OH, 2014, p. 660.
[76] S. Spangelo, D. Landau, S. Johnson, N. Arora, and T. Randolph, “Defining the requirements for the Micro Electric Propulsion systems for small spacecraft missions,” in *2015 IEEE Aerospace Conference*, Big Sky, 2015, pp. 1–16.
[77] R. W. Conversano and R. E. Wirz, “Mission Capability Assessment of CubeSats Using a Miniature Ion Thruster,” *J. Spacecr. Rockets*, vol. 50, no. 5, pp. 1035–1046, Sep. 2013.
[78] A. R. Tummala and A. Dutta, “An Overview of Cube-Satellite Propulsion Technologies and Trends,” *Aerospace*, vol. 4, no. 4, p. 58, Dec. 2017.
[79] A. S. Erickson, “China’ s space development history: A comparison of the rocket and satellite sectors,” *Acta Astronaut.*, vol. 103, pp. 142–167, 2014.
[80] M. Endo, “The Japanese Space Launch Program,” in *Handbook of Space Security: Policies, Applications and Programs*, K.-U. Schrogl, P. L. Hays, J. Robinson, D. Moura, and C. Giannopapa, Eds. New York, NY: Springer, 2015, pp. 899–920.
[81] J. N. Pelton, “Launch vehicles and launch sites,” in *Handbook of Satellite Applications*, Pelton, Joseph N., Madry, Scott, Camacho-Lara, Sergio, Ed. Springer Science+Business Media, 2016, pp. 1–15.
[82] A. C. Veclani and J.-P. Darnis, “European Space Launch Capabilities and Prospects,” in *Handbook of Space Security: Policies, Applications and Programs*, K.-U. Schrogl, P. L. Hays, J. Robinson, D. Moura, and C. Giannopapa, Eds. New York, NY: Springer New York, 2015, pp. 783–800.
[83] F. Bonaventure, S. Locoche, and A.-H. Gicquel, “De-orbitation studies and operations for spirale GTO satellites,” in *23rd International Symposium on Space Flight Dynamics*, Pasadena, California, 2013 [Online]. Available: http://issfd.org/ISSFD_2012/ISSFD23_CRSD1_3.pdf
[84] W. S. Kurth *et al.*, “Electron densities inferred from plasma wave spectra obtained by the Waves instrument on Van Allen Probes,” *J. Geophys. Res. [Space Phys]*, vol. 120, no. 2, pp. 904–914, Feb. 2015.
[85] T. Villela, C. A. Costa, A. M. Brandão, F. T. Bueno, and R. Leonardi, “Towards the Thousandth CubeSat: A Statistical Overview,” *International Journal of Aerospace Engineering*, vol. 2019, Jan. 2019 [Online]. Available: https://www.hindawi.com/journals/ijae/2019/5063145/. [Accessed: 12-Feb-2019]
[86] ISRO, “GSLV-F05 / INSAT-3DR Brochure.” Aug-2016 [Online]. Available: https://www.isro.gov.in/gslv-f05-insat-3dr/gslv-f05-insat-3dr-brochure-0. [Accessed: 03-Apr-2019]
[87] J. K. Ziemer, R. R. Wessen, and P. V. Johnson, “Exploring the science trade space with the JPL Innovation Foundry A-Team,” *Concurrent Engineering: Research and Applications*, vol. 26, no. 1, pp. 22–32, Mar. 2018.
[88] Analytical Graphics Inc., *Systems Tool Kit*. 2019 [Online]. Available: https://www.agi.com/products/satellite-design-and-operations
[89] The MathWorks, Inc., *Matlab*. 2018 [Online]. Available: https://se.mathworks.com/products/matlab.html
[90] Consortium led by the Royal Belgian Institute for Space Aeronomy (BIRA-IASB), *SPENVIS*. 2016 [Online]. Available: https://www.spenvis.oma.be
[91] J. R. Weiss, W. D. Smythe, and W. Lu, “Science traceability,” in *2005 IEEE Aerospace Conference*, Big Sky, MT, USA, 2005, pp. 292–299.

[92] Analytical Graphics Inc., “Technical Notes for HPOP,” *STK*. [Online]. Available: http://help.agi.com/stk/index.htm#hpop/hpopTechNotes.htm. [Accessed: 10-Mar-2019]
[93] D. Hastings and H. Garrett, *Spacecraft Environment Interactions, 1996*. Cambridge University Press: Cambridge, 2009.
[94] G. Beutler, *Methods of Celestial Mechanics: Volume I: Physical, Mathematical, and Numerical Principles*. Springer Science & Business Media, 2004.
[95] Analytical Graphics Inc., “Approximate Altitude Computation in STK,” *STK*, May-2019. [Online]. Available: http://help.agi.com/stk/index.htm#hpop/approximateAltitudeComputation.htm. [Accessed: 05-May-2019]
[96] Y. Wang and P. Gurfil, “The role of solar apsidal resonance in the evolution of geostationary transfer orbits,” *Adv. Space Res.*, vol. 59, no. 8, pp. 2101–2116, Apr. 2017.
[97] Y. Wang and P. Gurfil, “Dynamical modeling and lifetime analysis of geostationary transfer orbits,” *Acta Astronaut.*, vol. 128, pp. 262–276, Nov. 2016.
[98] C. Lucking, C. Colombo, and C. McInnes, “Mission and system design of a 3U CubeSat for passive GTO to LEO transfer,” in *63rd International Astronautical Congress*, Naples, 2012, p. 13.
[99] S. M. Seltzer, “Electron, Electron-Bremsstrahlung and Proton Depth-Dose Data for Space-Shielding Applications,” *IEEE Trans. Nucl. Sci.*, vol. 26, no. 6, pp. 4896–4904, Dec. 1979.
[100] A. Parsons, “Radiation Effects on CubeSats,” *The UNSW Canberra at ADFA Journal of Undergraduate Engineering Research*, vol. 10, no. 2, 2017 [Online]. Available: http://ojs.unsw.adfa.edu.au/index.php/juer/article/view/1092. [Accessed: 12-Apr-2019]
[101] R. Kingsbury *et al.*, “TID Tolerance of Popular CubeSat Components,” in *2013 IEEE Radiation Effects Data Workshop (REDW)*, San Francisco, CA, USA, 2013, pp. 1–4.
[102] P. Fortescue, G. Swinerd, and J. Stark, *Spacecraft Systems Engineering*. John Wiley & Sons, 2011.
[103] California Polytechnic State University, “Cubesat design specification,” Cal Poly SLO, San Luis Obispo, Rev.13, Feb. 2014.
[104] N. W. Peddie, “International Geomagnetic Reference Field,” *J. Geomagn. Geoelectr.*, vol. 34, no. 6, pp. 309–326, 1982.
[105] W. P. Olson, K. A. Pfitzer, and G. J. Mroz, “Modeling the magnetospheric magnetic field,” in *Quantitative Modeling of Magnetospheric Processes*, vol. 21, W. P. Olson, Ed. Washington, D. C.: American Geophysical Union, 1979, pp. 77–85.
[106] C. V. Voorhies, “On magnetic spectra of Earth and Mars,” *J. Geophys. Res.*, vol. 107, no. E6, p. 790, 2002.
[107] J. A. Penrod, “Feasibility of Using Lunar Magnetic Fields to Control CubeSat Attitude,” BSc, Faculty of the Graduate School, 2015 [Online]. Available: https://hanspeterschaub.info/Papers/grads/JamesPenrod.pdf
[108] B. Riwanto, “CubeSat Attitude System Calibration and Testing,” MSc, School of Electrical Engineering, 2015 [Online]. Available: http://urn.fi/URN:NBN:fi:aalto-201509184426. [Accessed: 10-Feb-2019]
[109] B. Charbaut, “Robust and Agile Attitude Control for Triple CubeSat Eye-Sat,” MSc, School of Engineering Sciences (SCI), 2018 [Online]. Available: http://www.diva-portal.org/smash/record.jsf?pid=diva2:1255169. [Accessed: 12-Apr-2019]
[110] H. E. Spence *et al.*, “Science Goals and Overview of the Radiation Belt Storm Probes (RBSP) Energetic Particle, Composition, and Thermal Plasma (ECT) Suite on NASA’s Van Allen Probes Mission,” *Space Sci. Rev.*, vol. 179, no. 1–4, pp. 311–336, Nov. 2013.
[111] R. Nymmik, “Initial conditions for radiation analysis: Models of galactic cosmic rays and solar particle events,” *Advances in Space Research*, vol. 38, no. 6, pp. 1182–1190, 2006.
[112] K. D. C. Simunac and T. P. Armstrong, “Solar cycle variations in solar and interplanetary ions observed with Interplanetary Monitoring Platform 8,” *J. Geophys. Res.*, vol. 109, no. A10101, 2004 [Online]. Available: http://doi.wiley.com/10.1029/2003JA010194
[113] H. Singer, L. Matheson, R. Grubb, and A. Newman, “Monitoring space weather with the GOES magnetometers,” in *Proc. SPIE 2812, GOES-8 and Beyond*, Denver, CO, United States, 1996

[Online]. Available: https://www.spiedigitallibrary.org/conference-proceedings-of-spie/2812/0000/Monitoring-space-weather-with-the-GOES-magnetometers/10.1117/12.254077.short?casa_token=vNPZdheB5j0AAAAA:3wG5koys_LqJCi2SSDYykpezH9gEqNt7dgv-r-Ai-o-1FZc7Ybjuo3HnWWAvZcxqyVlQUqxR

[114] Kongsberg Satellite Services, "KSAT LITE – FOR SMALL SATELLITES," *KSAT*. [Online]. Available: https://www.kongsberg.com/ksat/services/ksatlite/. [Accessed: 11-Feb-2019]

[115] SSC, "Ground Station Network," *SSC - Swedish Space Corporation*. [Online]. Available: https://www.sscspace.com/ssc-worldwide/ground-station-network/. [Accessed: 10-Mar-2019]

[116] ESA, "Estrack ground stations," *European Space Agency*, 18-Feb-2018. [Online]. Available: https://www.esa.int/Our_Activities/Operations/Estrack/Estrack_ground_stations. [Accessed: 02-Apr-2019]

[117] International Telecommunications Union-Radiocommunications Sector (ITU-R), "Effects of tropospheric refraction on radiowave propagation," International Telecommunications Union - Radiocommunications Sector (ITU-R), ITU-R P.834, Dec. 2017 [Online]. Available: https://global.ihs.com/doc_detail.cfm?document_name=ITU-R%20P.834&item_s_key=00439692#product-details-list

[118] AGI Inc., "Antenna Coordinate Systems," *STK - Antenna Coordinate Systems*, Jan-2019. [Online]. Available: http://help.agi.com/stk/index.htm#comm/antenna_coordinate_systems.htm%3FTocPath%3DAdd-on%2520Modules|Communications%2520%2526%2520Radar|Antenna%2520Models|_____2. [Accessed: 23-Jan-2019]

[119] International Amateur Radio Union, Region 1, "IARU-R1 VHF Handbook," IARU, Nov. 2018 [Online]. Available: http://www.ok2kkw.com/iaru/vhf_handbook_v8.12.pdf

[120] B. Klofas, "Upcoming amateur radio cubesats: the flood has arrived," in *AMSAT Annual Meeting and Space Symposium*, Houston, Texas, USA, 2013 [Online]. Available: https://klofas.com/papers/klofas_upcoming_cubesat_launches.pdf

[121] P. Niemelä and T. Nikkanen, "A1-GND-DD-01-v5-DRAFT Design of Ground Station Hardware." 2017.

[122] WiMo Antennen & Elektronik GmbH, "Yagi antennas for 2m and 70cm," *Wifi UMTS/3G GSM Antennas, Radio Amateur Antenna, coaxial cables assemblies, radio accessories*. [Online]. Available: https://www.wimo.com/yagi-antennas-wimo_e.html. [Accessed: 08-Apr-2019]

[123] WiMo Antennen und Elektronik GmbH, "WiMo Yagi Antennas," May 2004 [Online]. Available: http://www.radiomanual.info/schemi/ACC_antenna/Wimo_Yagis_broch.pdf

[124] Aalto University, "For radio amateurs," *Aalto University*, 30-Oct-2018. [Online]. Available: https://www.aalto.fi/en/spacecraft/for-radio-amateurs. [Accessed: 02-Apr-2019]

[125] A. M. Bagher, M. M. A. Vahid, and M. Mohsen, "Types of solar cells and application," *American Journal of Optics and Photonics*, vol. 3, no. 5, pp. 94–113, 2015.

[126] Finnish Centre of Excellence in Research of Sustainable Space, "FS1 Interface Control Sheet." May-2019.

[127] A. C. Tribble, *The Space Environment: Implications for Spacecraft Design - Revised and Expanded Edition*. Princeton University Press, 2003.

[128] G. L. Stephens *et al.*, "An update on Earth's energy balance in light of the latest global observations," *Nat. Geosci.*, vol. 5, no. 10, pp. 691–696, Sep. 2012.

[129] Atmospheric and Environmental Research, Inc. (AER), "SEET: SPACE ENVIRONMENT AND EFFECTS TOOL FOR AGI'S SYSTEMS TOOL KIT (STK)," AGI, Jun. 2015 [Online]. Available: http://help.agi.com/stk/LinkedDocuments/SEET_manual.pdf

[130] R. Hienonen, M. Karjalainen, and R. Lankinen, *Verification of the thermal design of electronic equipment*. Espoo: Technical Research Centre of Finland, 1997.

[131] R. Osiander and A. G. Darrin, "9 - Wireless MEMS for space applications," in *Wireless MEMS Networks and Applications*, D. Uttamchandani, Ed. Woodhead Publishing, 2017, pp. 197–214.

[132] A. R. Plastino and J. C. Muzzio, “On the use and abuse of Newton’s second law for variable mass problems,” *Celest. Mech. Dyn. Astron.*, vol. 53, no. 3, pp. 227–232, Sep. 1992.
[133] J. C. Pascoa, O. Teixeira, and G. Filipe, “A Review of Propulsion Systems for CubeSats,” in *Proceedings of the ASME 2018 International Mechanical Engineering Congress and Exposition*, Pittsburgh, PA, USA, 2018, pp. V001T03A039–V001T03A039.
[134] D. Gibbon and C. Underwood, “Low Cost Butane Propulsion Systems for Small Spacecraft,” in *Proceedings of the 15th AIAA/USU Conference on Small Satellites*, Logan, Utah, USA, 2001 [Online]. Available: https://digitalcommons.usu.edu/smallsat/2001/All2001/76/. [Accessed: 08-Apr-2019]
[135] Aurora Propulsion Technologies, “FS-2 RCS proposition: Resistojet thruster system for the FS-2 satellite.” 07-Mar-2019.
[136] P. Janhunen, “Electric Sail for Spacecraft Propulsion,” *J.PROPULSION*, vol. 20, no. 4, pp. 763–764, Jul. 2004.
[137] P. Janhunen, “Conversation in the Slack channel of Aalto Satellites,” 23-Apr-2019.
[138] N. Crisp, K. Smith, and P. Hollingsworth, “Small Satellite Launch to LEO: A Review of Current and Future Launch Systems,” *TRANSACTIONS OF THE JAPAN SOCIETY FOR AERONAUTICAL AND SPACE SCIENCES, AEROSPACE TECHNOLOGY JAPAN*, vol. 12, no. ists29, p. Tf_39–Tf_47, 2014.
[139] Hyperion Technologies B.V, “RW210,” 2018 [Online]. Available: https://hyperiontechnologies.nl/wp-content/uploads/2018/07/HT-RW210_V1.02_Flyer.pdf. [Accessed: 11-Feb-2019]
[140] NewSpace Systems (Pty) Ltd., “New Space stellar gyroscope NSGY-001,” NewSpace Systems (Pty) Ltd., Oct. 2018 [Online]. Available: http://www.newspacesystems.com/wp-content/uploads/2018/10/NewSpace-Stellar-Gyro_8b.pdf
[141] M. Rothacher, M. Meindl, M. Joss, and E. Styger, “Requirements for CubeSats: the Astrocast CubeSat Mission,” ETH Zürich, Riga, 2017 [Online]. Available: https://cddis.nasa.gov/2017_Technical_Workshop/docs/presentations/session1/ilrsTW2017_s1_Rothacher2.pdf
[142] D. M. Miles and et al., “A miniature, low-power scientific fluxgate magnetometer: A stepping-stone to cube-satellite constellation missions,” *Journal of Geophysical Research: Space Physics*, vol. 121, no. 11, pp. 839–860, 2016.
[143] A. J. Caffee and B. G. Drost, “Physical design in magnetic environment,” 1015308411-Dec-2018 [Online]. Available: https://patentimages.storage.googleapis.com/74/cf/46/6c0841b897d025/US10153084.pdf. [Accessed: 12-Feb-2019]
[144] H. C. Koons, J. E. Mazur, R. S. Selesnick, J. B. Blake, and J. F. Fennell, “The impact of the space environment on space systems,” AEROSPACE CORP EL SEGUNDO CA EL SEGUNDO TECHNICAL OPERATIONS, 1999 [Online]. Available: http://www.dtic.mil/docs/citations/ADA376872
[145] H.-S. Choi *et al.*, “Analysis of GEO spacecraft anomalies: Space weather relationships: SPACE WEATHER EFFECTS ON GEO SPACECRAFT ANOMALIES,” *Space Weather*, vol. 9, no. 6, Jun. 2011 [Online]. Available: http://doi.wiley.com/10.1029/2010SW000597
[146] S. T. Lai, K. Cahoy, W. Lohmeyer, A. Carlton, R. Aniceto, and J. Minow, “Chapter 16 - Deep Dielectric Charging and Spacecraft Anomalies,” in *Extreme Events in Geospace*, N. Buzulukova, Ed. Elsevier, 2018, pp. 419–432.
[147] J. E. Mazur, “An Overview of the Space Radiation Environment,” *Crosslink*, vol. 4, no. 2, pp. 10–14, 2003.
[148] R. Evans, H. B. Garrett, S. Gabriel, and A. C. Whittlesey, “A preliminary spacecraft charging map for the near earth environment,” in *Proceedings of the Spacecraft Charging Technology Conference*, Monterey, California, 1989.
[149] NASA, “Mitigating In-Space Charging Effects-A Guideline,” NASA Technical Standards System (NTSS), Washington, DC, NASA-HDBK-4002, Oct. 2017 [Online]. Available: https://standards.nasa.gov/standard/nasa/nasa-hdbk-4002. [Accessed: 04-Apr-2019]

[150] E. J. Daly, G. Drolshagen, A. Hilgers, and H. D. R. Evans, “Space environment analysis: Experience and trends,” in *Symposium Proceedings (ESA SP-392)*, ESTEC Noordwijk, 1996, p. 15.

[151] H. C. Polat, J. Virgili-Llop, and M. Romano, “Survey, statistical analysis and classification of launched CubeSat missions with emphasis on the attitude control method,” *Journal of Small Satellites*, vol. 5, no. 3, pp. 513–530, 2016.

[152] J. Wrobel *et al.*, “Versatile Structural Radiation Shielding and Thermal Insulation through Additive Manufacturing,” in *AIAA/USU Conference on Small Satellites*, Logan, 2013 [Online]. Available: https://digitalcommons.usu.edu/smallsat/2013/all2013/61/. [Accessed: 12-May-2019]

[153] D. Thomsen, W. Kim, and J. Cutler, “Shields-1, A SmallSat Radiation Shielding Technology Demonstration,” in *29th Annual AIAA/USU Conference on Small Satellites*, Logan, 2015 [Online]. Available: https://digitalcommons.usu.edu/smallsat/2015/all2015/84/. [Accessed: 12-May-2019]

APPENDICES

FORESAIL	
Project statement	Funded by the Finnish Academy of Science, the Finnish Centre of Excellence in Research of Sustainable Space (FORESAIL) encompasses three nanosatellite missions for the investigation of a multitude of kinetic processes in near-Earth space, while deploying novel methods for propulsion and space debris reduction.
FORESAIL-2	
MIssion goal	To demonstrate a feasibility to utilize and characterize a nanosatellite and its instruments for scientific purposes in a high-radiation environment.

Science Traceability Matrix (STM)

#	Science/Tech Goals	#	Science Objectives	Measurement Objectives	Measurement Requirements	Instruments	Instrument Reqs	Mission Reqs	Data Products	Potential Capability-Reducing Events
		1	Quantify the role of ULF waves (Pc5 and EMIC) for the response of the radiation belt electrons (e.g., decrease, deplete, no-change, pitch-angles, phase space densities) over a wide range of energies and locations as a function of solar wind structures (e.g., during coronal mass ejection ejecta and sheaths, stream interaction regions and fast streams) and magnetospheric activity.	Measure the energy spectrum of electrons	**Breakthrough:** Energy spectrum in the range of 30 keV–10 MeV along 30 lines of sight at a given time (6° angular resolution) with the energy resolution ΔE/E of 20%. **Enabling:** Energy spectrum in the range 800 keV to 8 MeV with the angular resolution of 15°. In the 300–1000 keV range, the energy resolution ΔE/E of 20%. In the 1–8 MeV range the energy resolution ΔE/E of 100%.	Relativistic Electron and Proton Experiment (**REPE**) telescope	Proton/e-discrimination ΔE / E ~ 0.2 **Breakthrough:** 6° angular resolution **Enabling:** 15° angular resolution	Scan the sky with spin axis perpendicular to the magnetic field vector Data rate 300 bit/s	Time history of electron fluxes per energy bin per pitch angle bin.	Missing observations for areas with significant geomagnetic activities Lost data due to the lack of data storage capacity and limited downlink Lost data due to single event upsets (SEUs)
			Percent completion of goal given full satisfaction of all contributing objectives: 100 %		Percent completion of Objective given full satisfaction of Measurement Requirements: 100 %					

FORESAIL	
Project statement	Funded by the Finnish Academy of Science, the Finnish Centre of Excellence in Research of Sustainable Space (FORESAIL) encompasses three nanosatellite missions for the investigation of a multitude of kinetic processes in near-Earth space, while deploying novel methods for propulsion and space debris reduction.
FORESAIL-2	
MIssion goal	To demonstrate a feasibility to utilize and characterize a nanosatellite and its instruments for scientific purposes in a high-radiation environment.

Science Traceability Matrix (STM)

#	Science/Tech Goals	#	Science Objectives	Measurement Objectives	Measurement Requirements	Instruments	Instrument Reqs	Mission Reqs	Data Products	Potential Capability-Reducing Events
1	What is the role of ULF waves in accelerating, transporting, and scattering of electrons in the Earth's radiation belts as a function of solar wind driving and magnetospheric activity?	2	Explore the impact of solar wind drivers and magnetospheric activity on the ULF Pc5 (2 mHz – 5 Hz) and EMIC (0.1–5 mHz) wave properties.	Measure magnetic field vectors in the 3 Cartesian coordinates.	**Breakthrough:** Magnetic field intensity in the 3 Cartesian coordinates with a frequency range from 1 mHz to 10Hz and with amplitudes between 0.1 nT to 1000 of nT (B). **Enabling:** Magnetic field intensity in the 3 Cartesian coordinates with a frequency range (Pc5) from 2 to 7 mHz. The burst mode is optional	Flux Gate Magnetometer (FGM)	Attitude control information. Sampling rate of 10 to 100Hz The maximum acceptable noise levels are 1 nT^2/Hz for 1 mHz waves and 10^-3 nT^2/Hz for 1 Hz waves The normal-mode measurements should be acquired continuously throughout orbit. The burst-mode measurements – for 1000 seconds at the apogee.	Attitude knowledge >1.5° Position knowledge 100 - 1000 km Sufficient satellite rotation speed to scan all space. Wide Magnetic Local Time (MLT) coverage. Orbit covering range between 2 to 5 Earth radii in altitude. Equatorial orbits are preferred Inclination < 45° Measurement over 400 orbits Data rate 100 bit/s Minimize influence of magnetic disturbance from spacecraft towards magnetometer	Time history of electric and magnetic fields.	Missing observations for areas with significant geomagnetic activities Lost data due to the lack of data storage capacity and limited downlink Lost data due to single event upsets (SEUs)
			Percent completion of goal given full satisfaction of all contributing objectives: 100 %		Percent completion of Objective given full satisfaction of Measurement Requirements: 100 %					

FORESAIL	
Project statement	Funded by the Finnish Academy of Science, the Finnish Centre of Excellence in Research of Sustainable Space (FORESAIL) encompasses three nanosatellite missions for the investigation of a multitude of kinetic processes in near-Earth space, while deploying novel methods for propulsion and space debris reduction.
FORESAIL-2	
MIssion goal	To demonstrate a feasibility to utilize and characterize a nanosatellite and its instruments for scientific purposes in a high-radiation environment.

Science Traceability Matrix (STM)

#	Science/Tech Goals	#	Science Objectives	Measurement Objectives	Measurement Requirements	Instruments	Instrument Reqs	Mission Reqs	Data Products	Potential Capability-Reducing Events
		3	Integrate the data with measurements by the other spacecraft in the solar wind and magnetosphere, and from ground-based facilities to resolve whether waves are externally transferred or internally generated waves (substorm activity). Characterise the response of electrons (e.g., decrease, deplete or have no-change)	TBD	TBD	TBD	TBD	TBD	TBD	TBD
	Relative value of science goal toward mission goal: 100 %		Percent completion of goal given full satisfaction of all contributing objectives: TBD %		Percent completion of Objective given full satisfaction of Measurement Requirements: TBD %					
		1	Characterize how wave properties (from ULF frequencies upwards to turbulent frequencies) such as frequency spectra, polarization, correlation lengths, etc. vary as waves travel from the upstream interplanetary medium through the magnetosphere, the radiation belts and into the ionosphere.	Measure plasma wave properties (electric and magnetic field fluctuations, plasma density).	See Science goal #1, Objective #2	See Science goal #1, Objective #2	See Science goal #1, Objective #2	See Science goal #1, Objective #2	See Science goal #1, Objective #2	See Science goal #1, Objective #2
					Percent completion of Objective given full satisfaction of Measurement Requirements: 100 %					
					Measure electric field intensity in in the 3 Cartesian coordinates with a frequency range from 1 mHz to 10Hz and with amplitudes between 0.1mV/m and 1000 of mV/m	Langmuir Probe or Faraday Cup or Antenna	TBD	TBD	TBD	TBD
					Percent completion of Objective given full satisfaction of Measurement Requirements: 50 %					
	How do ULF waves and turbulence transmit in the solar wind – magnetosphere – ionosphere system?				Electric current in tether	See Science goal #3, Objective #1	See Science goal #3, Objective #1	See Science goal #3, Objective #1	See Science goal #3, Objective #1	See Science goal #3, Objective #1
			Percent completion of goal given full satisfaction of all contributing objectives: 80 %		Percent completion of Objective given full satisfaction of Measurement Requirements: 50 %					

FORESAIL	
Project statement	Funded by the Finnish Academy of Science, the Finnish Centre of Excellence in Research of Sustainable Space (FORESAIL) encompasses three nanosatellite missions for the investigation of a multitude of kinetic processes in near-Earth space, while deploying novel methods for propulsion and space debris reduction.
FORESAIL-2	
MIssion goal	To demonstrate a feasibility to utilize and characterize a nanosatellite and its instruments for scientific purposes in a high-radiation environment.

Science Traceability Matrix (STM)

#	Science/Tech Goals	#	Science Objectives	Measurement Objectives	Measurement Requirements	Instruments	Instrument Reqs	Mission Reqs	Data Products	Potential Capability-Reducing Events
2	Relative value of science goal toward mission goal: 90 %	2	Characterize the spatial variation of wave properties in as large a range of L-shells and polar angles as possible, by having the spacecraft reach a wide range of locations in near-earth space.	Accumulate magnetic and electric fields over a range of altitudes and orbits	TBD	TBD	TBD	an elliptical orbit ranging from 2 to 5 Earth radii in altitude	Derived from magnetic field timeseries data.	TBD
			Percent completion of goal given full satisfaction of all contributing objectives: 100 %		Percent completion of Objective given full satisfaction of Measurement Requirements: 100 %					
		3	Characterize the temporal variations of the wave properties, as a function of solar wind driving conditions.	Accumulate magnetic and electric field data and compare / relate it to upstream conditions	Magnetic and electric field measurements of comparable rate and precision as measurements on spacecraft measuring solar wind conditions	TBD	TBD	Mission lifetime for at least 3 months	Derived from magnetic field timeseries data and correlation to other spacecraft	TBD
			Percent completion of goal given full satisfaction of all contributing objectives: 100 %		Percent completion of Objective given full satisfaction of Measurement Requirements: 100 %					
		1	Characterise the relationship between the Coulomb drag force and plasma density in plasmas (from LEO to plasma pause)	1. Measure change in spin rate resulting from switching on and off (step) tether voltage in sync with rotation (to get Coulomb drag)	Coulomb drag: 1 nN/m (resolution); max force: 500 nN per meter of tether length Gold tether: Measure difference in phase angle with resolution of 0.4° Aluminium tether: Measure difference in phase angle with resolution of 1.6°	Coulomb Drag Experiment (CDE) tether Attitude Determination System (ADS)	No conductive surface needed Max deflection 0.859372 deg Max tether tension 1 cN	Atittude knowledge of 0.4° or 1.6° depending on tether material Minimum angular momentum of 21 Nms for reeling tether out Data rate 10 bit/s	TBD	A DC motor fails to reel out the full length of tether Maximum deflection is exceeded and tether breaks away Lost data due to the lack of data storage capacity and limited downlink Lost data due to single event upsets (SEUs) One of ADCS sensors fails and it is not possible to measure change in spin rate
				Percent completion of Objective given full satisfaction of Measurement Requirements: 100 %						

FORESAIL	
Project statement	Funded by the Finnish Academy of Science, the Finnish Centre of Excellence in Research of Sustainable Space (FORESAIL) encompasses three nanosatellite missions for the investigation of a multitude of kinetic processes in near-Earth space, while deploying novel methods for propulsion and space debris reduction.
FORESAIL-2	
MIssion goal	To demonstrate a feasibility to utilize and characterize a nanosatellite and its instruments for scientific purposes in a high-radiation environment.

Science Traceability Matrix (STM)

#	Science/Tech Goals	#	Science Objectives	Measurement Objectives	Measurement Requirements	Instruments	Instrument Reqs	Mission Reqs	Data Products	Potential Capability-Reducing Events
3	How does the CD force depend on plasma parameters and tether voltage?	2	Characterise relationship between the Coulomb drag force and tether voltage	2. Measure tether current simultaneously (to get plasma density)	TBD	Coulomb Drag Experiment (CDE) tether Attitude Determination System (ADS)	Time resolution: 1 min or 1 second in a denser plasma environment	Data rate 1 bit/s	TBD	See Science goal #3, Objective #1
			Percent completion of goal given full satisfaction of all contributing objectives: 100 %		Percent completion of Objective given full satisfaction of Measurement Requirements: 100%					
				1. Measure change in spin rate resulting from switching different tether voltages in sync with rotation	See Science goal #3, Objective #1	Coulomb Drag Experiment (CDE) tether Attitude Determination System (ADS)	See Science goal #3, Objective #1	See Science goal #3, Objective #1	See Science goal #3, Objective #1	See Science goal #3, Objective #1
				Percent completion of Objective given full satisfaction of Measurement Requirements: 100 %						
				2. Measure tether current simultaneously	See Science goal #3, Objective #2	Coulomb Drag Experiment (CDE) tether Analog-to-Digital Converter (ADC)	See Science goal #3, Objective #2	See Science goal #3, Objective #2	See Science goal #3, Objective #2	See Science goal #3, Objective #2
	Relative value of science goal toward mission goal: 100%		Percent completion of goal given full satisfaction of all contributing objectives: 100 %		Percent completion of Objective given full satisfaction of Measurement Requirements: 100 %					

FORESAIL	
Project statement	Funded by the Finnish Academy of Science, the Finnish Centre of Excellence in Research of Sustainable Space (FORESAIL) encompasses three nanosatellite missions for the investigation of a multitude of kinetic processes in near-Earth space, while deploying novel methods for propulsion and space debris reduction.
FORESAIL-2	
MIssion goal	To demonstrate a feasibility to utilize and characterize a nanosatellite and its instruments for scientific purposes in a high-radiation environment.

Science Traceability Matrix (STM)

#	Science/Tech Goals	#	Science Objectives	Measurement Objectives	Measurement Requirements	Instruments	Instrument Reqs	Mission Reqs	Data Products	Potential Capability-Reducing Events
4	What are the novel radiation mitigation techniques? Relative value of technology goal toward mission goal: 50%	1	Software techniques: - Design and implementation of a fault-tolerant operating system architecture Hardware techniques: - Implementation of a distributed processor architecture for increased fault tolerance - Demonstrating the mitigation of TID-induced component degradation via localized component heating under bias Percent completion of goal given full satisfaction of all contributing objectives: 50%	On-board: Evaluating the functionality and change in electrical parameters of a set of discrete components as a function of total ionizing dose and annealing profile On the ground: - Evaluating the behavior of an implementation of the distributed processor architecture and/or the fault-tolerant operating system under irradiation	On-board: Discrete measurements of voltages with about 10 mV precision Discrete measurements of currents with about 100 uA precision Temperature measurements with <= 5'C precision Measurement frequency: no more than 1/minute Percent completion of Objective given full satisfaction of Measurement Requirements: 100%	**RME** board	On-board: Dedicated board floorspace on one of the boards, or dedicated experiment board Significant amount of energy for test component heating (how much will depend on thermal properties of the system)	Orbit with high-radiation environment Data rate < 116 bit/s	On-board: - Supply currents vs. time - Temperature vs. time - Error logs for complex ICs (memory and/or MCU)	Communication fails and no data on efficiency of applied radiation mitigation techniques

Mission Traceability Matrix (MTM)				
Mission Reqs	MIssion Design Reqs	Spacecraft Reqs	Ground System Reqs	Operations Reqs
From 01 Science Traceability Matrix	**Launch date:** Launch during forecasted high solar and geomagnetic activities is preferred **Mission length:** Minimum 6 months (> 400 orbits) **Orbit altitude requirement:** Minimum orbit altitude 180 km to ensure minimum mission length Maximum orbit altitude has to be more than 12756 km (> 2 Earth radii) **Geographic coverage:** Daily passes over region within latitude of 30 degrees North and South to provide dowlink capabilities for science data **Orbit local time:** Wide coverage of Magnetic Local Time (MLT) to meet science requirement of temporal sampling **Type of orbit:** Highly Elliptical (e > 0.7) Equatorial with i < 45 degree **Other:** Orbit has to cross Van Allen radiation belts to satisfy science requirement for high-radiation environment	**Stabilization:** Spin stabilized with spin axis perpendicular to the magnetic field vector **Mass:** <1530 g (around 1.5 kg) **Power:** >7W (Highest simultaneous power demand from instruments) **Volume:** 1652.75 cm3 (around 1.6U) (Sum of volumes of all instruments) **Data Rate:** 411 bit/s (all instruments producing measurements simultaneously) **Temperature Range for operation:** - 40°C to 85 °C (smallest range from all instruments) **Attitude knowledge:** > 0.4° (highest accuracy requirement) **Position knowledge:** 100 - 1000 km **Radiation shielding requirement:** > 10 krad to decrease rate of degradation of electronic components **Other:** Fit within nanosatellite class of spacecrafts (1-10 kg)	**Passes per day and duration:** Minimum 1 passes per day with average 60 minutes **Assumed antenna size:** high-gain (>15dB) Yagi antenna or 3 meter parabolic antenna **Data volume per day:** 4.44 Mbytes/day (Data storage) **Real time data:** None	**General spacecraft maneuver requirements and frequency:** De-tumble following orbit insertion to spin rate =< 36°/s . 1 time Spin up spacecraft <180 deg/s. 1 time Deploy tether . 1 time Stabilize spin axis pointed towards magnetic field vector. 1 time Point solar panels towards the sun. 1 time per orbit **Special maneuvers requirements:** None **Rationale for maneuvers:** Lower spin rate increases sampling rate and allows to scan larger areas of plasmasphere Larger spin rate produces required angular momentum (~20 Nms) and centrifugal force (~0.4 cN) to deploy tether. Pointing solar panels towards the sun ensures that electric power is available for science experiments **Ephemeris requirements:** Position knowledge of spacecraft within 100 - 1000 km range **Changes in viewing modes** New view mode per second to cover larger areas of plasmasphere

Mission Traceability Matrix (MTM)				
Mission Reqs	MIssion Design Reqs	Spacecraft Reqs	Ground System Reqs	Operations Reqs
Instrument Specific	Mission Reqs	Spacecraft Reqs	Ground	Operations
Flux Gate **Magnetometer** (FGM)	Attitude knowledge >1.5° Position knowledge 100 - 1000 km Sufficient satellite rotation speed to scan all space. Wide Magnetic Local Time (MLT) coverage. Orbit covering range between 2 to 5 Earth radii in altitude. Equatorial orbits are preferred Inclination < 45° Measurement over 400 orbits Data rate 100 bit/s Minimize influence of magnetic disturbance from spacecraft towards magnetometer	Based on HMC2003 **Stabilization:** spin stabilized with rate =< 36 deg/s (1°/s for sampling with 10Hz rate) **Mass:** 30 g **Power:** 15V x 20mA (> 0.3 W) **Volume:** 1.97x2.73x1.2 (>6.45 cm3) **Data Rate:** 100 bit/s (For burst mode of 100 Hz) **Temperature Range for operation:** -40°C to 85 °C **Attitude knowledge:** < 1.5° **Position knowledge:** 100 - 1000 km **Radiation shielding requirement:** > 10 krad to decrease rate of degradation for DIP **Other:** Minimize magnetic disturbance produced by spacecraft subsystems	**Passes per day and duration:** Minimum 2 passes per day with average 60 minutes **Assumed antenna size:** high-gain (>15dB) Yagi antenna or 3 meter parabolic antenna **Data volume per day:** 1.08 Mbyte/day (Data storage) **Real time data:** None	**General spacecraft maneuver requirements and frequency:** De-tumble following orbit insertion to spin rate =< 36°/s . 1 time **Special maneuvers requirements:** None **Rationale for maneuvers:** Lower spin rate increases sampling rate and allows to scan larger areas of plasmasphere **Ephemeris requirements:** Position knowledge of spacecraft within 100 - 1000 km range **Changes in viewing modes** New view mode per second to cover larger areas of plasmasphere

Mission Traceability Matrix (MTM)				
Mission Reqs	MIssion Design Reqs	Spacecraft Reqs	Ground System Reqs	Operations Reqs
Relativistic Electron and Proton Experiment (**REPE**) telescope	Scan the sky with spin axis perpendicular to the magnetic field vector Measurement over 400 orbits Data rate 300 bit/s	Based on PaTe **Stabilization:** spin stabilized with axis perpendicular (<5° of deviation) to the magnetic field vector **Mass:** < 820 g (PaTe with 1 telescope) **Power:** < 2 W **Volume:** > 1000 cm3 **Data Rate:** 300 bit/s **Temperature Range for operation:** -35°C to 149 °C (Based on test of Xilinx Artix-7 FPGA) https://www.dfrsolutions.com/instability-metastability-or-failure **Attitude knowledge:** Same as for magnetometer **Position knowledge:** Same as for magnetometer **Radiation shielding requirement:** > 10 krad to decrease rate of degradation	**Passes per day and duration:** Minimum 1 pass per day with average 60 minutes **Assumed antenna size:** high-gain (>15dB) Yagi antenna or 3 meter parabolic antenna **Data volume per day:** 3.24 Mbyte/day (Data storage) **Real time data:** None **Transmit frequency:** UHF or S-band **Power available for COM:** 1.2W **Downlink data rate:** 300 bit/s **Number of data dumps per day:** >= 1 **Spacecraft data destination:** Aalto University **Science data destination:** UTU, FMI, UH	**General spacecraft maneuver requirements and frequency:** De-tumble following orbit insertion and stabilize spin axis. 1 time **Special maneuvers requirements:** None **Rationale for maneuvers:** Target pointing increases sampling rate and allows to scan larger areas of plasmasphere **Ephemeris requirements:** Same as for magnetometer **Changes in viewing modes** New view mode per second to cover larger areas of plasmasphere

Mission Traceability Matrix (MTM)				
Mission Reqs	MIssion Design Reqs	Spacecraft Reqs	Ground System Reqs	Operations Reqs
Coulomb Drag Experiment (**CDE**) tether Attitude Determination System (**ADS**) Analog-to-Digital Converter (**ADC**)	Atittude knowledge of 0.4° or 1.6° depending on tether material Minimum angular momentum of 21 Nms for reeling tether out Data rate 10 bit/s (CD force) + 1 bit/s (plasma density)	Based on Plasma brake **Stabilization:** spin stabilized with rate =< 36 deg/s (1°/s for sampling with 10Hz rate) **Mass:** < 600 g **Power:** Reeling mode: 7W, Science mode: 0.6 W (CD force + Tether current) **Volume:** 6.7×8.4×9.6 (< 540.3 cm3) **Data Rate:** 11 bit/s **Temperature Range for operation:** - 55°C to 85 °C (Based on 12AV1000 screened package) **Attitude knowledge:** > 0.4° **Position knowledge:** None **Radiation shielding requirement:** > 10 krad to decrease rate of degradation for electronics	**Passes per day and duration:** Minimum 1 pass per day with average 60 minutes **Assumed antenna size:** high-gain (>15dB) Yagi antenna or 3 meter parabolic antenna **Data volume per day:** 118.8 kbyte/day **Real time data:** None	**General spacecraft maneuver requirements and frequency:** Spin up spacecraft <180 deg/s. 1 time **Special maneuvers requirements:** None **Rationale for maneuvers:** Increase spin rate to reel tether out **Ephemeris requirements:** Same as for magnetometer **Changes in viewing modes** New view mode per second to cover larger areas of plasmasphere
Radiation Mitigation Experiment (**RME**) board	Orbit with high-radiation environment Data rate <116 bit/s	**Stabilization:** None **Mass:** 80 g (Assuming the same size as OBC board) **Power:** > 2W (assuming power for heating) **Volume:** 9.4x9.4x1.2 (>106 cm3) (Based on dimensions of FS-1 PCB in avionics stack) **Data Rate:** <116 bit/s **Temperature Range for operation:** -40°C to 105 °C (Based on RM48L952 by Texas Instruments) **Attitude knowledge:** None **Position knowledge:** None **Radiation shielding requirement:** > 10 krad to decrease rate of degradation for a board	**Passes per day and duration:** Minimum 1 pass per day with average 60 minutes **Assumed antenna size:** high-gain (>15dB) Yagi antenna or 3 meter parabolic antenna **Data volume per day:** <1.25 Mbyte/day **Real time data:** None	**General spacecraft maneuver requirements and frequency:** None **Special maneuvers requirements:** None **Rationale for maneuvers:** None **Ephemeris requirements:** Same as for magnetometer **Changes in viewing modes** None

Appendix 3 STK with Matlab

```
% Launch STK and create a new scenario file
matlab = actxserver('STK11.application');
root = matlab.Personality2;
matlab.visible = 1;
root.NewScenario('FS2-3U-SD-CC-NB');
FS2atGTO = root.CurrentScenario;
installDirectory = root.ExecuteCommand('GetDirectory / STKHome').Item(0);

% Period of simulation
FS2atGTO.SetTimePeriod('1 Dec 2021 00:00:00.000','1 Feb 2023 00:00:00.000');

% Create a model of 3U CubeSat
FS2= root.CurrentScenario.Children.New('eSatellite', 'FORESAIL-2-3U');
FS2.Mass = 5; %kg
Bmass = FS2.Mass;


% Moment of Inertia
Bheight = .3405; % height of rectangular body (m)
Bwidth = .10; % width of rectangular body (m)
Bdepth = .10; % depth of rectangular body (m)
FS2.Inertia.Ixx = 1/12*Bmass*((Bheight)^2+(Bdepth)^2); % kgm^2
FS2.Inertia.Ixy = 0;
FS2.Inertia.Ixz = 0;
FS2.Inertia.Iyy = 1/12*Bmass*((Bwidth)^2+(Bheight)^2);
FS2.Inertia.Iyz = 0;
FS2.Inertia.Izz = 1/12*Bmass*((Bwidth)^2+(Bdepth)^2);

transmit = FS2.Children.New('eTransmitter', 'UHF transceiver');
txModel = transmit.Model;
antCntrl = txModel.AntennaControl;
antCntrl.SetEmbeddedModel('Isotropic');
antCntrl.EmbeddedModel.Efficiency = 85; %Percent

% Satellite attitude: spinning about sun vector
attitude = FS2.Attitude.Basic;
attitude.SetProfileType('eProfileSpinSun')
attitude.Profile.Rate = 6;  % rev/sec or 36 deg/s

% Create ground station located at Aalto University
OH2AGS = root.CurrentScenario.Children.New('eFacility', 'Aalto University');
receiver = OH2AGS.Children.New('eReceiver', 'Yagi Antenna');
OH2AGS.UseTerrain = true;

% Set altitude to a distance above the ground
OH2AGS.HeightAboveGround = .04;   % km

root.UnitPreferences.Item('LatitudeUnit').SetCurrentUnit('deg')
root.UnitPreferences.Item('LongitudeUnit').SetCurrentUnit('deg')

OH2AGS.Position.AssignPlanetodetic(60.18718,24.81760,0); % OH2AGS in Otaniemi, Espoo, Finland

%Scenario parameters
FS2.SetPropagatorType('ePropagatorHPOP'); % Using High Precision Orbit Propagator (HPOP)
```

```
    set(FS2.Propagator,'Step',1); % 1 min resolution
    GTO = FS2.Propagator.InitialState.Representation.ConvertTo('eOrbitStateClassical'); %
    GTO.SizeShapeType = 'eSizeShapeAltitude';  % Use Perigee/Apogee
    GTO.LocationType = 'eLocationTrueAnomaly'; % Use True Anomaly
    GTO.Orientation.AscNodeType = 'eAscNodeRAAN'; % Use RAAN
    GTO.SizeShape.PerigeeAltitude = 185;      % km
    GTO.SizeShape.ApogeeAltitude = 35786;       % km
    GTO.Orientation.Inclination = 27;         % deg
    GTO.Orientation.ArgOfPerigee = 180;       % deg
    GTO.Orientation.AscNode.Value = 7.5;      % deg
    GTO.Location.Value = 1.67885e-14;               % deg

    FS2.Propagator.InitialState.Representation.Assign(GTO);

    forceOnFS2 = FS2.Propagator.ForceModel;
    forceOnFS2.CentralBodyGravity.File = 'C:\Program Files\AGI\STK
11\STKData\CentralBodies\Earth\EGM2008.grv';
    forceOnFS2.CentralBodyGravity.MaxDegree = 21;
    forceOnFS2.CentralBodyGravity.MaxOrder = 21;
    forceOnFS2.CentralBodyGravity.UseOceanTides = 1;
    forceOnFS2.CentralBodyGravity.OceanTides.MaxDegree = 4;
    forceOnFS2.CentralBodyGravity.OceanTides.MaxOrder = 4;
    forceOnFS2.CentralBodyGravity.OceanTides.MinAmplitude = 0;
    forceOnFS2.CentralBodyGravity.UseSolidTides = 1;
    forceOnFS2.CentralBodyGravity.SolidTideType = 0; %Include both time-dependent and time-independent
contributions.
    forceOnFS2.CentralBodyGravity.UseSecularVariations = 1;

    forceOnFS2.ThirdBodyGravity.CentralBody = 'Sun';
    forceOnFS2.ThirdBodyGravity.Source = 0; %Central body file (all bodies): gravitational value from editable
central body file shipped with STK
    forceOnFS2.ThirdBodyGravity.CentralBody = 'Moon';
    forceOnFS2.ThirdBodyGravity.Source = 0;

    forceOnFS2.Drag.Use=1;
    forceOnFS2.Drag.DragModel.Type=0; %Spherical
    forceOnFS2.Drag.DragModel.Cd=2.2;
    forceOnFS2.Drag.DragModel.AreaMassRatio=0.002; % m^2/kg
    forceOnFS2.Drag.DragModel.AtmosphericDensityModel=13;%The Drag Temperature Model (DTM), 2012
version
    forceOnFS2.Drag.DragModel.LowAltAtmosphericDensityModel=8; % NRLMSISE 2000
    forceOnFS2.Drag.DragModel.BlendingRange = 30; %km
    forceOnFS2.Drag.DragModel.SolarFluxGeoMag.AgVeSolarFluxGeoMagUseFile=1;
    forceOnFS2.Drag.DragModel.SolarFluxGeoMag.File='C:\ProgramData\AGI\STK 11
(x64)\DynamicEarthData\SpaceWeather-v1.2.txt';
    forceOnFS2.Drag.DragModel.SolarFluxGeoMag.GeomagFluxUpdateRate=2; %Daily
    forceOnFS2.SolarRadiationPressure.Use=0;

    forceOnFS2.Drag.DragModel.SolarFluxGeoMag.GeomagFluxSrc=1; %Read Ap from file.

    integrate = FS2.Propagator.Integrator;
    integrate.DoNotPropagateBelowAlt=-1e6;
    integrate.IntegrationModel=3; % Runge-Kutta-Fehlberg integration method of 7th order with 8th order
error control for the integration step size.
    integrate.StepSizeControl.Method=1; % Relative error
    integrate.StepSizeControl.ErrorTolerance=1e-13;
    integrate.StepSizeControl.MinStepSize=0.1;
```

```
    integrate.StepSizeControl.MaxStepSize=30;
    integrate.Interpolation.Method=1; %Lagrange: interpolates position and velocity separately
    integrate.Interpolation.Order=7;

FS2.Propagator.Propagate;

%Evaluating access between FORESAIL-2 and Ground Station in Otaniemi
access = OH2AGS.GetAccessToObject(FS2);
access.ComputeAccess()

acsInt = access.ComputedAccessIntervalTimes;
accessDataProvider = access.DataProviders.Item('AER Data').Group.Item('Default');
dataProviderElements = {'Time';'Azimuth';'Elevation';'Range'};
for i = 1:1:acsInt.Count
  [start, stop] = acsInt.GetInterval(i-1);
  dataProviderResult = accessDataProvider.ExecElements(start,stop,1,dataProviderElements);

  timeValues = cell2mat(dataProviderResult.DataSets.GetDataSetByName('Time').GetValues);
  azimuthValues = cell2mat(dataProviderResult.DataSets.GetDataSetByName('Azimuth').GetValues);
  elevationValues = cell2mat(dataProviderResult.DataSets.GetDataSetByName('Elevation').GetValues);
  rangeValues = cell2mat(dataProviderResult.DataSets.GetDataSetByName('Range').GetValues);
end

% Parameters for orbital lifetime analysis
root.ExecuteCommand('SetLifetime */FORESAIL-2-3U DragCoeff 2.2 ReflectCoeff 1.5 DragArea 0.01
SunArea 0.09 Mass 5 DecayAltitude 100 FluxSigmaLevel 2 2ndOrder On Rotate On Graphics On
DensityModel DTM2012');

% lifetime
result = root.ExecuteCommand('Lifetime */FORESAIL-2-3U');

disp(result.Item(0))

split_result = regexp(result.Item(0), ' ', 'split');

decay = [split_result{8} ' ' split_result{9} ' ' split_result{10} ' ' split_result{11}]
numOrbits = str2num(split_result{13})
orbLifetime = str2num(split_result{17}) %days

root.ExecuteCommand('SetAnimation * StartAndCurrentTime "1 Dec 2021 00:00:00.00" EndTime "1 Dec
2023 00:00:00.00" TimeStep 0.5');

% Thermal conductivity

k = 121.2; % W/m/C
A = 0.03; % m^2
dT = 92.3; % C
t = 1320; % seconds
L = 0.006; % m

Qj = (k*A*dT/L)/1000 % kW

Qw = ((Qj*1000)*t)/10^6 %MJ
```

Appendix 4 Risk Assessment Matrix

#	Mission challenges	Negative effect	Cause	Probability [142]	Severity [145]
1	Total Ionizing Dose (TID)	Degradation of microelectronics	Trapped protons Trapped electrons Solar protons	HIGH Total of 3 events	MODERATE Leads to a decrease in science return but does not fail the mission entirely.
2	Displacement Damage Dose (DDD)	Degradation of optical components and some electronics Degradation of solar cells	Trapped protons Trapped electrons Solar protons Neutrons	HIGH Total of 14 events	MODERATE Leads to a decrease in science return but does not fail the mission entirely.
3	Single Event Effects (SEE)	Data corruption Noise on images System shutdowns Electronic component damage	GCR heavy ions Solar protons and heavy ions Trapped protons Neutrons	HIGH (2) SEU - Cosmic Ray 15 events SEU - Solar Particle 9 events SEU - SAA 20 events SEU - Uncategorized 41 events Total of 85 events	MODERATE Leads to a decrease in science return but does not fail the mission entirely. Spacecraft can recover.
4	Surface Erosion	Degradation of thermal, electrical, optical properties Degradation of structural integrity	Particle radiation Ultraviolet Atomic oxygen Micrometeoroids Contamination	LOW Atomic oxygen 1 event	LOW Brings minor issues to the mission
5	Surface Charging	Biasing of instrument readings Power drains Electrical discharges leading to physical damage	Dense, cold plasma Hot plasma	LOW 1 event Plasma effects 4 events	MODERATE Leads to a decrease in science return but does

					not fail the mission entirely.
6	Electrostatic Discharges (ESD)	Component failure Phantom commands		HIGH (1) ESD - Internal Charging 74 events ESD - Surface Charging 59 events Uncategorized 28 events Total: 161	HIGH Leads to the failure of the mission
7	Deep Dielectric Charging / Non-ionising Energy Loss (NIEL)	Biasing of instrument readings Electrical discharges leading to physical damage	High-energy electrons		
8	Structure Impacts	Structural damage Decompression	Micrometeoroids Orbital debris	LOW 10 events	HIGH
9	Drag	Torques Orbital decay	Neutral thermosphere	LOW 1 event	MODERATE Leads to a decrease in science return but does not fail the mission entirely.
10	Thermal swings	Malfunctioning of electronic components Degradation of onboard battery lifetime Structural damage due to strain from a thermal expansion	Fast and frequent changes in eclipse periods	MODERATE Frequency is 2 times per day Slow, time in eclipse is around 30 minutes	MODERATE Leads to a decrease in science return but does not fail the mission entirely.
11	Communication disruption	Temporary loss of a communication link between the CubeSat and ground station	Ionospheric irregularities	LOW 1 event	LOW Brings minor issues to the mission. Recoverable.

12	Attitude Control Disruption	Temporary loss of control over the attitude of the CubeSat	Large storm-time magnetic field fluctuations	LOW 5 events	LOW Brings minor issues to the mission. Recoverable.

Telemetry producers, types and rates

Subsystem and Telemetry Type		Data production rate	
OBC			
	Nominal HK	13,3	bits/s
	Event Data	1,3	bits/s
EPS			
	Nominal HK	13,3	bits/s
ADCS			
	Nominal HK	13,3	bits/s
	Sensor Dump	1,3	bits/s
Propulsion			
	Nominal HK	13,3	bits/s
	Sensor Dump	1,3	bits/s
REPE			
	Science mode	317	bits/s
	Uncompressed science data	300	bits/s
	HK Data	6	bits/s
	Metadata (attitude, timestamps, etc.)	11	bits/s
	Calibration mode (Pulse height data)	500	bits/s
CDE tether			
	Standby	64	bits/s
	Reeling	128	bits/s
	Science mode	11	bits/s
Magnetometer			
	Nominal HK	1	bit/s
	Science mode	100	bits/s
Radiation mitigation experiments			
	Nominal HK	13,3	bits/s
	Science mode	116	bits/s
Compression rate		21%	Estimated using RADMON data

Downlink requirements in science mode

On-board storage / Required downlink rate	**4,6**	**Mbytes per day**
Compressed data	971	kbytes per day
Downlink datarate	8,0	kbit/s
Required downlink time	16,18	min per day

Subsystem	Planned Volume (cm3)	Contingency (%/cm3)		Volume with contingency (cm3)	Fraction	
					3U	6U
Avionics stack	710,4	20%	142,1	852,5	28,42%	14,21%
Structure	103,9	20%	20,8	124,6	4,15%	4,15%
ADCS						
3 Reaction wheels	28,2	20%	5,6	33,8	1,1%	0,0
Gyroscope	64,4	20%	12,9	77,2	2,6%	0,0
Propulsion	300,0	50%	150,0	450,0	15,00%	7,50%
Payloads	1 652,8					
REPE	1 000,0	20%	200,0	1 200,0	40,0%	0,2
Flux Gate Magnetometer	6,5	10%	0,6	7,1	0,2%	0,0
RME board	106,0	20%	21,2	127,2	4,2%	0,0
CDE tether	540,3	25%	135,1	675,4	22,5%	0,1
Total	2 859,6		688,3	3 547,8	118,26%	63,29%
Free space	140,45			−547,83	−18%	37%

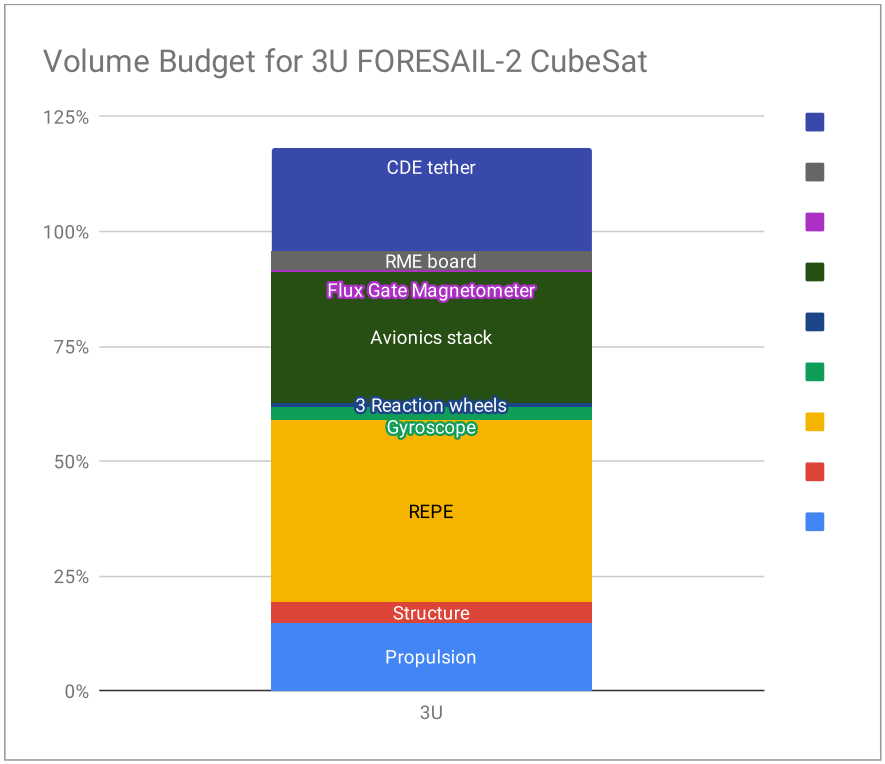

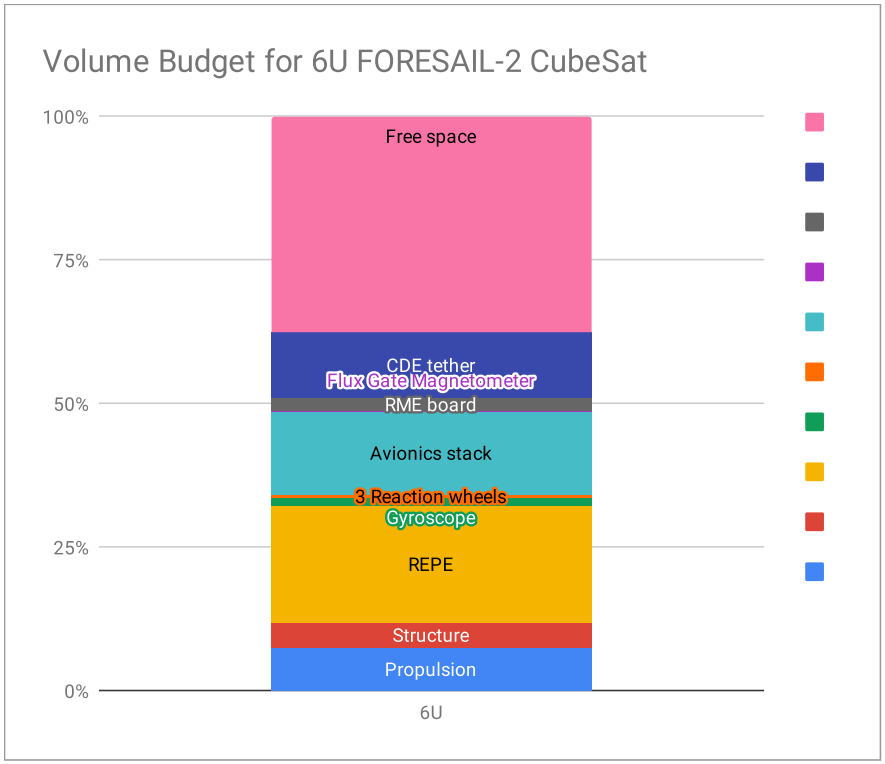

Subsystem	Planned Mass (g)	Contingency (%/g)		Mass with contingency (g)	Fraction
OBC					**1,5%**
OBC board	80,0	10%	8,0	88,0	1,5%
EPS					**16,9%**
EPS Board	80,0	10%	8,0	88,0	1,5%
Solar panels	520,0	20%	104,0	624,0	10,8%
Batteries	186,0	10%	18,6	204,6	3,5%
Battery board	60,0	10%	6,0	66,0	1,1%
ADCS					**5,0%**
3 Reaction wheels	96,0	20%	19,2	115,2	2,0%
Gyroscope	100,0	20%	20,0	120,0	2,1%
Sun sensors	46,0	20%	9,2	55,2	1,0%
UHF					**2,7%**
UHF board	80,0	20%	16,0	96,0	1,7%
Antennas	50,0	20%	10,0	60,0	1,0%
Propulsion					**11,4%**
Propellant	120,0	20%	24,0	144,0	2,5%
Dry mass	350,0	20%	70,0	420,0	7,2%
Control board	80,0	20%	16,0	96,0	1,7%
Structure					**26,7%**
Rails	466,0	20%	93,2	559,2	9,6%
Top plate	112,0	20%	22,4	134,4	2,3%
Bottom plate	112,0	20%	22,4	134,4	2,3%
Avionics Shielding	562,0	20%	112,4	674,4	11,6%
Harnessing and integration	40,0	20%	8,0	48,0	0,8%
Payloads					**35,7%**
REPE	1 000,0	20%	200,0	1 200,0	20,7%
Flux Gate Magnetometer	100,0	10%	10,0	110,0	1,9%
RME board	80,0	10%	8,0	88,0	1,5%
CDE tether	480,0	25%	120,0	600,0	10,3%
Retroreflectors	60,0	20%	12,0	72,0	1,2%
Total	4 860,0			5 797,4	
				Avionics	26,2%

Load	Power Consumption (W)	Average Duty Cycle (%)							
		Safe mode	Nominal	Telemetry downlink	First observation phase	Spin up	CDE demonstration	Second observation phase	Third observation phase
OBC	0,30	50%	50%	100%	100%	100%	100%	100%	100%
ACS	1,00								
- 3 Reaction wheels	1,89	50%	90%	100%	100%	0%	0%	100%	50%
ADS	0,25								
- Gyroscope	0,20	0%	100%	100%	100%	100%	100%	100%	50%
- Sun Sensors	0,05	100%	100%	100%	100%	100%	100%	100%	100%
Propulsion	2,00								
- RCS	0,50	25%	50%	100%	100%	0%	0%	100%	50%
- Propulsion	1,50	0%	0%	0%	0%	100%	0%	100%	0%
EPS	0,20	100%	100%	100%	100%	100%	100%	100%	100%
UHF	2,86								
- Receiving	0,36	80%	80%	10%	80%	80%	80%	90%	50%
- Transmitting	2,50	20%	20%	90%	20%	20%	20%	10%	50%
REPE	2,50								
- *Standby*	0,0001	0%	100%	100%	0%	100%	100%	0%	0%
- Science Mode	2,5	0%	0%	0%	100%	0%	0%	100%	0%
Magnetometer	0,50								
- Standby	0,0001	0%	100%	100%	0%	100%	100%	0%	0%
- Science Mode	0,50	0%	0%	0%	100%	0%	0%	100%	0%
CDE tether	7,60								
- Standby	0,0001	0%	100%	100%	0%	0%	0%	0%	100%
- Plasma density	0,60								
- CD force		0%	0%	0%	0%	0%	0%	100%	0%
- Reeling	7,00	0%	0%	0%	0%	0%	100%	0%	0%
RME board	2,50								
- *Experiment mode*	0,50	0%	0%	0%	0%	0%	0%	0%	100%
- Heating	2,00	0%	0%	0%	0%	0%	0%	0%	100%
Total	19,71	2,3	3,3	5,4	6,9	3,0	8,5	8,8	5,8
Power production	20,7	6,89							

A9.1 Trade space on tether deployment

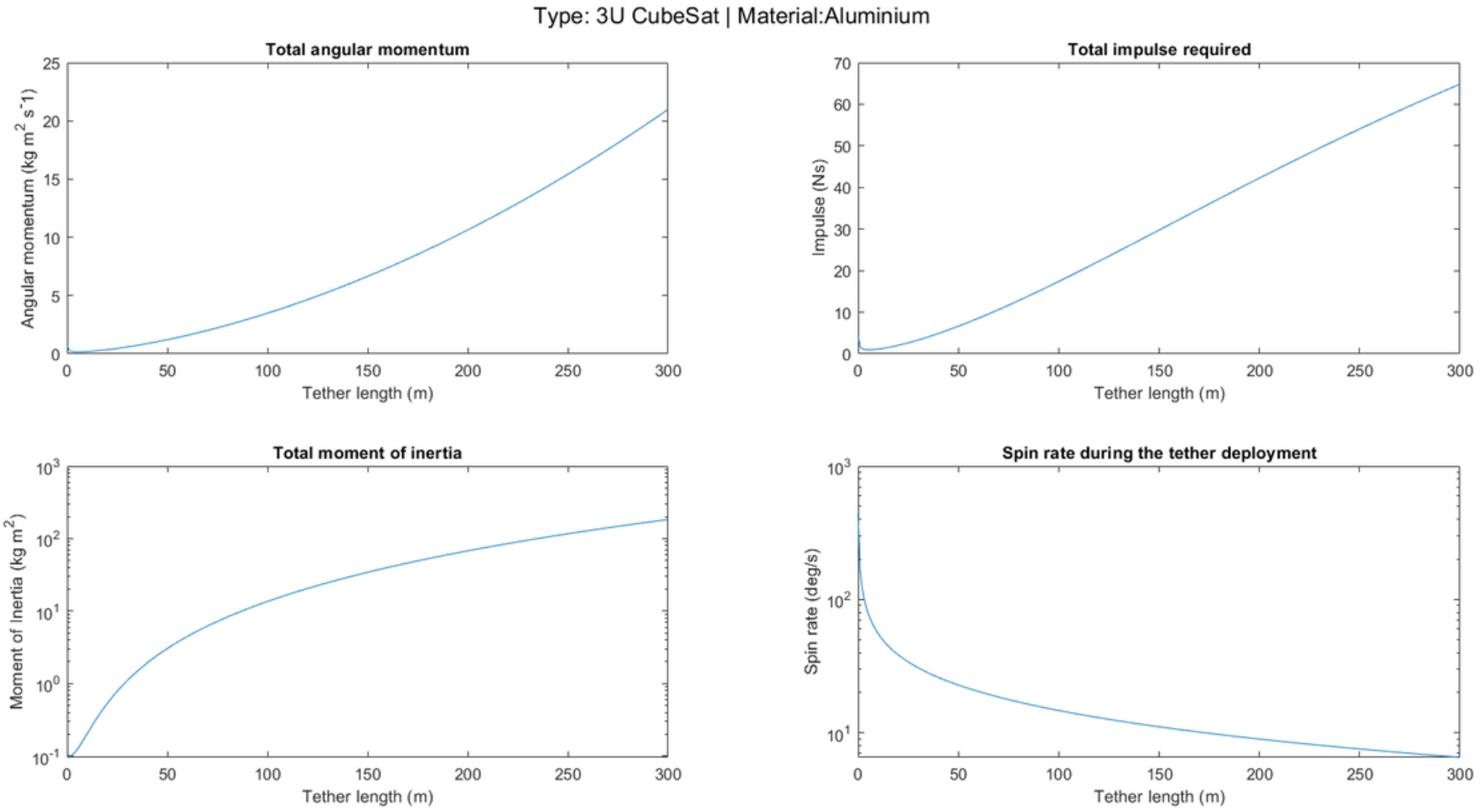

A9.2 Trade space on tether deployment

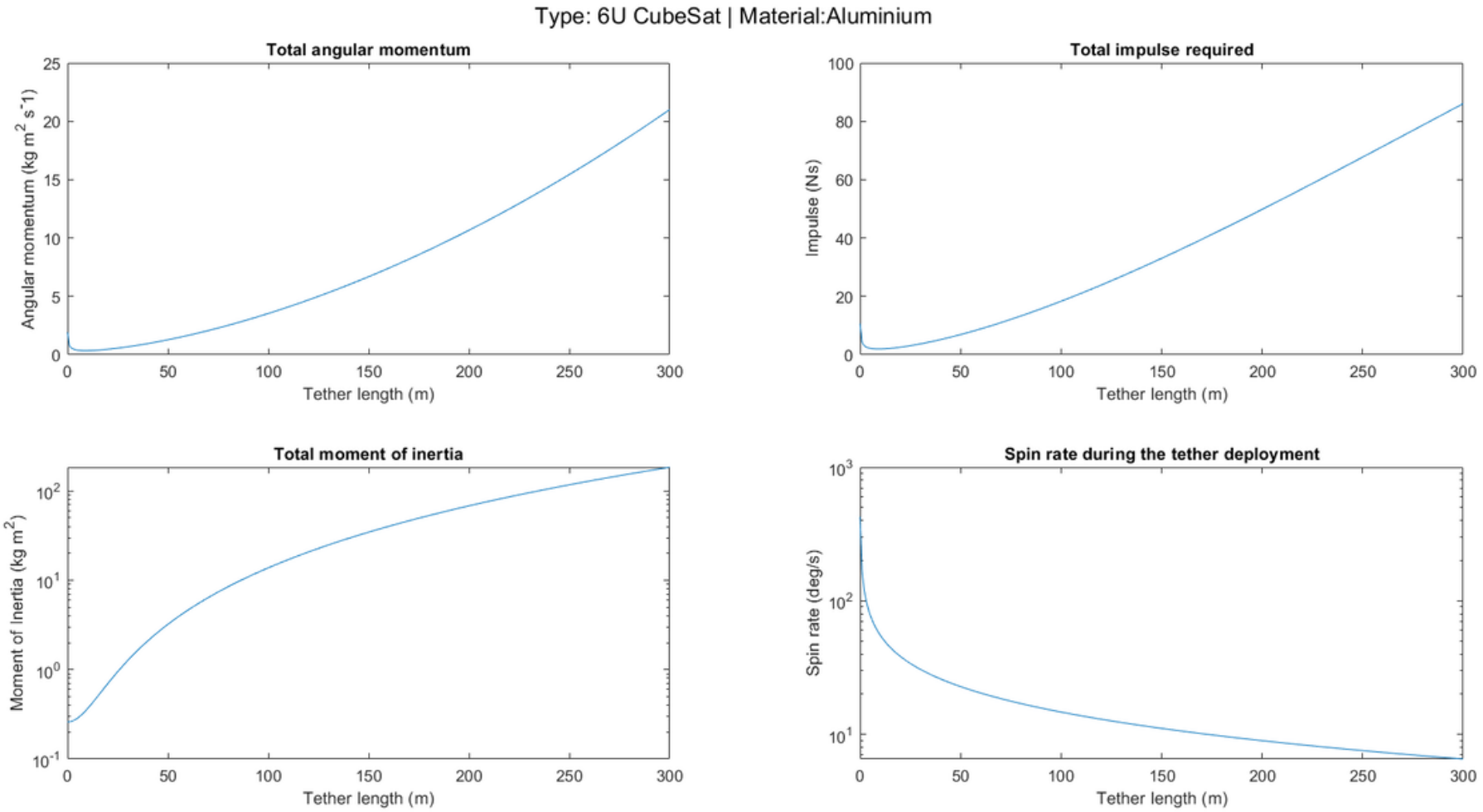

A9.3 Trade space on tether deployment

Type: 3U CubeSat | Material:Gold

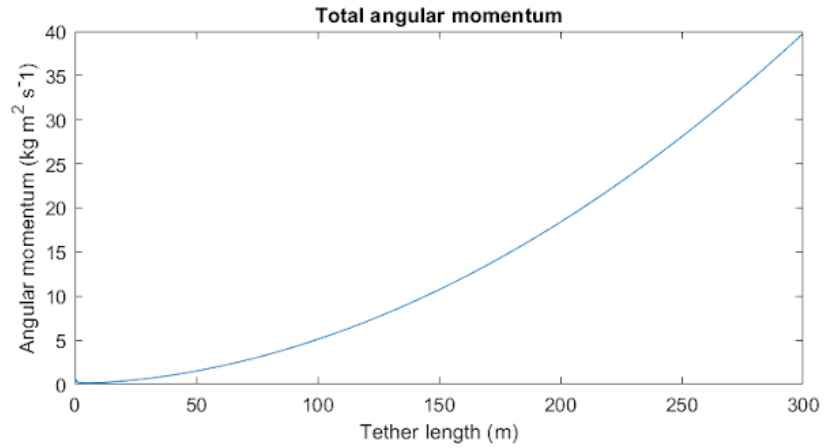

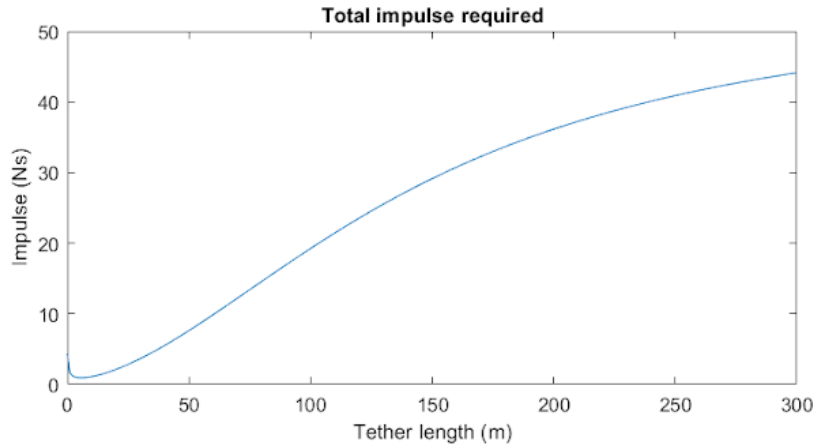

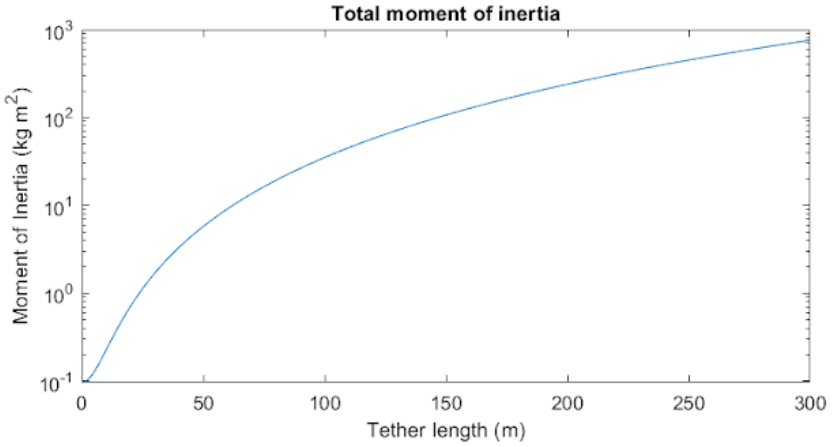

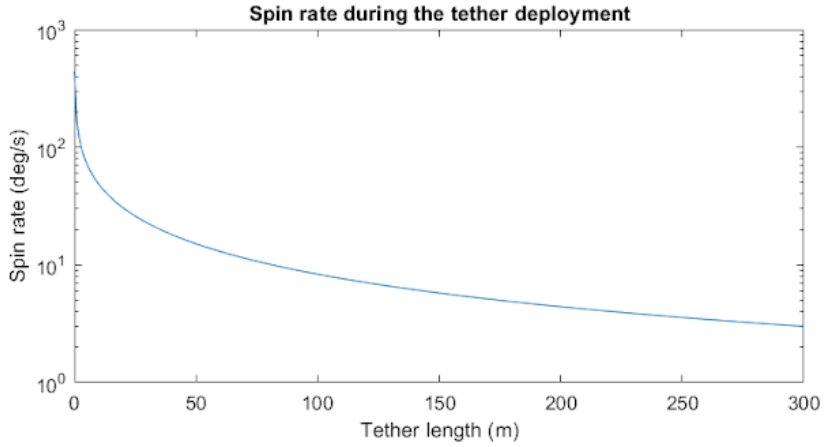

A9.4 Trade space on tether deployment

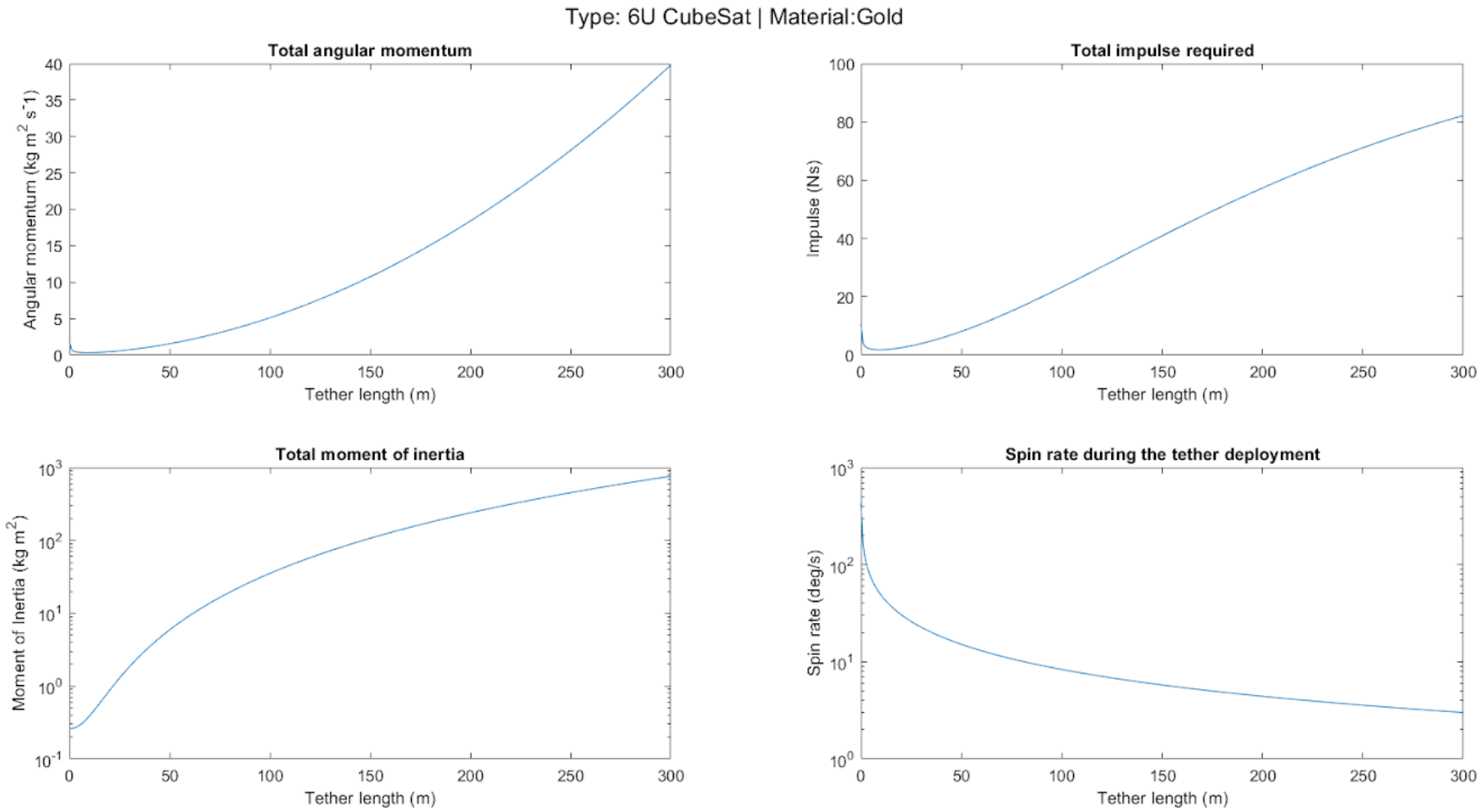

Appendix 10 Mission operation phases